STUDIES OF THE TOWNSEND DISCHARGE IN CAESIUM VAPOUR AND OF THE FORMATIVE TIME LAG IN MERCURY VAPOUR

by

A.A.W.M. Garamoon, B.Sc.

Being a thesis submitted to the
University of Keele in candidature
for the Degree of Doctor of Philosophy

Department of Physics,
University of Keele,
Keele,
Staffordshire.

October, 1968.

SYNOPSIS

Due to the great difficulties in working with caesium, investigation of the breakdown characteristics of caesium vapour in the Townsend discharge (and of the alkali metal vapours generally) has been neglected compared to other gases (i.e. inert gas and hydrogen). In the present investigation a new technique has been developed which enabled the characteristics of a caesium discharge to be determined in two Pyrex glass discharge tubes. Breakdown potential measurements at a fixed electrode separation have been carried out in the range of $p_o d$ from 0.11 to 1 mm.Hg.cm., using nickel electrodes which were covered with caesium. Minimum breakdown potentials of 308 and 332V were found at $p_o d$ of 0.22mm. Hg. Also measurements of first Townsend ionization coefficients have been obtained in the range of E/p_o from 50 to 600 $V.cm^{-1}.mm.Hg^{-1}$., which enabled the second Townsend ionization coefficients to be estimated in the range of E/p_o from 525 to 600$V.cm^{-1}.mm.Hg^{-1}$

Formative time-lags have been measured in Townsend discharge in mercury vapour using a stainless steel anode and liquid mercury pool cathode for a reduced pressure range from 0.5 to 5.8mm.Hg. The results covered a range of E_s/p_o from 138 to 450$V.cm^{-1}.mm.Hg^{-1}$ In the range of E_s/p_o below 350$V.cm^{-1}.mm.Hg^{-1}$, the measured formative time-lags were found to depend on the gap geometry. Analysis of the measured time-lags using Davidson's theory showed that the predominant secondary ionization processes leading to electrical breakdown were the emission of secondary electrons from the mercury cathode by positive ions (coefficient γ) and by delayed radiations (coefficient δ_1/α). These delayed radiations were found

to be produced in the volume destruction of the $^3p_2$ metastable mercury atoms in two body collisions with the ground state mercury atoms. Values of the coefficients γ and δ_1/α have been calculated as functions of E_s/p_o, and it has been found that the δ_1/α secondary process predominates at low values of E_s/p_o while the γ process is important only at high E_s/p_o.

ACKNOWLEDGEMENTS

I wish to express my thanks to:

Professor D.J.E. Ingram, who kindly provided the laboratory facilities.

Professor D.E. Davies*, for his supervision of the early stages of the work.

Dr. N.A. Surplice, for his constant supervision, guidance and helpful discussion during the last two years.

My friends and colleagues in the electron physics group at Keele, for their valuable discussion and in particular Mr. R.J. D'Arcy.

Mr. F. Rowerth and his staff for their technical assistance.

Mrs. J. Royston-Bishop for the typing and presentation of this thesis.

U.A.R. Ministry of Higher Education for the award of a grant to carry out this work.

To my parents for their foresight.

* Now Professor D.E. Davies at the University of La Trobe, Australia.

CONTENTS

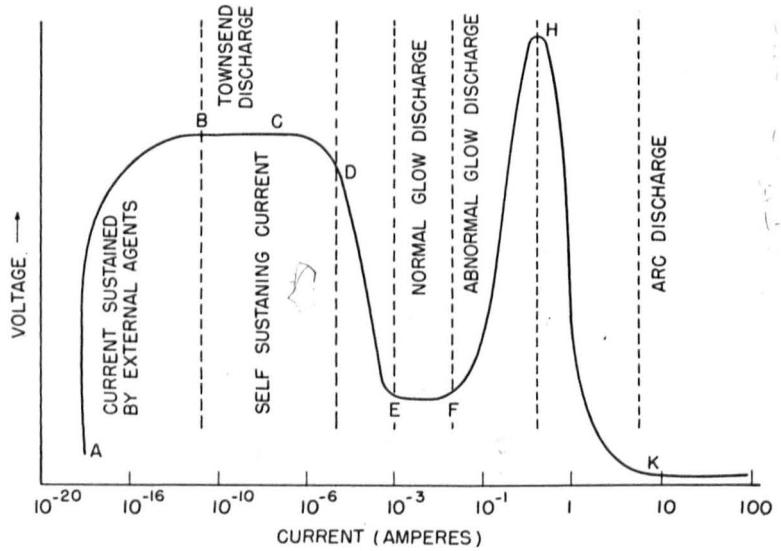

Classification of discharges.

fig.1

CHAPTER I

BASIC PROCESSES IN A LOW PRESSURE TOWNSEND GAS DISCHARGE.

1.1. INTRODUCTION.

The flow of electricity through a gas is often called a discharge. It was given that name many years ago (1), presumably because gases are normally very good insulators. It is of course well known that an electrified body in a gas - air for example - retains its charge indefinitely. But when the air is exposed to ultra-violet light, X-rays, or radiations from radio-active material, the electrified body loses its charge, showing that the air has become conducting.

The study of gaseous conduction is classified into different discharge regions according to the current flowing through the gas fig( ). The fundamental phenomenon that is common to all these regions is the interaction of electrons with the atoms of a gas with the production of ions and excited atoms. Any theory of gaseous conduction in an electric field attempts to derive relationships between the excitation and ionization coefficients and the nature and state of the gas, the gas pressure, the field strength, the nature of the cathode and other parameters. The theory, nevertheless, is incomplete in itself without experimental data to support it and therefore experimental investigation of these parameters is required. In the glow and arc regions distortion of the electric field, by the high currents, adds difficulties to the understanding of the fundamental processes taking place in the discharge. Such difficulties can be eliminated by confining the measurements to the low current Townsend region and it is in this region in which this work has been carried out.

1.2 BEHAVIOUR OF ELECTRONS MOVING THROUGH A GAS UNDER THE INFLUENCE OF AN ELECTRIC FIELD.

Consider a swarm of electrons moving through a gas under the influence of an electric field of very low intensity. Under these conditions the electron energies will be very small and the majority of them will suffer elastic collisions with the gas atoms (or molecules). Cravath (2) showed that an electron will lose approximately $2.66 \frac{m}{M}$ of its energy in an elastic collision with a gas atom, where m and M are the masses of electron and gas atom respectively. Since $m << M$ in most cases, then the electrons will lose only a negligible fraction of their energies and will be scattered in all directions. But due to the influence of the electric field their path is bent until, if no further collisions occur, they once more travel parallel to the field.

Now we have a swarm of electrons moving randomly in all directions with a mean random velocity, but possessing an average drift velocity in the direction of the applied field. The drift and the mean random velocity are quite different in order of magnitude. At low electric field strengths the drift velocity is usually about three orders of magnitude less than the mean random velocity, however, as the field strengths increase to higher values, few electrons will be moving in directions other than the electric field direction and the drift and the random velocity will be nearly equal. The mean energy of the electrons and the electron energy distribution will be determined by the amount of energy gained by the electrons from the electric field and the energy lost in collisions

with gas molecules. At low gas pressure the collision frequency is low, or more precisely the electron mean free path, λ , is large, and as the mean electron energy is directly proportional to λ , then the mean electron energy will be high at low gas pressures, but if the gas pressure is increased, the electron mean free path will be decreased, and consequently the electrons will suffer many more collisions with a corresponding loss of energy and the mean electron energy will be decreased. However, if the electric field strength is increased, so that the electrons can gain greater amount of energy from the field between collisions, the mean electron energy will be once more increased. Hence it can be seen, that, it is the ratio of the field strength to the gas pressure, E/p, which will determine the mean energy of the electrons moving through a gas under the influence of an electric field. Usually the pressure p is reduced to the pressure p_o at 0^oC.

On the assumption that the gas atoms were relatively at rest, low energy electron densities were present, electrons lost a fraction of their energy in elastic collisions, no inelastic collisions occurred and the mean free path of the electrons were independent of their velocities, Penning and Druyvesteyn (3) calculated the electron energy distribution function, given by

$$f(\varepsilon) = C\varepsilon^{\frac{1}{2}} e^{-0.55\left(\frac{\varepsilon}{\bar{\varepsilon}}\right)^2}$$

where $\bar{\varepsilon}$ is the electron mean energy and C is constant.

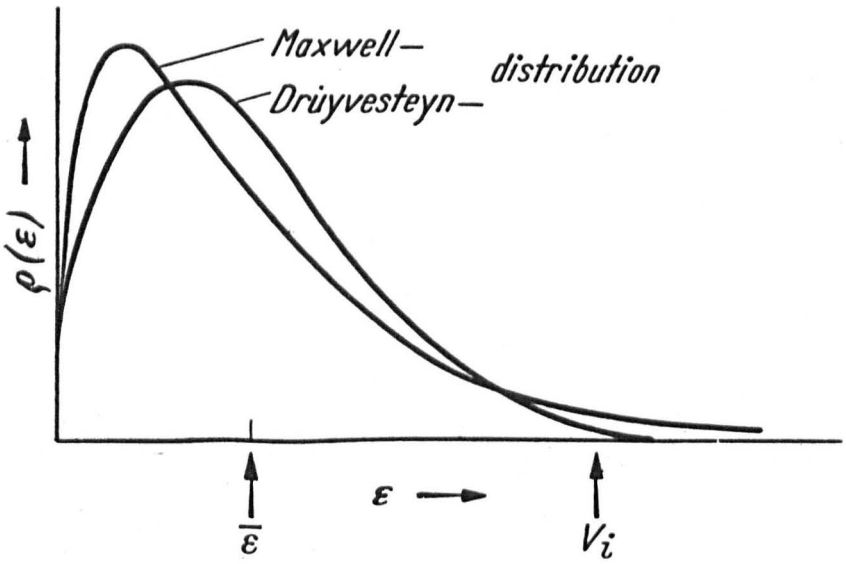

Electron energy distribution ϱ as a function of the energy ε for the same mean energy $\bar{\varepsilon}$ and the same number of electrons (the same area covered by the curve).

MAXWELL distribution: $\varrho(\varepsilon) = C' \varepsilon^{\frac{1}{2}} - \frac{\varepsilon}{\bar{\varepsilon}}$;

DRUYVESTEYN distribution: $\varrho(\varepsilon) = C \varepsilon^{\frac{1}{2}} e^{-0.55\left(\frac{\varepsilon}{\bar{\varepsilon}}\right)^2}$

fig.2

The form of the distribution is shown in fig.(2) and is compared with Maxwell-Boltzmann distribution for the same number of electrons. Although the equation does not predict a maximum energy, it can be seen that the curve approaches the energy axis more quickly than the Maxwellian, and has a smaller number of electrons with high energies compared to the large number of electrons with small and medium energies.

So, any increase of the parameter E/p will be followed by an increase in the mean electron energy together with an increase in the number of electrons in the high energy tail. Eventually energy will be lost by electrons to vibrational and rotational states of the gas molecules and to molecular dissociation, and the electrons in the high energy tail will be able to raise the atoms to excited states above the ground state with a corresponding loss of a large fraction of their energies. Further increase of the parameter E/p provides the electrons with energies sufficient to cause ionization of gas atoms and thus causes further loss of their energies. Therefore, at very low mean electron energy the Druyevesteyn distribution will hardly change due to elastic collisions. But as the mean electron energy increases (i.e. as E/p increases) the electrons will start losing a large proportion of their energies in inelastic collisions and there will be also a change in their mean free paths (Ramsauer's effect (4)). Under these circumstances, the conditions laid down by Druyvesteyn in his derivation of the energy distribution function are not upheld.

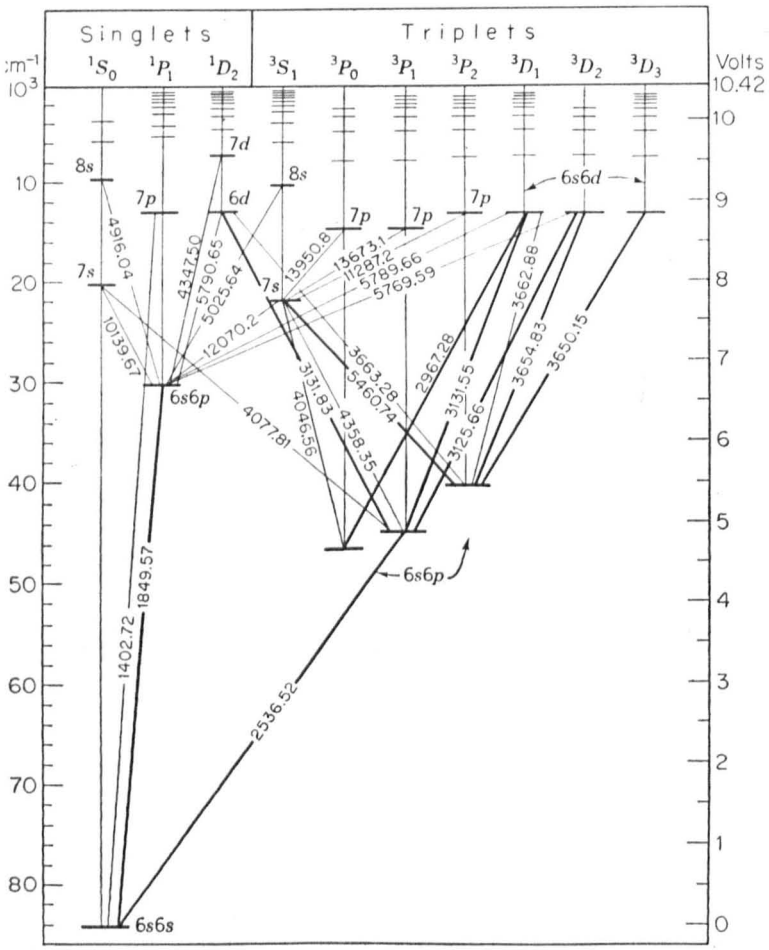

The most important energy levels and spectral lines for the neutral mercury atom.

fig.3

Probably the effect of these inelastic collisions is to decrease the number of electrons in the high energy tail. Now the two most important inelastic collisions by electrons (excitation and ionization) will be discussed in more detail.

1.3 EXCITATION BY ELECTRONS

An atom is said to be excited when an electron is lifted from the ground level to a higher energy level. The most important energy levels and spectral lines of the neutral mercury atom are shown in fig.(3). The probability of excitation to a certain energy level is often called the "excitation function", defined as the number of electron collisions leading to the required transition, divided by the total number of collisions per electron. This probability is, in general, of the order or smaller than 10^{-2}. The reason for such low probability is, that, two conditions must be satisfied before an electron can excite an atom.

a) The energy of the electron must exceed the excitation potential of the atom for the particular level under consideration.

b) Linear and angular momentum about the common centre of mass must be conserved.

Thus the change in the angular momentum of the system, δp , during the collision must balance the difference in the angular momentum of the atom in its initial and final state.

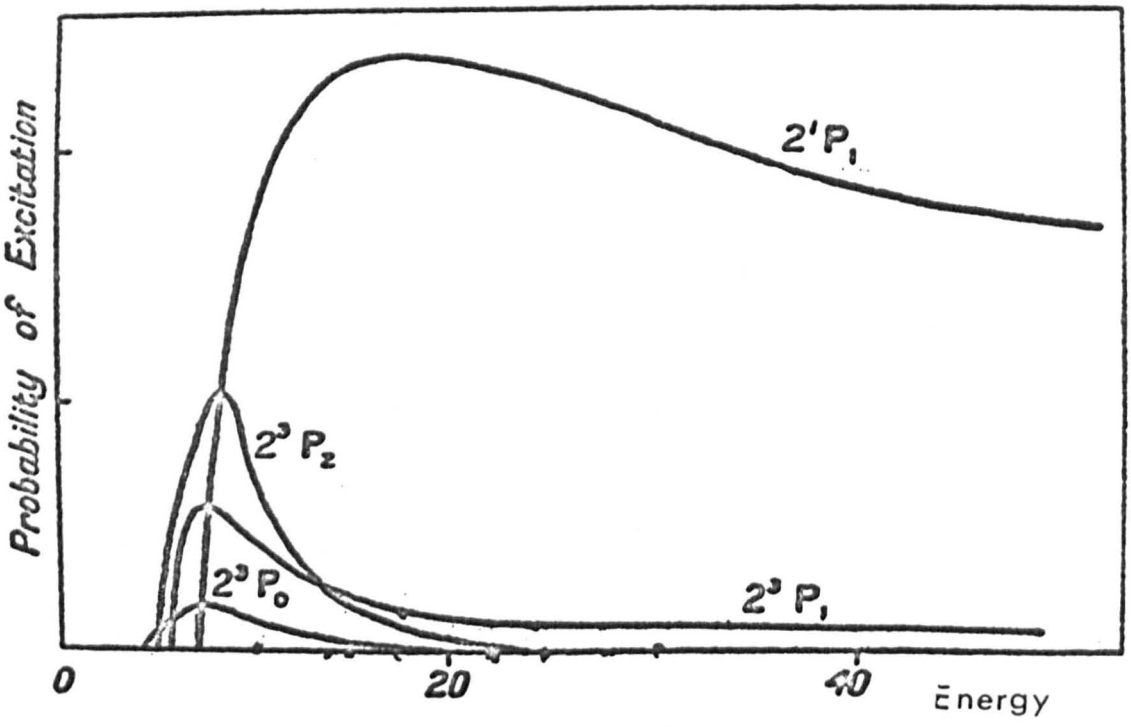

Excitation Funetions P States Hg

fig.4

Hence

$$\delta p = \frac{h}{2\pi} \quad \delta j \qquad 1.1$$

where $\delta j = L + S$, δj is the change in the inner quantum number.

L and S are the orbital and spin quantum numbers respectively. It follows from condition (b), that if an electron carries the exact energy necessary to excite an atom, it will be stationary after the collision and it has to hit precisely at the right angle to satisfy equation (1.1). Since only a negligible number of electrons fulfil this condition, therefore the excitation probability would be expected to be zero at the critical excitation potential of a certain state. On the other hand, it would be expected that the probability of excitation to increase as the electron energy exceeds the critical potential, as the electron itself can carry away the excess energy in a direction which satisfies the angular momentum condition. This can be seen clearly from the excitation functions of the four P states of mercury shown in fig.(4), as calculated by Penny (5).

The transitions $6^1S_o \rightarrow 6^1P_1$ (singlet-singlet) and $6^1S_o \rightarrow 6^3P_1$ (singlet-triplet) might have been expected to have roughly the same excitation function as each one of them has $\delta j = 1$, but as it can be seen from fig.(4), the singlet-singlet state has a large excitation function and broad maxima. On the other hand

the singlet-triplet state has a low excitation function and very sharp maxima. The reason for this difference as given by Francis(6) is that in singlet-singlet transition, the total spin quantum number S is unchanged and thus the spins of the two valency electrons are unchanged. In singlet-triplet transition, S changes from 0 to 1 and hence one of the electrons must have its spin vector reversed. For elements with strong spin-orbit coupling like Hg this can be brought about by electron impact. For elements with weak coupling like He, the reverse of the spin vector can occur only when the impact electron itself is captured by the atom and one valence electron is expelled. This electron change can occur only in a narrow energy range and, therefore, the excitation function has a sharper maxima than for Hg. Such necessary conditions are not attached to singlet-singlet transition nor to atoms with one valence electron (e.g. C_s atoms) and therefore the maxima is broad.

When the atom is excited to a higher energy state, it may in most circumstances, remain in this state for about 10^{-8} seconds before it returns (directly or via other states) to the ground state, such state is called resonance state (or normal state) and the subsequent emitted radiation is called resonance radiation. However, it may be excited into a state from which it cannot fall spontaneously, or at least the probability of such a transition is extremely small. Such a state is called a metastable state and the transition from this state to the ground state would break the

selection rules (which are $\delta L = \pm 1$ and $\delta j = \pm 1$ or o and not from j = o to j = o). It follows that the probability of the reverse process, excitation into metastable state from the ground state is very small or nearly equal to zero. Metastable states have a mean life-time of about 10^{-2} secs., but in most discharge conditions they are destroyed within this time either through collisions with ground states atoms and with discharge tube wall or by further excitation to normal excited states usually by absorption of light quanta. Metastable states are usually found among the lower energy levels since there are few lower levels into which the electrons can fall. Metastable states can be filled also by collisions of atoms in resonance states with atoms in the ground states. For example, in mercury discharge the metastable state 6^3P_o can be produced in a collision between an atom in the state 6^3P_1 and an atom in the ground state 6^3S_o (7) as follows

$$Hg(6^3P_1) + Hg(6^1S_o) \rightarrow Hg(6^3P_o) + Hg\ 6^1S_o) + \Delta$$

Due to the relatively long life of atoms in metastable states, they can play a very important part in gas discharges by releasing secondary electrons from the cathode as will be seen in section (1.8.6).

1.4 IONIZATION BY ELECTRONS.

Ionization of an atom by electron can be regarded as an extreme form of excitation, in which the electron is removed to

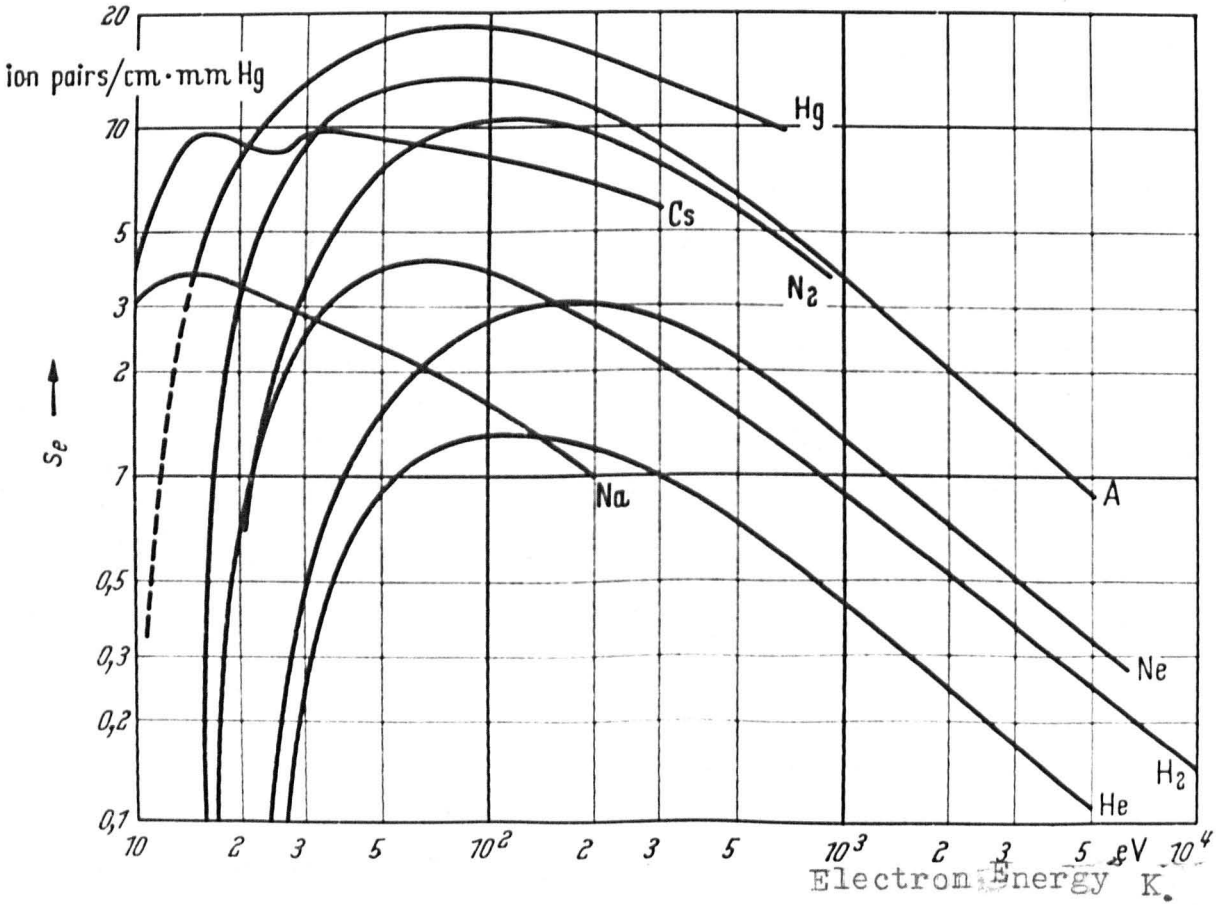

Measured values ofthe ionization efficiency Se as a function of the primary electron energy K.

fig.5

infinity. For an electron to do that its energy must exceed the ionization potential of the atom. Thus as we increase the parameter E/p, the mean electron energy will be increased, therefore electrons in the high energy tail of the distribution will not only be capable of exciting the gas atoms but also of producing singly charged positive ions; and with a further increase in energy the possibility of production of multiply charged ions arises.

The ionization efficiency, S_e is, usually, defined as the number of ion pairs produced by one electron moving 1 cm. through the gas at a pressure 1 mm. Hg and 0 °C fig. (5) shows measured values of the ionization efficiency S_e, as a function of the primary electron energy K for various gases and vapours. Efficiency of ionization is zero for electron energy equal to the ionization potential of the gas atom. The maxima of S_e lies for the majority of gases between about 80 & 120 e V. (with the exception of the alkali vapours whose maxima is between 15 and 30 eV.) and the corresponding values of S_e lie between 1 & 20 ions/ cm.
It can be seen from fig. (5) that the rule that the ionization efficiency is larger for lower ionization potentials is not generally applicable.

So far it has been assumed that electrons collide with atoms in the ground state. A gas which has been previously ionized usually contains a considerable number of excited atoms and a large number of slow electrons. Ionization can then be produced by a

relatively slow electron of energy E_s, in collision with an atom which has been previously raised to an excited state E_e,

$$E_s > E_i - E_e$$

where E_i is the ionization potential of the atom. An important case arises when E_e is a metastable level E_m, since the chance of a collision is greater than for a resonance level, due to their relatively long life. The rate of ionization by this process is proportional to the square of the current passing through the discharge.

1.5 THE TOWNSEND FIRST IONIZATION COEFFICIENT.

The quantities outlined above are determined from experiments in which mono-energetic beams of electrons are used. Hence the probability of ionization or the ionization efficiency S_e cannot be directly related to gas discharge conditions, unless the electron energy distribution is known. As it has been seen before it is the value of the ratio E/p which determines the mean energy of electron swarm moving through a gas. If the value of E/p is changed, then not only will the electron energy distribution be modified but the possibility arises of a change in the probabilities of excitation and ionization due to the change in the number of electrons in the high energy tail of the distribution.

It is possible, however, to define a coefficient α, similar to the ionization efficiency S_e under gas discharge conditions, as follows:

If we consider n electrons moving through a gas at a pressure p under the influence of a uniform electric field E between two plane-parallel electrodes, then the number of ion pairs dn produced by these electrons in a distance dx will be proportional to n and dx, thus

$$dn = \text{constant } ndx$$

or

$$dn = \alpha ndx \qquad 1.2$$

where the constant α is the electron multiplication factor and is known as the Townsend First Ionization Coefficient or the primary ionization coefficient.

If N_o electrons per second originate from the cathode , x=o,

and the inter-electrode separation is d cm., then the number N_d of electrons per sec., which will appear at the anode, x = d, can be found by integrating equation (1.5.1) as follows

$$\int_{N_o}^{N_d} \frac{dn}{n} = \int_o^d \alpha \, dx$$

or $$N_d = N_o \, e^{\alpha d}$$

which in terms of current can be expressed as (1),

$$I = I_o \, e^{\alpha d} \qquad 1.3$$

where the constant I_o is the photo electric current which is usually provided by external irradiation of the cathode. The factor α is defined as the average number of ion pairs produced from ionizing collisions in the gas per primary electron advancing one centimetre in the direction of the applied field. As α is expected to change with the electron energy, it is usually measured at a constant E/p. The photo-electrons must advance a distance do before they acquire a constant mean energy and the ionization process becomes steady (9). Equation (1.3) must therefore be altered to

$$I = I_o \, e^{\alpha(d-do)} \qquad 1.4$$

It is assumed in the above derivation that the field is uniform, therefore the current density should be so small that space charge does

not disturb the field. The currents involved in these experiments are usually in the range 10^{-13} to 10^{-8} A(10). A coefficient η analogous to α can be defined as the average number of ion-pairs produced by an electron falling through a potential difference of one volt. The current equation can be written in this case as

$$I = I_o \, e^{\eta(V - V_o)} \qquad 1.5$$

where V_o is a correction factor corresponding to d_o. From their definitions, the coefficient η can be related to α by

$$\eta = \frac{\alpha}{E} \qquad 1.6$$

In practice, either d or v can be treated as the independent variable and α or η can be found from the slope of the curve of log I against d or V respectively at different values of the ratio E/p.
Since the controlling factor in ionization by collision is the average energy an electron has gained along a mean free path in the field direction therefore α is expected to be a function of the pressure at a certain value of E/p, or

$$\alpha/p = f(E/p).$$

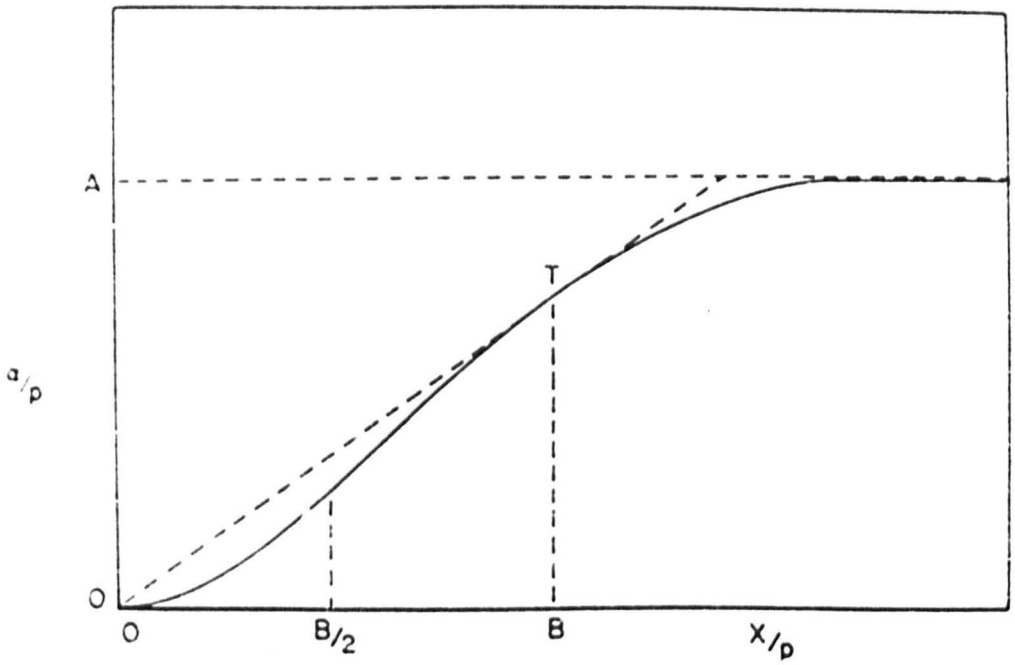

Characteristic curve for a/p, plotted against X/p

fig.6

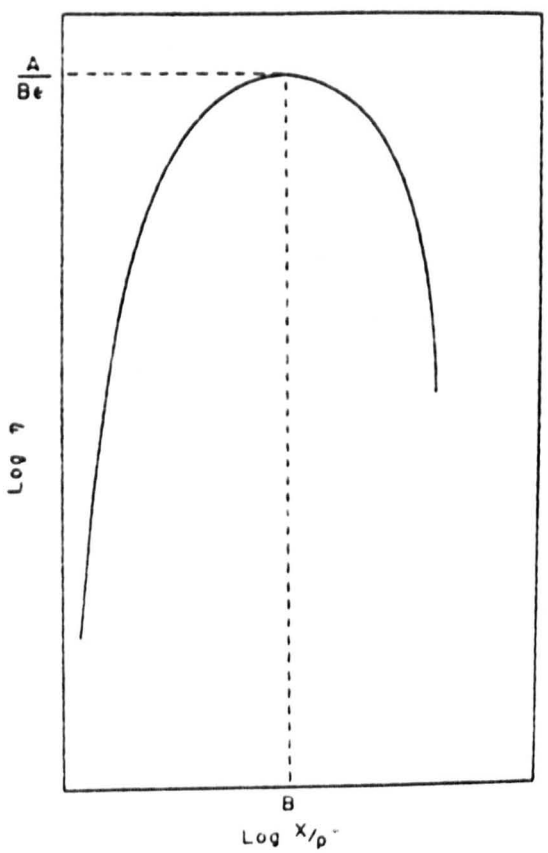

Characteristic curve for $\log \eta = \log (a \cdot V)$ against $\log X/p$.

fig.7

1.6 THE EVALUATION OF α/p AS A FUNCTION OF E/p.

One of the earliest attempts to relate α to the fundamental atomic properties was made by Townsend(1). His theory assumes that the field is so strong that electrons always travel in the direction of the field and the probability of ionization is zero for energies less than the ionization energy, eV_i, and is unity for energies equal or greater than eV_i, i.e. $eE\,\lambda_i \geq eV_i$ where E is the strength of the applied electric field, λ is the electron mean free path and V_i is the ionization potential.

On this assumption Townsend derived the relation

$$\alpha/p = \frac{1}{\eta_i}\, e^{-V_i/\lambda_i E/p}$$

or

$$\alpha/p = A\, e^{-Bp/E} \qquad 1.7$$

where $B = V_i/\lambda_i$ $A = \frac{1}{\lambda_i}$ (λ_i is the mean free path an electron must travel before it is capable of ionizing an atom). A typical plot of the function (1.7) is shown in fig.(6) which is characterised by an elongated letter S shape. In terms of η the relation is

$$\eta = \frac{\alpha}{E} = \frac{A}{E}\, p\, e^{-Bp/E} \qquad 1.8$$

fig.(7) shows a plot of the quantity η, rising steeply at low E/p,

reaching a maximum of $\eta - A/Be$ at E/p = B (Stoletow point of maximum ionization efficiency (8)) and then declining again. The peak of the η versus E/p curve fixes the minimum point on the Paschen curve (see section 1. 9). By suitable choice of the constants A and B, Townsend's theory could only be made to give reasonable agreement with the experiment over a limited range of E/p.

In a more recent theoretical calculation, Emeleus, Lunt and Meek (11) derived an expression for α/p, which allows the insertion of the appropriate velocity distribution and the experimentally determined values of ionization probabilities and electron drift velocities.

The expression of α/p is given by

$$\alpha/p = P/v \int_{c_i}^{\infty} c.P_i(c).\ f(c).\ dc \qquad 1.9$$

where c is the mean velocity of the electron

c_i is the velocity an electron must attain before being capable of ionizing gas atoms.

v is the mean drift velocity of the electron in the direction of the applied field.

f(c) is the velocity distribution function.

p(c) is the probability of ionization per cm. at pressure of 1 mm.Hg.

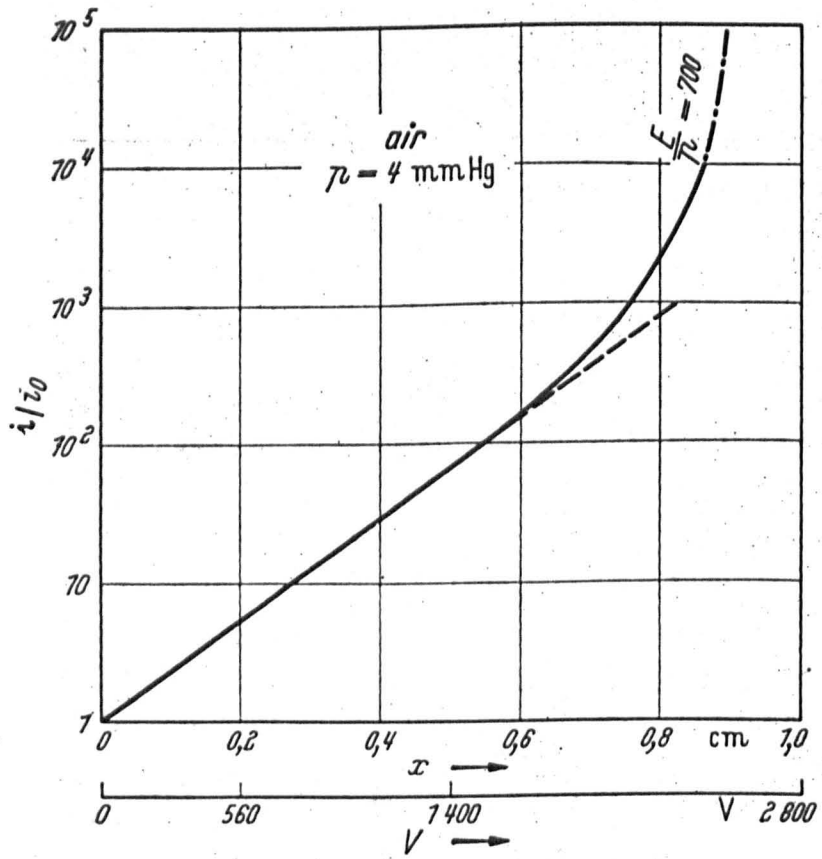

Multiplication i/i_0 as a function of the electrode spacing d or the applied voltage V at a constant and high value of E/p (700 V/cm. mm. Hg) in air at 4 mm. Hg.

fig.8

Assuming a Maxwellian distribution, good agreement between experiment and theory was found for the diatomic gases, air, nitrogen, hydrogen and oxygen, however the agreement was bad for argon.
As it can be seen, until the energy distribution and more precise measurements of ionization probability are known, Emeleus, Lunt and Meek theory would not meet any wide application.

1.7 THE CURRENT EQUATION AT LARGE VALUES OF ELECTRODE SEPARATION.

Fig. (8) shows a plot of log I/I_o as a function of d in air at a pressure 4 mm.Hg. and E/p = 700 volts/am.mm.Hg. At small values of d, the curve is practically a straight line as predicted by equation (1.4). At larger values of d however, the curve seems to increase faster than linearly, finally becoming vertical at $d = d_s$. At this distance d_s a breakdown occurs (characterised by a spark) and the current seems to increase without a limit.

The explanation for the deviation of the graph from a straight line is that at larger electrode distance the electrons which are released from the cathode consists of two groups, the primary ones which are liberated from the cathode (by external irradiation) forming a current I_o and secondary electrons which must originate from agents created by the primary electron avalanche.

Under these conditions, equation (1.4) must be modified(to represent the variation of current at large values of d) as follows

$$I = \frac{Io \quad e^{\alpha(d-d_o)}}{1 - \frac{\omega}{\alpha}\left(e^{\alpha(d-d_o)} - 1\right)} \qquad 1.10$$

where ω/α is known as the generalised secondary ionization coefficient or Townsend second ionization coefficient and is a function of E/p. ω/α describe all the processes leading to secondary electron production and it can be defined as the average number of secondary electrons produced per ionizing collision in the gas.

1.8 POSSIBLE SECONDARY PROCESSES.

1.8.1 INTRODUCTION.

In Townsend discharge there are three possible sources of secondary electron production. These are (1) positive ions, (2) photons, and (3) normal excited and metastable atoms. Each of these can, under suitable conditions, be capable of ionization in the gas or electron emission from the cathode surface. These secondary processes will now be discussed in more detail.

1.8.2 IONIZATION OF THE GAS BY POSITIVE ION COLLISION.

According to the classical treatment the ion loses half of its energy in collision with the gas atom. Thus an ion will be capable of ionizing an atom on collision if its energy is greater than $2eV_i$, where V_i is the ionization potential of the atom (12). In early experimental measurements, Varney (13) has indicated that positive ion energies greater than 300 eV were necessary before any ionization could

even be detected. Recently, however, Horton and Millest (14) have shown that ionization of neutral helium atoms could occur at energies greater than 49.4 eV which is at about the theoretical minimum potential of $2V_i$ (ionization potential of helium is 24.7V). However it has been shown (14) that the energy of positive ions differs little from that of the gas atoms even up to moderate values of E/p. The energy of the gas atoms at ordinary temperatures is only a fraction of $2eV_i$ for any gas and therefore it is unlikely that this process of secondary electron production is important for the values of E/p used in most gas discharge measurements.

1.8.3. IONIZATION BY NORMAL EXCITED ATOMS AND METASTABLE ATOMS COLLISIONS.

In pure gases, collisions between excited atoms and those in the ground states cannot lead to ionization, since the ionization energy is greater than the excitation energy. This process of ionization can be of considerable importance in a gas mixture where the excitation potential of one gas is higher than the ionization potential of the other. The cross-section of such a process can be very large when the excited atom is in a metastable state. Penning and Addink(15) have shown that small amounts of argon in neon have considerable effect on the conductivity of neon which they referred to the presence of metastable neon atoms whose excitation potential (16.55V) exceeds the ionization potential of argon (15.68 V). This shows the necessity, when in experiments in pure gases with low ionization potential (like C_s and Hg), to achieve low ultimate air pressures to remove all the oxygen and nitrogen which possess high energy metastable states. When two excited atoms collide

atomic and molecular ions can be produced if the sum of the excitation energies is greater than the ionization energy. The process is most efficient at high pressures and at high current densities where the excited atoms have a high density and especially when the excited atoms are in metastable states.

1.8.4. PHOTO-IONIZATION OF THE GAS.

Since radiation is a form of energy, a photon may excite or may ionize an atom if it has the right amount of energy corresponding to the atomic energy state in question. Thus, an atom in the ground state can only be ionized by a photon of frequency ν if

$$h\nu \geq eV_i \qquad 1.11$$

where V_i is the ionization potential and h is Plank's constant. The process is most efficient when the photon gives up the whole of its energy to the atom, that is, when $h\nu = eV_i$. [redacted]. Photo-ionization by a cumulative process has been observed in caesium vapour (16) and in mercury vapour by Rouse and Giddings (17) when they discovered that mercury vapour is ionized by absorption of resonance radiation (2537A^{o}). Houtermans (7) has shown later that during irradiation of mercury vapour, metastable atoms Hg (^{3}Po) are formed by collisions of resonance atoms, Hg($3P_1$), with atoms in the ground state, Hg($^{1}S_{o}$) according to the

reaction $Hg\ (^3P_1) + Hg\ (^1S_o) \rightarrow Hg(^3P_o) + Hg(^1So) + \Delta$

where $\Delta = 0.218$ eV is the energy difference between the $^3P_1$ and ^3P_o states which is converted into kinetic energy of the Hg atoms. From experiments with quenching gases Houtermans deduced that collisions between atoms in the $^3P_1$ and ^3P_o states produce positive molecular Hg ions and electrons

$$Hg\ (^3P_1) + Hg\ (^3P_o) \rightarrow Hg_2^* \rightarrow Hg_2^+ + e \qquad 1.12$$

where Hg_2^* is a temporary molecule in an excited state.

The process satisfies conservation of energy since the ionization potential of the Hg_2 molecule is approximately 9.6 V_i the excitation potentials of the $Hg(^3P_o)$ and the $Hg\ (^3P_1)$ atoms are 4.66 and 4.86V respectively and the heat of dissociation of 0.06eV as well as the kinetic energy has to be included in the formation of the molecule.

Recently Tan and Von-Engel (18) found that the associative ionization cross-section of reaction (1.12) of the order 5×10^{-14} cm.^{2} and the cross-section for the reverse process, dissociative recombination into excited atoms, to be the same order as the forward process. Due to the high dissociative recombination cross-section and the small concentration of the state ^3P_o and the low excitation probability to the state ^3P_o the cumulative ionization is unlikely to be important in mercury discharge at low pressure and small current.

Photo-ionization can also occur by stepwise process when a photon (of energy $h\nu < E_i$) gets absorbed by an atom which has been previously excited to normal or metastable state, provided

$$h\nu \geq E_i - E_e, (E_m)$$

where E_i is the ionization energy, E_e and E_m are the excitation energies of the normal and metastable states respectively. The process can be very effective at high concentration of excited state, which is again likely at high gas pressures and high discharge current. Photo-ionization, however, can be very important in gas mixtures when the resonance radiation of one type of atom has energy greater than or equal to the ionization energy of the second type. The process has been used by Loeb and Meek (19) and Reather (20) to explain the streamer mechanism.

In brief, therefore, the contribution of the gaseous secondary processes to ω/α is negligible except possibly at high pressures. In gas mixtures, however, the effects can be quite important.

1.8.5 ELECTRON EMISSION FROM THE CATHODE BY POSITIVE IONS.

When a positive ion approaches a cathode surface (solid or liquid) it may be reflected as positive or negative ion; reflected as an unexcited or excited atom, cause sputtering of the surface; or cause electrons to be emitted (a) due to the kinetic energy given up on impact, and (b) due to its potential energy (21).

The emission of electrons from a cathode surface due to the

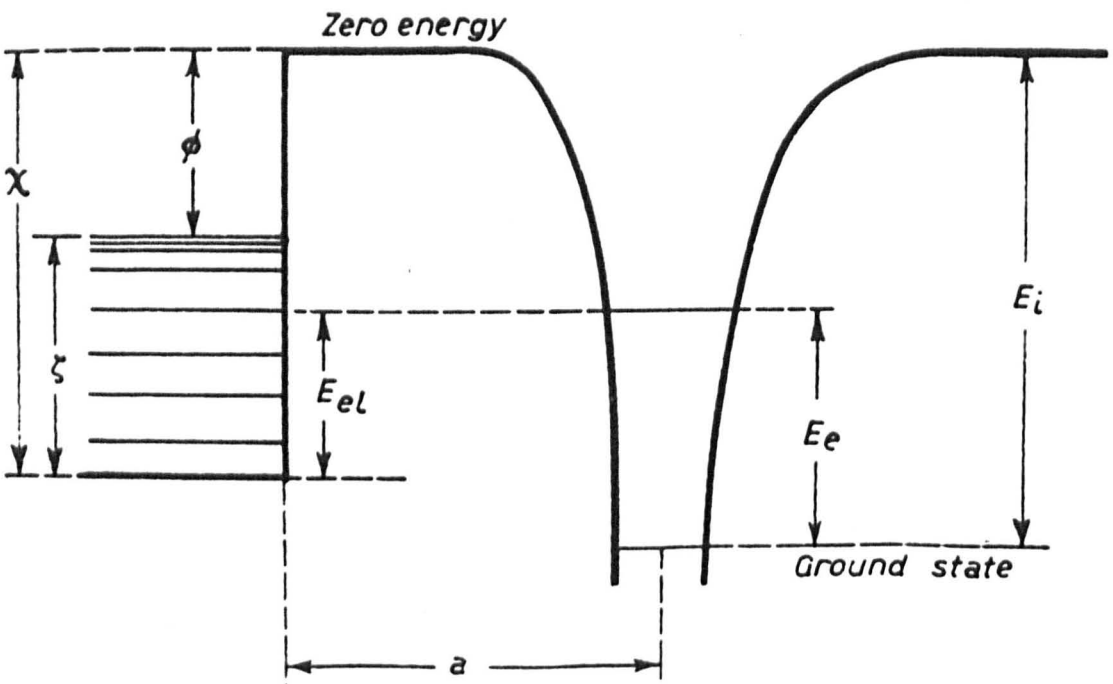

Energy diagram of a positive ion near a metal

ϕ, work function of the metal E_{ep}, occupied level in the metal E_e, Unoccupied level in the ion. E_i ionization potential of the ion ψ, the maximum depth of the fermi level in electron volt. a, the distance between the ion and the metal.

Fig. 9

incidence of high energy positive ions is thought to be a thermionic effect due to intense local heating of the cathode at the point of impact (22). This is supported by the fact that the energy distribution of the ejected electrons is that which would be expected from thermoicnic emission (23).

For low energy positive ions, electron emission can be caused by two mechanisms which are independent of the kinetic energy of the ion and dependent only on its potential energy. The first is a two-step process, in which the positive ion captures an electron from the conduction band of the metal into a level of equal energy in the ion as long as such a level is unoccupied fig.(9). If an excited atom is formed, the transition is most likely to occur when, $\phi = E_i - E_e$

where ϕ = work function of the metal

E_i = ionization energy of the gas atom

E_e = excitation energy of the gas atom.

In most cases the excited atom collides with the cathode surface within a ~~the~~ short time that radiation does not occur. It is most likely that in the second step, the excited atom gives up its energy to the cathode and there is subsequent emission of another electron from the metal. The condition for the second step is that the energy of the final ejected electron $E = E_e - \phi$

$$\therefore \quad E = E_i - 2\phi$$

Hence if $E_i > 2\phi$ and $E_e > \phi$ an electron may be emitted by this mechanism.

The second alternative mechanism is also possible if the positive ion can penetrate the potential barrier before capturing an electron. In this process two electrons are involved at the same time, one being captured by the ion and the other being emitted. From the above discussions it can be seen that the electron emission by positive ions at moderate values of E/p is dependent not only on the energy of the ions but also on the work function of the cathode and hence on the cathode surface conditions.

1.8.6. ELECTRON EMISSION FROM THE CATHODE BY EXCITED ATOMS.

Excited atoms, in general, can liberate electrons on collision with the cathode surface provided that $E_e \geq \phi$, where E_e is the excitation energy and ϕ is the work function of the cathode. Under gas discharge conditions, normal excited atoms return to the ground state, within a time of about 10^{-8} secs., thus there is little or no chance for these atoms to diffuse to the cathode and cause an electron emission. However due to the relative long lifetime of a metastable atom, it can diffuse to the cathode and liberate an electron with energy $E \leq E_m - \phi$ where E_m is the excitation energy of the metastable atom. Since metastable atoms are uncharged, and most of them formed near the anode, only a fraction of them will diffuse to the cathode. The number of those diffusing to the cathode, will depend on the electrodes separation (d) as well as on the electrodes diameter (D). Assuming infinitely plane parallel electrodes, Newton (24) has shown that the electron emission coefficient, Y_m per metastable atoms formed

in the gas as,

$$Y_m = \text{Constant } (N + \frac{1}{\alpha d})$$

where N is the mean free path of metastables moving in a gas of normal atoms. Thus Y_m falls as d increases even if the electrodes are to be of infinite diameters. With electrodes of finite dimensions, Y_m is likely to be reduced further by diffusion of metastable from the discharge volume as shown by Molnar (25).

However the yield or average number of electrons produced per incident metastable atom can be quite high (26).

e.g. 10^{-2} for Hg metastable atoms on Hg

0.4 for A metastable atoms on C_s

1.8.7 PHOTO-ELECTRIC EMISSION FROM THE CATHODE.

Light quanta produced in gas discharge are of two main types : resonance radiation, resulting from the decay of normal excited atoms or metastable atoms that have been raised to some higher excited states, and non-resonance radiation as the result of a collision which sufficiently perturbs the metastable state to give rise to radiation by breaking the selection rules. The resultant photons will be capable of emitting electrons from the cathode surface if, $h\nu \geq \phi$

where ν is the frequency of the radiation and h is the plank's constant.

Not all of the photons produced in the gas succeed in striking the cathode. The number of photons reaching the cathode will depend on the gap geometry and also on the absorption coefficient of the photons in the gas; however, only a fraction of the incident photons will get absorbed by the cathode and cause emission of electrons from the metal, which escape into the gas (27). The photo-electric efficiency depends on the nature and state of the cathode surface (i.e. on the work function) and on the energy of the incident radiation. The efficiency generally increases with the increase in the energy of the incident radiation up to a maximum value and then begins to fall due to the fact that the more energetic radiation will emit electrons at greater depth in the metal and only few of these will be able to escape from the surface. The efficiency depends also on the angle of the incidence and on the polarization of the incident radiation. Many measurements have been carried out to investigate this effect using monochromatic radiation and prepared surfaces, but it is not fruitful to attempt to compare these conditions with those which exist in gas discharge where a range of photon energies are incident on a cathode surface whose work function is difficult to specify. The contribution of the photo-electric emission is expected to be high at low values of E/p, where photons are produced in great

number due to the high efficiency of excitation.

1.8.8. SUMMARY OF THE SECONDARY IONIZATION PROCESSES.

Each secondary process mentioned in the above sections can be represented by an ionization coefficient which is average number of electrons contributed by that process per primary ionizing collision in the gas. If all or some of these processes are taking part in the secondary ionization, then the generalised secondary ionization coefficient ω/α will be the sum of the individual coefficients (9). At low values of pressure and moderate values of E, it is the cathodic processes which are important. It is to be expected therefore that in a mercury discharge the action of metastable atoms, photons and positive ions at the cathode will constitute the major source of secondary electrons.

1.9 BREAKDOWN CRITERION IN UNIFORM FIELD.

From fig. (8) it can be seen that at a small inter-electrode distance d, the current I is dependent on I_o. Thus if the photo-current I_o is cut off, then the current I will cease to zero. However as d is increased to a sufficiently large value d_s, the slope of the graph becomes infinite and the current, I, flowing through the gap is limited only by the external circuit, and breakdown occurs. The physical significance of this phenomenon is that the current I in the gap is no longer a function of I_o. In other words, the current has

become self-maintained and will continue to flow even if the current I_o is reduced to zero. It can be seen from equation (1.10) that for the current to be finite when I_o is made equal to zero, the denominator must become zero.

Hence, $1 - (\omega/\alpha)_s \left[e^{\alpha(d_s - d_o)} - 1 \right] = o$ at constant E/p 1.13

Townsend used this criterion for a self-maintained discharge (or for breakdown). For any value of the sparking distance d_s in the equation there is a corresponding value of $(\omega/\alpha)_s$

In terms of η the breakdown criterion is

$$1 - (\omega/\alpha)_s \left[e^{\eta (V_s - V_o)} - 1 \right] = o \text{ at constant E/p} \qquad 1.14$$

where V_s is the breakdown potential and is defined as the minimum voltage required for a very small current to flow between the electrodes without the assistance of any external agency capable of producing electrons in the gas or at the cathode.

The term $e^{\eta V_s}$ is much greater than unity and hence the breakdown voltage can be represented by

$$V_s = (- \log \omega/\alpha)/\eta \qquad 1.15$$

Since ω/α is involved criterion (1.15), then the sparking potential will depend not only on the gas but also on the nature and condition of the cathode, since ω/α is dependent on the work function of the cathode. Thus high sparking potentials will be associated with low values of ω/α (or high values of ϕ), and low sparking potentials will be associated with high values of ω/α (or low values of ϕ).

Since α/p (or η) and ω/α are functions of E/p ($=V_s/P_{d_s}$),

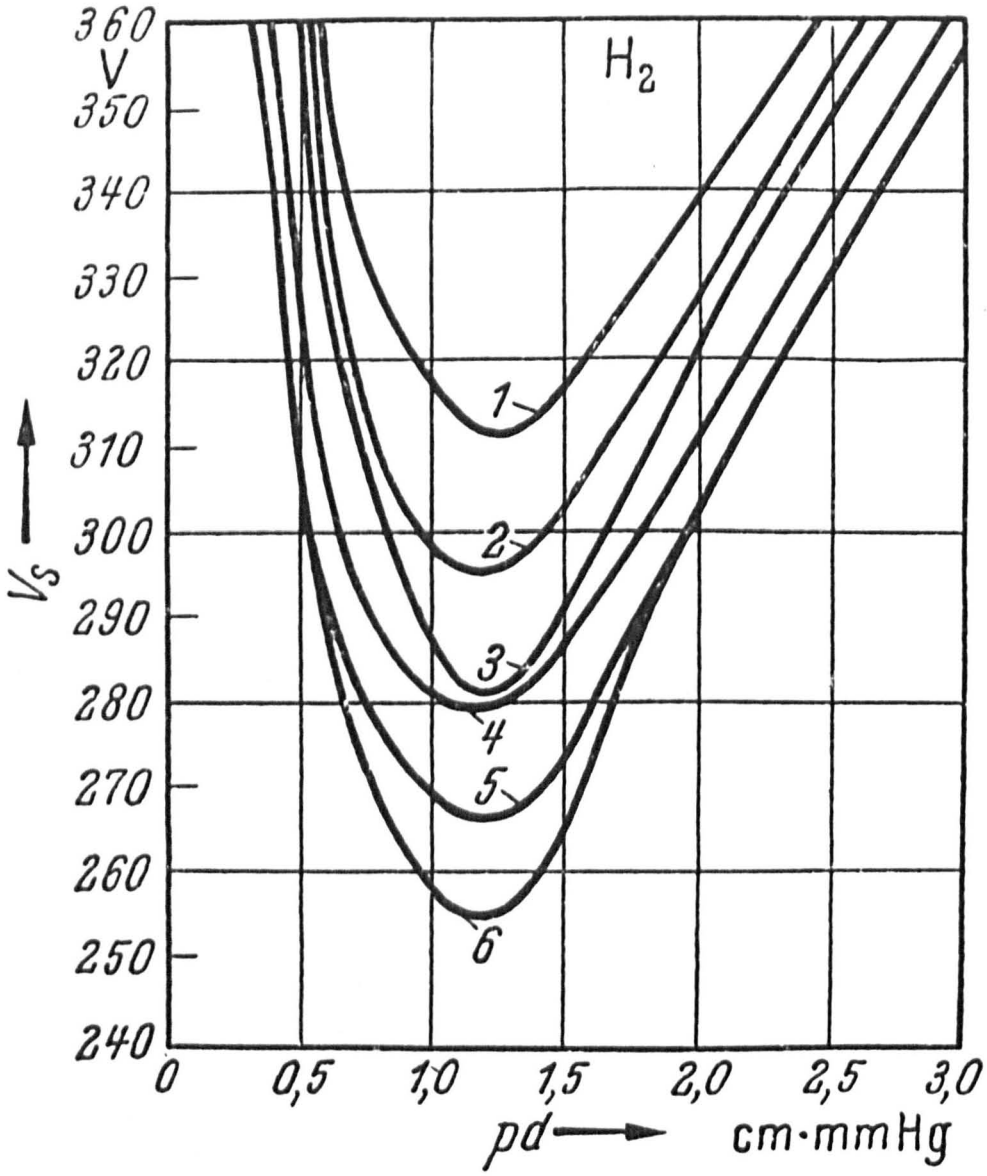

Breakdown voltage V_s as a function of $p\,d$ for various cathodes on hydrogen: *1* Steel cathode, *2* copper, *3* oxidised steel, *4* nickel, *5* pure aluminium, *6* commercial aluminium.

fig.10

it can be shown (28) V_s is a function of the product pd_s only for a given gas and a given cathode and this is known as Paschen's law. Typical Paschen curves in hydrogen are shown in fig. (10) for different cathode materials from which can be clearly seen the effect of the work functions of different cathode materials on the sparking potential (breakdown potential).

It is important to remember that the derivation of Paschen's law assumes that ω/α is a function of E/p only. If ω/α is a function of p or d_s then Paschen's law will not be obeyed, that is for a given gas and a given cathode, V_s will not be a function of pd_s only but will also depend on the indivudal values of pressure p and the electrode separation d_s. Such deviation will result if either non-uniform field conditions arise or if photons and excited atoms are lost from the discharge volume. Deviation from Paschen's law was observed by Overton (29) in mercury discharge where metastable atoms and photons are important sources as secondary ionization processes.

1.10 DISTINGUISHING SECONDARY IONIZATION PROCESSES IN GAS DISCHARGE

A decision as to the relative importance of the secondary processes cannot be provided by considering the current growth curves since each process leads to an equation of the same analytical form as the general Townsend formula (1.10), with ω/α being a composite coefficient depending on which combination of secondary processes is operative. However, consideration of the variation of the generalised

secondary coefficient ω/α with E/p can sometimes provide some indirect information on the nature of the secondary mechanisms. For example secondary emission due to the impact of positive ions on the cathode is mainly due to the potential energy of the positive ions. As the potential energy does not depend on E/p, it is to be expected that ω/α would not change greatly other than to show a small increase as E/p increases if the positive ions action at the cathode is dominant. Photo-emission can sometimes be recognised from sharp peaks in the curve of ω/α against E/p. These peaks usually exist, at low values of E/p, as the concentration of the number of photons increases due to the increase in the ratio of the excitation to ionization collisions in the gas.

Secondary mechanisms can be distinguished more easily if the time taken for a gap to break down is compared to the time taken for a different species to reach the cathode. For instance if photo-emission is dominant, the time taken will depend on the lifetime of the excited states, the point of origin and the nature of the photons. In the case of unscattered photons a time of the order 10^{-6} sec. will be expected which is negligible compared to the time taken for the positive ions to drift to the cathode = 10^{-5} sec. Diffusion of metastable atoms to the cathode involves a delay time of the order 10^{-3} sec. The total time taken for the breakdown of a gap to take place after the application of the breakdown voltage is the sum of the statistical

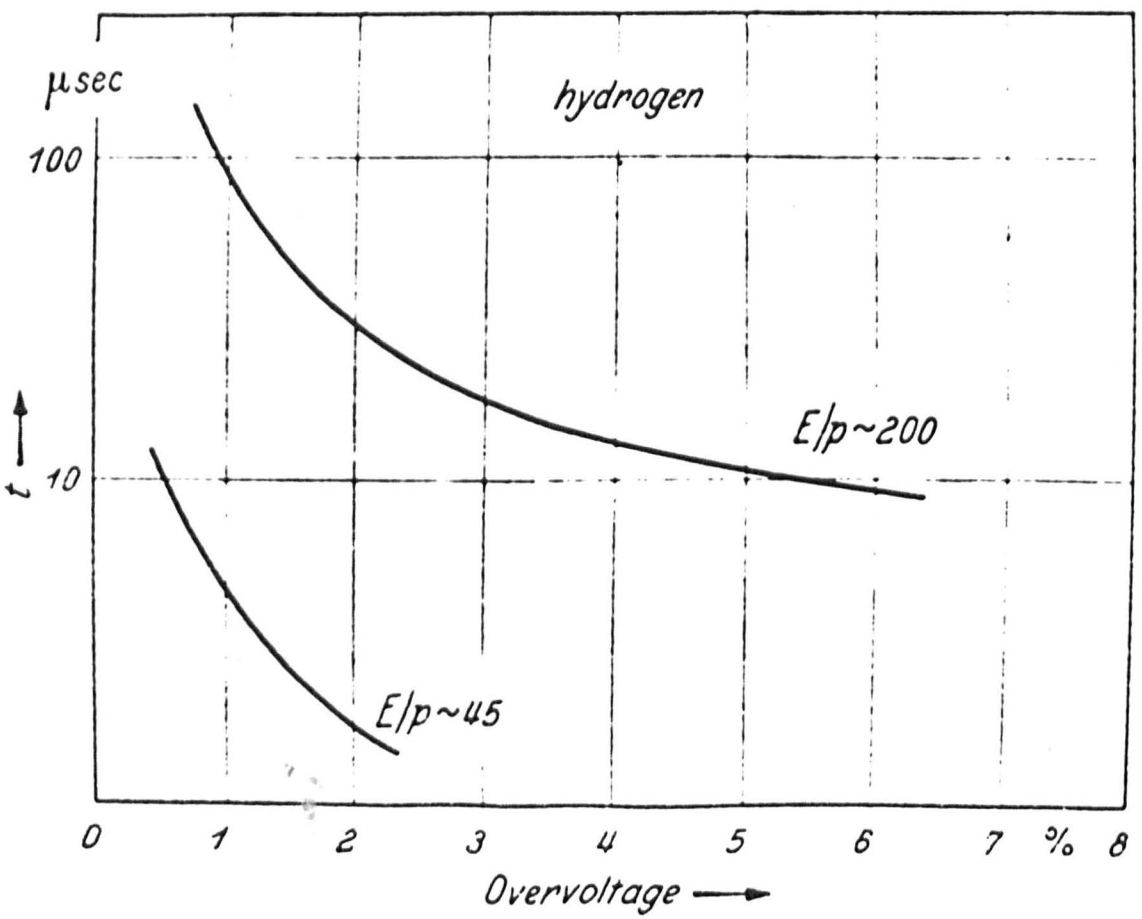

Formative time lags in hydrogen.

fig.11

time lag (S.T.L.) and the formative time lag (F.T.L). The S.T.L. is the time which elapses between the application of the voltage and the appearance of an initiatory electron in the gap. The F.T.L. is defined as the time taken for breakdown to occur after the appearance of the initiatory electron. In practice the S.T.L. can be reduced to zero by irradiating the cathode with ultra violet light, thus ensuring an adequate supply of initial electrons all the time. By this way the measured time lag will be equal to the formative time lag. Typical experimental curves in hydrogen are shown in fig. (11). The formative time lag can be predicted theoretically in certain simple cases by assuming values for the secondary ionization coefficients which are thought to be operative. Comparison of these calculated time lags with the experimentally measured values provide approximate values of the fractional contribution of different secondary processes to the generalised secondary ionization coefficient, provided an agreement can be found between the calculated and the measured time lags. This method has been used in the present study of identifying the secondary ionization processes involved in onset of breakdown in low pressure mercury discharge under uniform field conditions.

CHAPTER II

DAVIDSON'S THEORY FOR THE TEMPORAL GROWTH OF IONIZATION

2.1 INTRODUCTION

There are two approaches to the temporal growth of ionization in a Townsend discharge. The approach of Hornbeck (30) and Varney (31) and of Molnar (32) is aimed at the direct measurement of the secondary coefficient as a result of the action of positive ions and metastables at the cathode. The second approach, which in this thesis is presented in its most complete form, is due to Davidson. In this approach Davidson developed a theory which enables the formative time lag to be calculated if the ionization coefficients are known. Assuming values for the secondary ionization coefficients of the possible secondary processes in a particular gas, the formative time lag can be calculated and compared with the experimental value. The coefficients are adjusted until agreement is found between the theoretical and the experimental formative time lags. In this way the importance of various secondary ionization processes can be estimated. Three solutions for the temporal growth of current were developed by Davidson. Each was developed on the assumption that a different combination of secondary processes is active in the gas. The original theory developed by Davidson (33), gave an exact solution to the problem of ionization growth in hydrogen where only two secondary processes are operative. These two processes are the emission of electrons from the cathode by

positive ions (γ process) and undelayed photons (δ process). The main theory (34), discussed in section (2.2), takes into account the action of metastable atoms (ε process) and scattered resonance radiation (δ process). However this theory was modified later (35) to allow for the destruction of metastable atoms in the gas. This modified theory is discussed in section (2.3).

2.2 THEORY OF TEMPORAL GROWTH OF IONIZATION INVOLVING THE ACTION OF METASTABLE ATOMS AND DELAYED PHOTONS AT THE CATHODE.

Davidson (34) regards the motion of scattered resonance radiation in the gas as a diffusion process. Photons emitted by atoms which have been excited to normal states in collision with the primary electrons may be strongly absorbed by ground state atoms and after a short mean time interval, τ re-emitted with scattering. They thus proceed to the cathode by a process of diffusion due to repeated scattering. Since metastable atoms are uncharged, their motion is entirely due to diffusion and may reach the cathode by this process if not destroyed in the gas.

The formulae employed to represent the diffusion of repeatedly scattered photons resemble the formulae which represent the diffusion of metastable atoms and advantage is taken of this fact. The two cases were referred to as cases (b) and (a) respectively.

To investigate the spatial and temporal growth produced by processes depending on diffusion, it is assumed that initially the only secondary processes are of this type. It is further assumed, both in case (a) and in case (b), that the internal destruction produces no active photons capable of reaching the cathode either directly or by diffusion. After considering these two cases, Davidson generalised the treatment to include the case where all possible secondary processes are acting at the cathode, such as undelayed photons and positive ions processes.

Consider two plane parallel electrodes, of separation d, with the cathode ($x=o$) being exposed to a constant radiation producing a photo-electric current I_o. At time zero a potential of magnitude $V > V_s$ (where V_s is the breakdown potential at a particular value of pd) applied to the electrodes and maintained. Considering a region of the gas at a distance x, the basic diffusion equation which the active particles satisfy is given (34) as

$$\frac{\partial n(x,t)}{\partial t} = - \frac{\partial j(x,t)}{\partial x} + \alpha_1 e^{\alpha x} i_-(t-\frac{x}{w_-}) - \frac{n(x,t)}{\tau_1} \qquad (2.1)$$

where,

$n(x,t)$ is the spatial density of the active particles at a distance x from the cathode at time t.

$j(x,t)$ is the current density in the x-direction of the active particles.

i_- is the electron current density at the cathode.

w_- is the electron drift velocity.

α is the average number of electrons generated by an electron per centimetre path length in the direction of the field, (the primary ionization coefficient).

α_1 is the average number of active particles generated by an electron per centimetre path length in the direction of the field.

$\frac{1}{\tau_1}$ is the fraction of the active particles destroyed per unit time by collision with unexcited atoms. It is assumed that destruction of metastable atoms by electrons can be neglected. For this reason the theory is not applicable for high current densities where the field would in any case be distorted by space charge.

In the steady state, the diffusion coefficient D for the active particles is related to the current density, j, by

$$j = - D \frac{dn}{dx} \qquad 2.2.$$

Assuming D to be constant in space and time, the term $-\partial \frac{j(x,t)}{\partial x}$ in equation (2.1) can be replaced by $D \frac{\partial^2 n(x,t)}{\partial x^2}$

Thus the diffusion equation (2.1) becomes

$$\frac{\partial n(x,t)}{\partial t} = D \frac{\partial^2 n(x,t)}{\partial x^2} + \alpha_1 e^{\alpha x} i_- \left(t - \frac{x}{w_-}\right) - \frac{n(x,t)}{\tau_1} \qquad 2.3$$

The diffusion coefficient D is defined differently for cases (a) and (b). In case (a), $D = D_m$ which is an ordinary atomic or molecular diffusion coefficient and is given approximately as $\frac{1}{3} \ell_m \bar{v}$, where ℓ_m

is the mean free path of the metastable atoms, and $\bar{v}$ their mean kinetic velocity.

In case (b), $D = D_p$ which is given approximately as

$$Dp = \frac{1}{3} \ell_p^2 / \{\tau + (\ell p/_c)\}\{ 1- F_1 \} \qquad 2.4$$

when the current density of bound photons is neglected F_1 is the fraction of the original momentum retained by photons on remission from the bound state, ℓ_p is the collision mean free path of the photons, τ is the mean time for which a photon remains bound before being released (or the mean lifetime of the excited atomic state) and c/ℓ_p is the fraction of free photons which become absorbed per unit time. However, the current of photons is not accurately monochromatic, and since their absorption by atoms is a resonance phenomena, hence any spatial variation in their frequency distribution will be accompanied by a spatial variation in ℓ_p and hence in D_p. Thus it is not certain that an accurate equation will be obtained on inserting D_p into the diffusion equation (2.3), with D assumed to be constant in space and time. Thus the diffusion equation (2.3) with constant D may not apply to trapped radiation with the same accuracy as it does to metastable atoms.

Considering the boundary conditions of equation (2.3) at the electrodes, Davidson assumes that the fraction g of active particles

which get destroyed at the cathode must not be greater than $\frac{1}{5}$ of the number of the active particles N which strike the cathode per unit time. In case (a), the number of the active particles which strike the cathode per unit time

$$N = \tfrac{1}{4} n\bar{v}$$

thus

$$D \frac{(\partial n)}{\partial x} = g \tfrac{1}{4} n\bar{v}$$

therefore

$$n = h \frac{\partial n}{\partial x} \quad \text{at} \quad x = o \qquad 2.5$$

where

$$h = \frac{4D}{g\bar{v}} = \frac{4}{g\bar{v}} \quad \frac{1}{3} \ell_m \bar{v} = \frac{4\ell_m}{3g} \qquad 2.6$$

If G is the fraction of active particles destroyed on striking the anode (x = d),

then

$$n = -H. \frac{\partial n}{\partial x} \qquad \text{at } x = d \qquad 2.7$$

where

$$H = \frac{4}{3} \ell_m / G.$$

If a fraction g_1 of the active particles destroyed at the cathode causes the emission of an electron, and if there is an externally maintained electron current density at the cathode I_o, then the electron current density at the cathode is given as

$$i- = I_o + g_1 D_m \left(\frac{\partial n}{\partial x} \right) \qquad \text{at } x = o \qquad 2.8$$

In case (b) similar expressions can be derived taking into account that

$$N = \tfrac{1}{4} Nc \,/\, (c\tau / \ell_p) + 1$$

Thus in the similar expression for n's (at the cathode and anode), h and H are given by

$$h = \frac{4}{3} \ell_p \,/\, (1-F_1)g$$

and

$$H = \frac{4}{3} \ell_p / (1-F_1)\, G.$$

Before considering the solutions for temporal growth, Davidson considered the solutions for a steady state. Since in steady state i_- and n are constant in time, the diffusion equation (2.3) becomes

$$D \frac{d^2 n}{dx^2} + \alpha_1 \, i_- \, e^{\alpha x} = \frac{n}{\tau_1} \qquad 2.9$$

with the boundary consitions (2.5), (2.7) and (2.8), equation (2.9) is integrated to give

$$\frac{i_-}{I_o} = 1/\left\{1 - \frac{\delta_1}{\alpha^2 - \mu^2} \left[\frac{e^{\alpha d} - \cosh \mu d - \alpha(\sinh \mu d)/\mu}{(\sinh \mu d)/\mu} \right] \right\} \qquad 2.10$$

providing g and G are large enough to make h = H = o

where, $\delta_1 = g_1 \alpha_1$

and $\mu = 1/\sqrt{D\tau_1}$

when μd (but not αd) is a small fraction, equation (2.10) reduces to

$$\frac{i_-}{I_o} = 1/\left[1 - \frac{\delta_1}{\alpha^2 d}\left(e^{\alpha d} - \alpha d - 1\right)\right] \qquad 2.11$$

If however αd is greater than 5, the electron current density at the cathode i_- will be given by

$$\frac{i_-}{I_o} = 1/\left(1 - \frac{\delta_1 e^{\alpha d}}{\alpha^2 d}\right) \qquad 2.12$$

If the conditions leading to (2.12) hold, the secondary coefficient due to metastable atoms ε is shown (9) to be given by $\delta 1/ \alpha d$. When metastable atoms and trapped radiation are acting simultaneously, the δ_1 in this expression must be replaced by the sum of the δ_1's of the separate processes.

Considering the temporal growth, Davidson gives the solution for the current growth in two forms. One is valid at all times. The other is valid only for time t where $\frac{t}{T}$ is a small fraction, e.g. $\frac{1}{4}$, T being the active particle transit time. In case of metastable atoms transit time $T = \frac{d^2}{D} = \frac{3d^2}{2v}$. Since solution in this range of small t/T is of limited practical use, this thesis will concentrate on the solution which is valid at all times. The gas is assumed to be free from active particles and electrons up to time, t = o, at which the externally generated cathode current I_o is established. Concerning the quantities $n(x,t)$ and $i_-(t)$ the following boundary conditions are given as sufficient to determine these quantities at all times:

(i) at $t < o$, $n(x,t) = i_{-}(x,t) = o$

(ii) at $t > o$, $i_{-}(t) = I_o + g_1 D \frac{\partial n(x,t)}{\partial x}$ 2.13

(iii) at $t > o$, $n(o,t) = n(d,t) = o$

(iv) at $t > o$, the differential diffusion equation (3) holds throughout the gas.

The following contour integrals are given as solutions which satisfy the four conditions.

$$\frac{n(x,t)}{I_o} = \frac{i\alpha_1}{\pi D} \int_C \frac{z\, e^{D(z^2 - \mu^2)t}}{(z^2 - \mu^2)\,\theta} \left[(1 - e^{-2zd}) e^{\psi x} + (e^{(\psi - z)d} - 1) e^{-zx} + (e^{-2zd} - e^{(\psi - z)d})\, e^{zx} \right] dz \qquad 2.14$$

$$\frac{i_{-}(t)}{I_o} = \frac{i}{\pi} \int_C \frac{z e^{D(z^2 - \mu^2)t}\, (z^2 - \psi^2)(1 - e^{-2zd})dz}{(z^2 - \mu^2)\,\theta} \qquad 2.15$$

where $\psi = \alpha - D(z^2 - \mu^2)/W_{-}$ 2.16

$\theta = \xi + 2\delta_1 z\, e^{(\psi - z)d} - (2\delta_1 z + \xi)\, e^{-2zd}$ 2.17

$\xi = \{Z + \psi\}\ \{(Z - \psi)F - \delta 1\}$ 2.18

$F = 1$ 2.19

The purpose of introducing the function F, whose value in the present case is unity, will appear later. The contour C(42), which is traversed clockwise, is a quarter of an infinite circle, the centre of the circle being at the origin and the centre of the arc being on the positive real

axis. At all positive times, Davidson showed that $i_-(t)/I_o$ is the real part of

$$A + \Sigma \frac{2f\,\lambda(\lambda^2 - \psi^2)(1 - e^{-2\lambda d})\; e^{D(\lambda^2 - \mu^2)t}}{(\lambda^2 - \mu^2)\,(\partial\theta/\partial\mathbb{Z})_\lambda} \qquad 2.20$$

The summation extends over all values λ of $\mathbb{Z}$ (other than 0 and ψ) which satisfy $\theta(\mathbb{Z})=0$ and which lie on the positive real or positive imaginary axes or in the quadrant bounded by them. f is a factor which is unity for the poles on the axes of the plane of integration and 2 for any poles inside the quadrant. A is given by the right hand side of equation (2.10). The character of λ all values of which lie on the axes depends on the sign of the quantity, A. If A is positive, λ can have a real value which will be less than μ. In this case the ratio $\frac{i_-(t)}{I_o}$ in (2.20) reduces to A at large times, thus a steady state is established. When A is negative, the case when the breakdown potential is exceeded, one of the values of λ is real and greater than μ and thus contributes to the current equation (2.20), a term which increases exponentially with time.

The treatment can be generalised to include the secondary processes of positive ions and unscattered photons at the cathode. This can be achieved by adding to the boundary condition (ii) in (2.13) the integral expressions which represent these secondary actions, viz.

at $t > o$,

$$i_- = I_o + g_1 D \frac{\partial n(x,t)}{\partial t} + \gamma I_+(o,t) + \delta \int_o^d i_- \bar{e}^{\mu_1 x} \, dx \qquad 2.21$$

where γ and δ / α are secondary ionization coefficients due to positive ions and undelayed photons respectively and μ_1 is the absorption coefficient. To satisfy these modified boundary conditions, the function F, which was previously taken as unity has to be replaced by:

$$F = 1 - (\delta / \psi) (e^{\psi d} - 1) - (\alpha \gamma / \phi) (e^{\phi d} - 1) \qquad 2.22$$

where $\phi = \alpha - D(g^2 - \mu^2) / W$

and $$\frac{1}{W} = \frac{1}{W_-} + \frac{1}{W_+} \qquad 2.23$$

W_- and W_+ are drift velocities of electrons and positive ions respectively.

The constant A can be replaced by

$$1/ \{ 1 - \omega / \alpha \, (e^{\alpha d} - 1) \}$$

where $\omega / \alpha = \gamma + \delta / \alpha + \varepsilon / \alpha$

If the time lag is of the same order as the transit time of the active particles, W_- can be considered infinite and therefore the expression $i_-(t - x/W_-)$ in the diffusion equation (2.3) can be replaced by $i_-(t)$. ϕ and ψ may be replaced also by α since

$$\psi = \alpha - D(g^2 - \mu^2)/W_- \text{ and } \phi = \alpha - D(g^2 - \mu^2) / W$$

If there is negligible destruction of the diffusing particles in the gas, μ can be neglected and putting $f = 1$, the complete modified solution is given by

$$\frac{i_-(o,t)}{I_o} = \frac{1}{1 - \frac{\omega}{\alpha}(e^{\alpha d}-1)} + \frac{2(\lambda^2 - \alpha^2)(1-e^{-2\lambda d})\, e^{D\lambda^2 t}}{\lambda \left(\frac{\partial \theta}{\partial Z}\right)_\lambda} \qquad (2.25)$$

By differentiating equation (2.17)

$$\left(\frac{\partial \theta}{\partial Z}\right)_\lambda = 2\lambda F - \delta_1 - 2\delta_1(\lambda d - 1) e^{(\alpha - \lambda)d} - e^{-2\lambda d}\left[2Fd(\alpha^2 - \lambda^2) + 2d\,\delta_1(\alpha - \lambda) + 2\lambda F + \delta_1\right] \qquad (2.26)$$

where λ is given the real value of Z satisfying $\theta(Z)=o$, where

$$\theta(Z)=(\alpha - Z)\{(\alpha + Z)F + \delta_1\} e^{-2Zd} + 2\delta_1 Z e^{(\alpha - Z)d} - (\alpha + Z)\{(\alpha - Z)F + \delta_1\} = o \qquad (2.27)$$

When the processes of metastable atoms, positive ions and undelayed radiation are the only secondary processes operative at the cathode, F is given as

$$F = 1 - (\gamma + \delta/\alpha)(e^{\alpha d} - 1) \qquad (2.28)$$

$$\omega/\alpha = \gamma + \epsilon/\alpha + \delta/\alpha \qquad (2.29)$$

and

$$\delta_1 = \frac{(\epsilon/\alpha)\,\alpha^2 d\left[e^{\alpha d} - 1\right]}{e^{\alpha d} - \alpha d - 1} \qquad (2.30)$$

The procedure for calculating the formative time lag t, or the time required for the current to be self-maintained, is as follows:

(1) The externally maintained current I_o is determined.

(2) The value of ω/α is determined from the Townsend breakdown criterion, by measuring the field at which the current is just self-maintained. The value of α at this field is used to calculate ω/α It is necessary to assume that ω/α does not vary appreciably with the overvoltage ΔV. In other words ω/α determined at the sparking potential, $\Delta V = o$, is assumed to remain the same for the higher over voltages used in formative time lag measurements ($\Delta V = V - V_s$, where V is the voltage at which the F.T.L. is measured and V_s is the breakdown potential, $V > V_s$).

(3) The values of the secondary ionization coefficients γ, δ/α ε/α are chosen such that $\gamma + \delta/\alpha + \varepsilon/\alpha = \omega/\alpha$. In practice the γ and δ/α components are so much faster than ε/α component that they cannot be distinguished from each other, they are therefore taken together.

(4) The value of α is selected for the value of E/p existing at the overvoltage ΔV to be considered.

(5) δ_1 and F are then determined from equation (2.30) and (2.28).

(6) The real solution λ is then determined from equation (2.27).

(7) The value of λ obtained is inserted in equation (2.26) and $\left(\frac{\partial \theta}{\partial \xi}\right)_\lambda$ is determined.

(8) From equation (2.25) Dt can then be calculated. t is the time

required for the current to reach the value $i_{(o,t)}$ of self-maintained current, and D is the diffusion coefficient. If D is known, t is then determined.

In this way the formative time lag can be calculated for several small values of overvoltages at a particular value of E/p, for a given choice of secondary ionization coefficients. The choice of these coefficients is adjusted in an attempt to get agreement with experimentally measured curves of formative time lag as a function of overvoltage.

It is of interest to observe that if the ε / α value is chosen as zero

$\delta_1 = o$ and the expression for $\theta(Z)$ becomes

$$\theta(Z) = (\alpha + Z) (\alpha - Z)F \left[e^{-Zd} - 1 \right]$$

In general F is not zero. The solutions for $\theta(Z) = o$ are then

$$Z = \pm\alpha \text{ and } o$$

These are the trivial solutions mentioned before, which are not included in the summation. Thus in this case (when $\varepsilon/\alpha = o$) there is no real solution for λ .

2.3 MODIFICATION OF THE TEMPORAL GROWTH THEORY TO ALLOW FOR THE DESTRUCTION OF METASTABLE ATOMS IN THE GAS.

Beside the processes which have been discussed in the previous section (2.2) there are other secondary ionization processes which,

while contributing to the growth, nevertheless introduce an appreciable delay between the original electron-atom exciting collisions and the release of cathode electrons. For example, delayed photo-electron emission can result from photons released in the de-excitation of metastable atoms, in which the atoms lose their energy in collisions with the ground state atoms in the following ways (Biondi(36)),

(i) by further excitation of a metastable atom to a radiating state when the energy difference is sufficiently small.

(ii) by perturbation of the metastable state in such a way that a collision-induced non-resonance photon is emitted in a transition to the ground state which breaks the selection rule.

(iii) by the production of a short-lived excited molecule in collision with two ground-state atoms.

In accounting for ionization growth in Argon, Menes (37) has examined the delayed photoelectric action of radiation produced by the destruction of argon metastable atoms in three-body collisions to form excited diatomic molecules, which then undergo radiative dissociation according to the reaction

$$A_{met} + 2A \rightarrow A_2^* + A, \quad A_2^* \rightarrow 2A + \text{photon}.$$

This process is pressure dependent, and the effective delay in the arrival of the photons at the cathode is determined by the three-body collision frequency (which is proportional to p^2) and the natural life time of the excited molecules. In helium, however, Phelps (38) has

shown that the main source of non-resonance photons in this gas appears to be the destruction of the $2\ ^1S$ metastable atoms in two-body collisions with neutral atoms at a rate proportional to p. A further mechanism of delayed photoelectric emission is that caused by resonance photons which was thought to reach the cathode by a diffusion process similar to that of metastable atoms. Phelps, has shown that the transport of resonance photons in the gases (which he considered) is in accordance with the Holstein (39) and Biberman (40) process. In this process resonance photons undergo repeated absorption by ground state atoms which are thus excited and re-emit them, so that photons are in effect retained by atoms for a total time of $n\tau_o$, where n is the number of such absorbing collisions and τ_o is the average life-time of the excited atoms. Taking into account dipole-dipole interactions and spectral line broadening has led to an estimate of n from the relation

$$n = 0.87 \left(\frac{3\pi^2 d}{\lambda_o}\right)^{\frac{1}{2}} \qquad (2.31)$$

Thus the average total delay time τ_1 by this mechanism is given by

$$\tau_1 = \tau_o n$$

where d is the gap separation and λ_o the wave length of the centre of the broadened resonance spectral line.

On the assumption that any or all of these secondary ionization processes are active in the gas, Davidson (35) extended his temporal

growth theory and derived two types of solution. One of these is a simple exponential solution where the current $i_k(x,t)$ of each type, K, of active particles is of the form,

$$i_k(x,t) = i_k(x,o)\ e^{\lambda t} \qquad (2.33)$$

in which the constant λ is the same for all types present, is real and not zero. The spatial densities of the active particles contain this same exponential term. Such a solution was shown to be applicable to the complicated case suggested by Phelps (38) where molecular ions and molecular metastables are included.

The procedure by which the simple exponential solution is derived, is as follows:

Formulae are set up for each of the ratios

$$i_k(o,t) \,/\, i_-(o,t) = f_k(\lambda) \qquad (2.34)$$

In setting up these expressions for the f_k'S all the differential equations and boundary conditions will have been used except the cathode electron boundary condition which is given by the following equation

$$\left.\begin{aligned} & i_-(o,t) = I_o(t) + g(t) \\ & \text{where} \quad g(t) = \Sigma_k\ \gamma_k\ i_k(o,t) \end{aligned}\right\} \qquad (2.35)$$

where $i_-(o,t)$ is the cathode electron current, at time t, $I_o(t)$ is the externally maintained current, $g(t)$ is the electron currents generated

by the secondary action of the various types (suffix k) of active particles, i_k (o,t) is the active particle current at the cathode and γ_k is its secondary ionization coefficient. The expression for each f_k will be a function of λ (but not time) and will be valid for all values of λ . Inserting these f_k's expressions into the cathode boundary electron boundary condition (2.35) gives

$$1 - \Sigma \gamma_k \ f_k \ (\lambda) = o \quad , \text{ for } I_o(t) = o \tag{2.36}$$

and $$i_-(o,t) = i_-(o,o)\ e^{\lambda t} = \frac{I_o(t)}{1 - \Sigma \gamma_k \ f_k} \ , \text{ for } I_o \neq o \tag{2.37}$$

Thus a simple exponential solution exists only in the case $I_o(t) = o$. In that case it exists if λ has a real value satisfying the equation

$$F(\lambda) = 1 - \Sigma \gamma_k \ f_k(\lambda) = o \tag{2.38}$$

λ varies continuously with the applied potential, V. At every value of V, there is an infinite number of λ's (real and imaginary) which satisfy, $F(\lambda) = o$. However the value of λ of the simple exponential solution is the one which is real and which goes through zero as V goes through the value V_s (the breakdown potential). This can be easily seen from the breakdown criterion as follows.

If $i(o,t) = i\ (o,o)e^{\lambda t}$

then $e^{\lambda t} = \frac{i(o,t)}{i(o,o)}$

At the breakdown voltage $V = V_s$, the secondary current at the cathode i(o,t) must be just sufficient to maintain the discharge,

i.e. $i(o,t) = i(o,o)$ so that $e^{\lambda t} = 1$ and therefore $\lambda = o$.

For the case where there is a constantly maintained cathode electron current I_o (produced by external illumination) and no initial active particles are present, Davidson writes an expression for the electron current $i_-(o,t)$ at the cathode as

$$\frac{i_-(o,t)}{I_o} = A - \Sigma B_\lambda e^{\lambda t} \qquad (2.39)$$

The expression is valid at all times $t > o$. A and B's have an explicit expression. The summation contains λ of the simple exponential solution and all other λ's which satisfy $F(\lambda) = o$.

At sufficiently large time t, the terms containing all these other λ's become relatively negligible in comparison with the λ of the simple exponential solution, and the general solution (2.39) reduces to

$$\frac{i_-(o,t)}{I_o} = A - Be^{\lambda t} \qquad (2.40)$$

when $V > V_s$, λ is positive and for large t the term A can be neglected and expression (2.40) reduces to

$$\frac{i_-(o,t)}{I_o} = -B e^{\lambda t} \qquad (2.41)$$

Phelps (38) derived an expression similar to the simple exponential expression (2.33) which can be re-written as

$$i_-(o,t) = C e^{\lambda t} \qquad (2.42)$$

The constant C was determined by an initial arbitrary distribution of active particles which is absent in the present problem. Expression (2.40) is an explicit expression from which the current due to a specific cause can be calculated.

At this point, Davidson turned his attention to derive the general solution when the secondary electron emission from the cathode is due to positive ions and delayed radiation. With a maintained I_o from time zero, the cathode electron boundary conditions become

$$\text{at } t < o \ , \qquad i_-(o,t) = o$$

$$\text{and at } t > o \ , \quad i_-(o,t) = I_o + \frac{\delta_1}{\tau_1} e^{-t/\tau_1} \int_o^d e^{\alpha x} dx \int_o^{t_1} i_-(o,t_1 - \tfrac{x}{w}) \cdot 2.43$$

$$e^{t_1/\tau_2} \, dt_1 + \alpha\gamma \int_o^d i_-(o,t - \tfrac{x}{w}) \, e^{\alpha x} dx$$

These conditions are satisfied by the following contour integral

$$i_-(o,t) = \frac{I_o}{2\pi i} \int_C \frac{e^{Pt} \, dP}{P \, F(P)} \tag{2.44}$$

$$\text{where } F(P) = 1 - \frac{\delta_1 (e^{\psi d} - 1)}{(1-p\tau_1)\psi} - \frac{\alpha\gamma (e^{\phi d} - 1)}{\phi} \tag{2.45}$$

$$\psi = \alpha - P/W_- \quad \text{and} \quad \phi = \alpha - P/W \tag{2.46}$$

and

δ_1/α is the delayed photon secondary ionization coefficient defined

as the number of secondary electrons released from the cathode by this process per primary ionizing collision in the gas.

α is the first Townsend ionization coefficient.

γ is the secondary ionization coefficient for positive ions, defined as the number of electrons released from the cathode by this process per primary ionizing collision in the gas.

d is the gap distance.

$\frac{1}{W} = \frac{1}{W_-} + \frac{1}{W_+}$, W_- is the electron drift velocity and W_+ is the positive ion drift velocity.

When non-resonance photons are the active ones at the cathode, τ_1 will be the average lifetime of the metastable states. If, on the other hand, the delayed resonance photons are the active ones, τ_1 will be the average total delay time before they strike the cathode surface.

From equation (2.39) the electron current can be calculated for given values of the various assumed secondary coefficients.

Expression (2.39) is valid for $t > o$, and can be written in detail as,

$$\frac{i_-(o,t)}{I_o} = \frac{1}{F(o)} + \Sigma_\lambda \frac{e^{\lambda t}}{\lambda \partial F(\lambda)/\partial\lambda} \qquad (2.47)$$

i.e. $A = \frac{1}{F(0)}$ and $B = \frac{-1}{\lambda \partial F(\lambda)/\partial\lambda}$ (2.48)

$$\frac{1}{F(0)} = 1/\{1 - (\frac{\delta_1}{\alpha} + \gamma)(e^{\alpha d} - 1)\} \qquad (2.49)$$

As explained above, (2.47) can be approximated to

$$\frac{i_-(o,t)}{I_o} = A - Be^{\lambda t} \qquad (2.50)$$

and at large t, equation (2.50) can be reduced further to

$$\frac{i_-(o,t)}{I_o} = - Be^{\lambda t} \qquad (2.51)$$

λ is the real value of P which satisfies the equation $F(p) = o$

and $$\frac{\partial F(\lambda)}{\partial \lambda} = \frac{\delta_1}{W_- \psi^2(1 - \lambda\tau_1)^2}\left[W_- \psi\tau_1(e^{\psi d} - 1) + (1 + \lambda\tau_1)\{(\psi d - 1)e^{\psi d} + 1)\}\right]$$

$$+ \frac{\alpha\gamma}{W \phi 2}\left[(\phi d - 1)\, e^{\phi d} + 1\right] \qquad (2.52)$$

The total secondary ionization coefficient ω/α (for this combination) is given by $\omega/\alpha = \delta_1/\alpha + \gamma$ (2.53)

Thus by applying equation (2.50) or (2.51) to a particular gas the formative time lag due to the simultaneous action of delayed radiation and positive ions at the cathode can be calculated when the various coefficients are known. The formative time lag can be calculated for several values of overvoltage for a given choice of secondary ionization coefficients, at different values of E/p_o. The choice of these coefficients, at each particular value of E/p_o is adjusted in an attempt to get agreement with experimentally measured curves of formative time lag as a function of overvoltage. However since one or

more delayed photo electric mechanisms may be active, τ_1 (delay time) should be treated as a variable, beside the secondary ionization coefficients. If an agreement is found between calculated and measured formative times over the full range of the curve of the formative time lag at a particular value of E/p_o, then the delayed photon process characterised by the particular delay time τ_1 (at which the agreement is found) will be responsible for the observed ionization growth. This method of calculation is adopted in the present analysis and its full detail is given in chapter (6.2.3).

For the case when the secondary electron emission from the cathode is due to the simultaneous action of positive ions (γ process) and undelayed photons (δ process), the current growth equation can be predicted from the above theory as follows. Excitation of gas atoms by electron impact takes place with the primary ionization and, after negligible delay time ≈ the life time (10^{-8} sec.) of the excited states) spontaneous de-excitation occurs. The resulting photons travel through the gas to the cathode in a time < d/c (c is the velocity of light) which is negligible. Thus the time taken for the undelayed radiation to reach the cathode after the excitation by primary electrons is negligible compared to the time ($\approx 10^{-3}$ sec.) involved in the case of delayed radiation and can be considered as zero. Therefore the temporal growth of ionization current when the secondary ionization is due the δ and γ processes

at the cathode can be obtained by putting $\tau_1 = o$ in the above expressions of the modified theory. Hence the electron current i_- flowing at time t at the cathode can be given by

$$i_-(o,t) = \frac{I_o (1 - e^{\lambda t})}{1 - (\gamma + \delta/\alpha)(e^{\alpha d} - 1)} \qquad (2.54)$$

λ is given the value which makes $F(\lambda) = o$

where $$F(\lambda) = 1 - \frac{\gamma\alpha}{\phi}(e^{\alpha d} - 1) - \frac{\delta}{\psi}(e^{\psi d} - 1) \qquad (2.55)$$

$$\phi = \alpha - \frac{\lambda}{W} \qquad (2.56)$$

$$\psi = \alpha - \frac{\lambda}{W_-} \quad \text{(if the absorption of the photons in the gas is negligible).}$$

$$\frac{1}{W} = \frac{1}{W_+} + \frac{1}{W_-} \qquad (2.57)$$

and $$\omega/\alpha = \gamma + \frac{\delta}{\alpha} \qquad (2.58)$$

I_o is the externally maintained current.

W_- and W_+ are the electron and positive ion drift velocity respectively

γ is the secondary ionization coefficient for positive ions.

δ/α is the undelayed photon secondary ionization coefficient defined as the number of secondary electrons released from the cathode by this process per primary ionizing collision in the gas.

Expression (2.54) is the approximate expression developed by Davidson (33) for the interpretation of ionization growth in hydrogen.

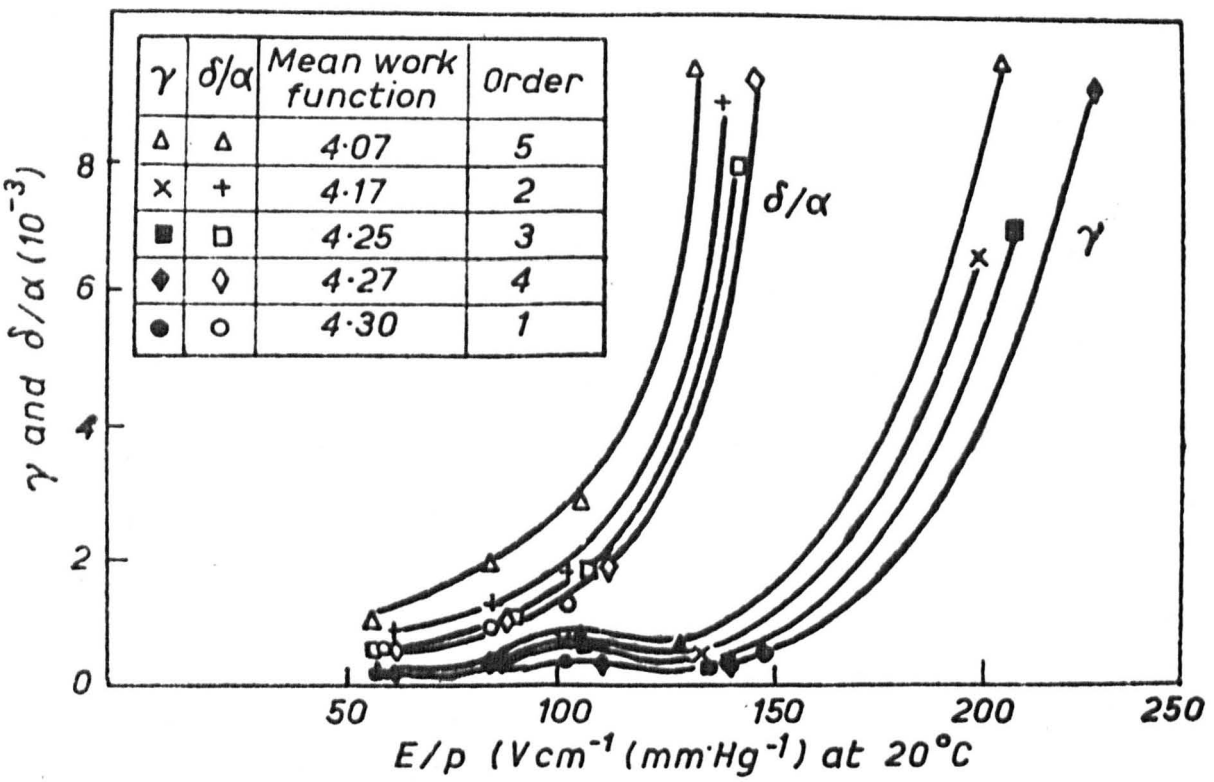

The influence of the work function on the secondary coefficients in hydrogen.

fig.12

Bartholomeyczyk (41) solution for the same case (undelayed photon and positive ion secondary cathode processes) neglects I_o and does not take correct account of initial distributions of the active particles in the gap.

2.4 CONCLUSION.

In applying Davidson's growth equations, the essential test (9) is to find what combination of secondary processes will give rise to the measured growth times over a wide range of E/p. An agreement of predicted values with any particular observed value of t_f is nearly always possible for a specific value of $E/_p$, but the agreement over a wide range is a stringent test. From the previous equations it has been seen that the growth time depends greatly on the value of the primary ionization coefficient (and therefore on purity of the gas) and on the value of secondary coefficient (which depends on the work function of the cathode). Therefore, it is desirable to measure these coefficients and the time lags under the same conditions, if it is possible.

A successful application of Davidson theory was carried out for hydrogen (43,44) where positive ions (γ- process) and undelayed photons ($\delta'\alpha$ process) were found to be the active secondary processes. The influence of the work function of the cathode on these two processes is shown in fig. (12).

In helium, however, application of Davidson's approach led to the conclusion (45) that the dominant secondary process is the photo-electric emission from the cathode (δ_1 / α) due to the incidence of delayed non-resonance photons produced by the destruction of metastable 2^1S atoms in two-body collisions in the gas, in the range of E/p < 13 $V.cm^{-1}.mm.Hg^{-1}$. At high E/p >38, positive ions were found to be dominant.

In mercury vapour, time lag measurements were carried out by Overton (see section 3.2). Analysis of the results at two values of E/p_o (358 and 391 $V.cm^{-1}.mm.Hg^{-1}$) lead to the conclusion that delayed radiation and positive ions are dominant secondary processes at these values of E/p. However no agreement could be found at other values of E/p.

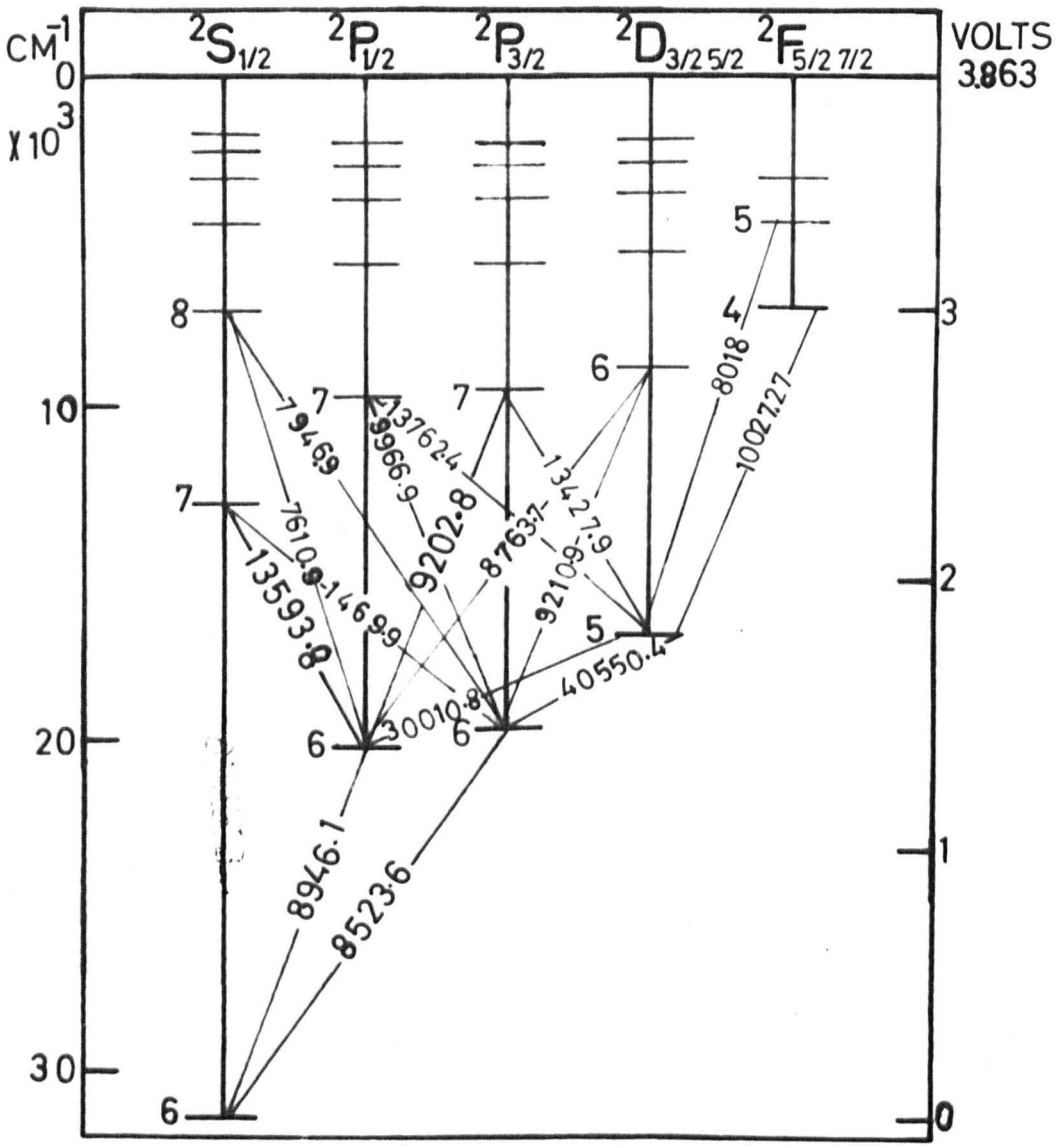

THE MOST IMPORTANT ENERGY LEVELS AND SPECTRAL LINES FOR THE NEUTRAL CAESIUM ATOM.

Fig. 13

CHAPTER III

REVIEW OF THE PREVIOUS EXPERIMENTAL WORK.

3.1 PREVIOUS WORK IN CAESIUM.

3.1.1 INTRODUCTION

The electrical properties of the alkali metals are of much interest from several points of view. They are interesting as components of stellar atmosphere and other plasmas, because their low ionization potentials (~ 4-5V) lead to high ionization probabilities and put them in the role of electron donors. However, among the alkali metals caesium has the lowest ionization potential of 3.893V. The most important energy levels and spectral lines of the neutral caesium atom are shown in fig.(13). It can be seen that the caesium atom can possess (apart from two excited states $6^2P_{1/2,\ 3/2}$ of energies ≈ 1.45 e.V.) a considerable number of excited states with energies greater than 2 e.V. above the ground state. The importance of these states lies in the fact that associative ionization processes can take place in a caesium discharge (46) since the ionization energy of atomic caesium is 3.893 e.V. and that of the molecular caesium is 3.19 e.V. However associative ionization processes are dependent on thepressure and the current flowing in the discharge. Thus the efficiency of these processes is high in high current caesium discharge. In low current discharge, however,(Townsend discharge) these excited

states can contribute to the breakdown mechanism by releasing secondary electrons from the cathode (either by the collision of the excited atoms or by incidence of the emitted radiation) since in most cases any metal cathodes get contaminated with caesium and attain a work function around 2 e.V.

A great deal of work has been carried out concerning the breakdown mechanisms and characteristics of caesium vapour in the high current discharge because of its important industrial applications and now, due to the more recent development of gas discharge devices, a detailed study of the breakdown charcteristics of caesium vapour at low pressures is necessary in order to assist in obtaining a clear picture of the fundamental processes involved in the caesium vapour discharge.

Due to the experimental difficulties created by the great chemical reactivity of caesium ,there has not been reported any work on caesium vapour in the Townsend region apart from the paper published by Bratescu (40) on breakdown potentials in caesium vapour. The results and the technique of Bratescu will now be discussed in the following section.

3.1.2 THE EXPERIMENT OF BRATESCU

The discharge tube was made of "Rasotherm" glass of diameter 4.9 cm. The discharge tube was coated from the inside with a protective covering (Bestunmungen) which allowed the temperature to be taken

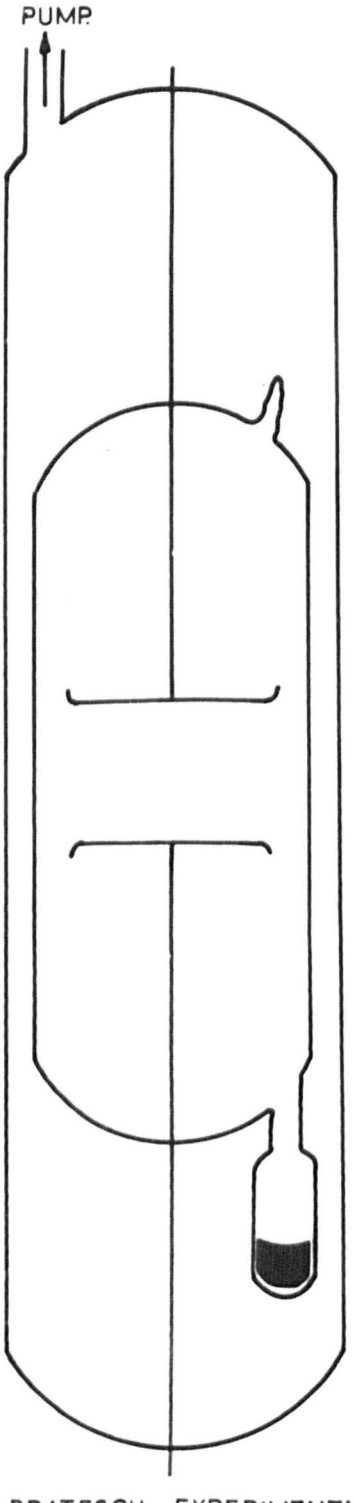

BRATESCU EXPERIMENTAL TUBE.

Fig. 14

above 300°C. A side-arm containing a caesium reservoir was attached to the tube. This side-arm was maintained at lower temperature than the tube while taking the measurements.

The electrodes were made of nickel sheets and had Rogowski profile to reduce the field distortion. They were fastened on to the discharge tube by a tungsten wire of diameter 1 mm., which also served as electrical connection to the external circuit. The electrodes were 3.7 cm. in diameter and 2.61cm., apart. A diagram of the discharge tube is shown in fig. (14).

The tube was heated at 450°C under vacuum for several hours. The ultimate pressure obtained after baking at the above temperature was of the order of 10^{-5} mm.Hg. The pure caesium metal was introduced into the discharge tube after several distillations under vacuum. After finishing the distillation, the tube was sealed and put into another tube, which was connected to the vacuum system during the actual running of the discharge. The purpose of the second tube was to prevent (when leaks develop) air penetrating into the discharge tube. The main discharge tube was mounted into the outside tube by the tungsten wires which held the electrodes. By heating the tube in an electric oven (its specification was not mentioned in the paper) various gas pressures of C_s vapour could be obtained. The pressure was calculated from the expression (48)

$$\log_{10}(\text{p (mm. Hg.)}) = -\frac{A}{T} - B \log_{10} T + C$$

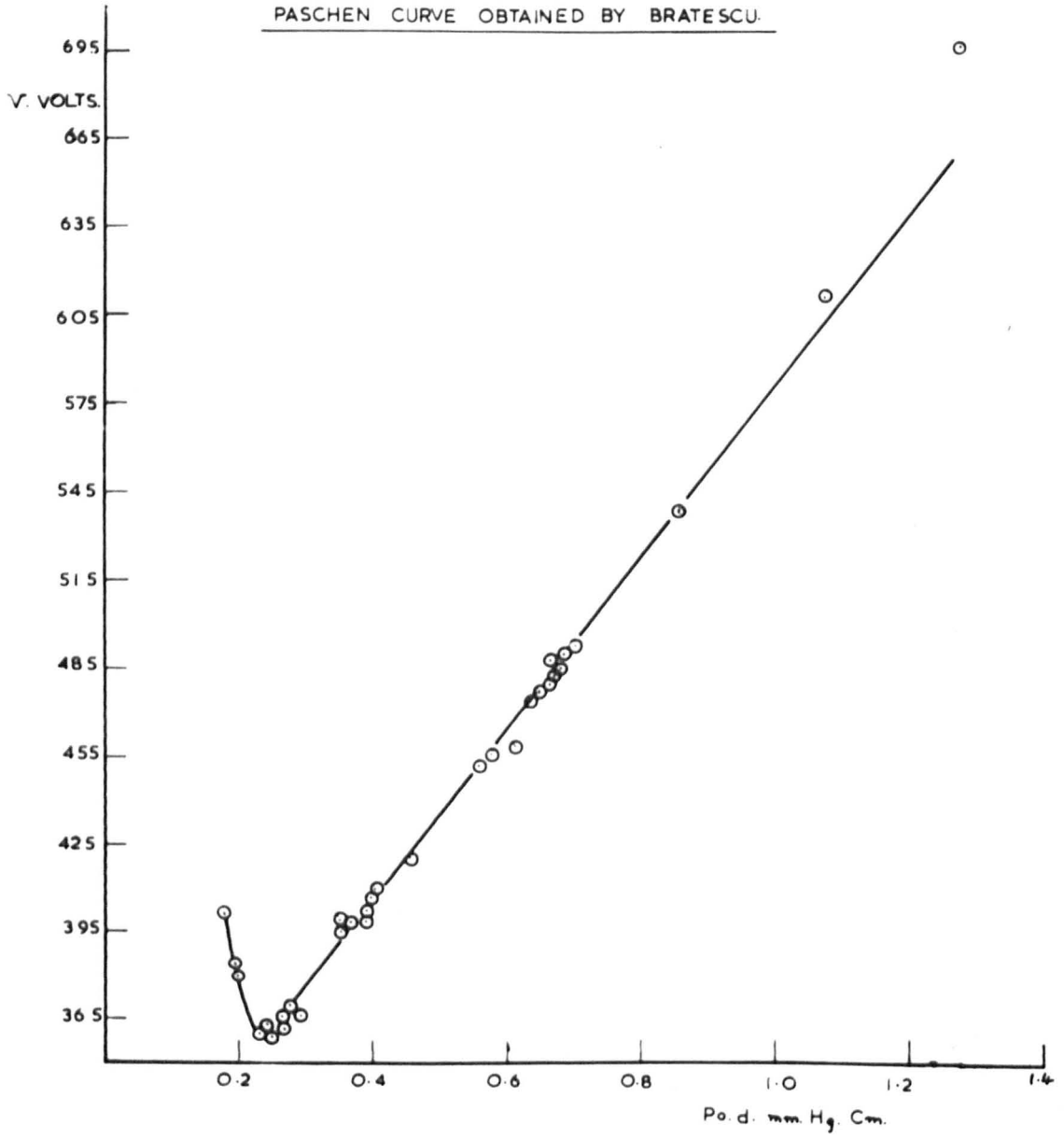
PASCHEN CURVE OBTAINED BY BRATESCU.
V. VOLTS.
695
665
635
605
575
545
515
485
455
425
395
365
0·2
0·4
0·6
0·8
1·0
1·2
1·4
Po. d. mm. Hg. Cm.

Fig. 15

where A = 4042, B = 1.4, C = 11.176

and T is the temperature of the side-arm in kelvin degrees.

The pressure p obtained from the above formula was within an accuracy of 10%, and was reduced to the pressure p_o at 0^oC.
A potential of 1200 volts supplied by a bank of dry batteries was taken through a potential divider and was applied across the discharge tube through a resistance R ($0 \leq R \leq 5000\ \Omega$). The potential across the tube was measured by a Chauvin-Arnoux voltmeter. The breakdown potential was taken as that value of voltage at which the applied potential falls by a small value, and the discharge light appeared. The breakdown potential as a function of $p_o d$ (p_o is the reduced vapour pressure and d is the electrode separation) is shown in fig. (15). The minimum value of the breakdown potentials, V_{min} in caesium vapour and those of potassium and sodium (48) are shown in table (3.1).

Metal	Cathode	$P_o d_{min}$	V_{min}(volts)
Sodium	Nickel	0.04	355
Potassium	Potassium	0.33	229.5
Caesium	Nickel	0.244	360.2

Comparing these values of V_{min}, Bratescu concluded that the values of breakdown potential (i.e. Paschen curve) obtained in caesium vapour using nickel cathode would resemble those values if a caesium cathode were used. It is highly probable that the work function of his nickel

cathode was nearly equal to that of a caesium cathode (49). However, as it can be seen from table (3.1) that value V_{min} for caesium is higher than those values of the other alkali metals, especially potassium, despite the fact that caesium has got the lowest ionization potential and work function. The reason for the high values of breakdown potentials could be attributed firstly to the loss of photons and excited atoms from the discharge volume since the ratio of the gap separation, d, to electrode diameter, D, ≈ 0.7. In caesium discharge, photons and excited atoms are expected to be active processes, in the breakdown mechanism, and therefore a higher voltage is needed to subsidise for the loss of these particles. Secondly the poor ultimate pressure obtained in his experiment (10^{-5}mm.Hg.) as well as the undegassed electrodes could have been a source of impurities(of mainly oxygen and nitrogen) which could easily change the breakdown mechanism of a metal like caesium. Further discussion and comparison of Bratescu's results with those obtained by the present author will be presented in chapter (6.1).

3.2. PREVIOUS WORK IN MERCURY.

3.2.1. INTRODUCTION

This part of chapter (3) contains a review of the experimental work relevant to the problem of evaluating and identifying the secondary processes involved in the low pressure mercury discharge.

Secondary Ionization Coefficients as a function of E/p
(Smith)

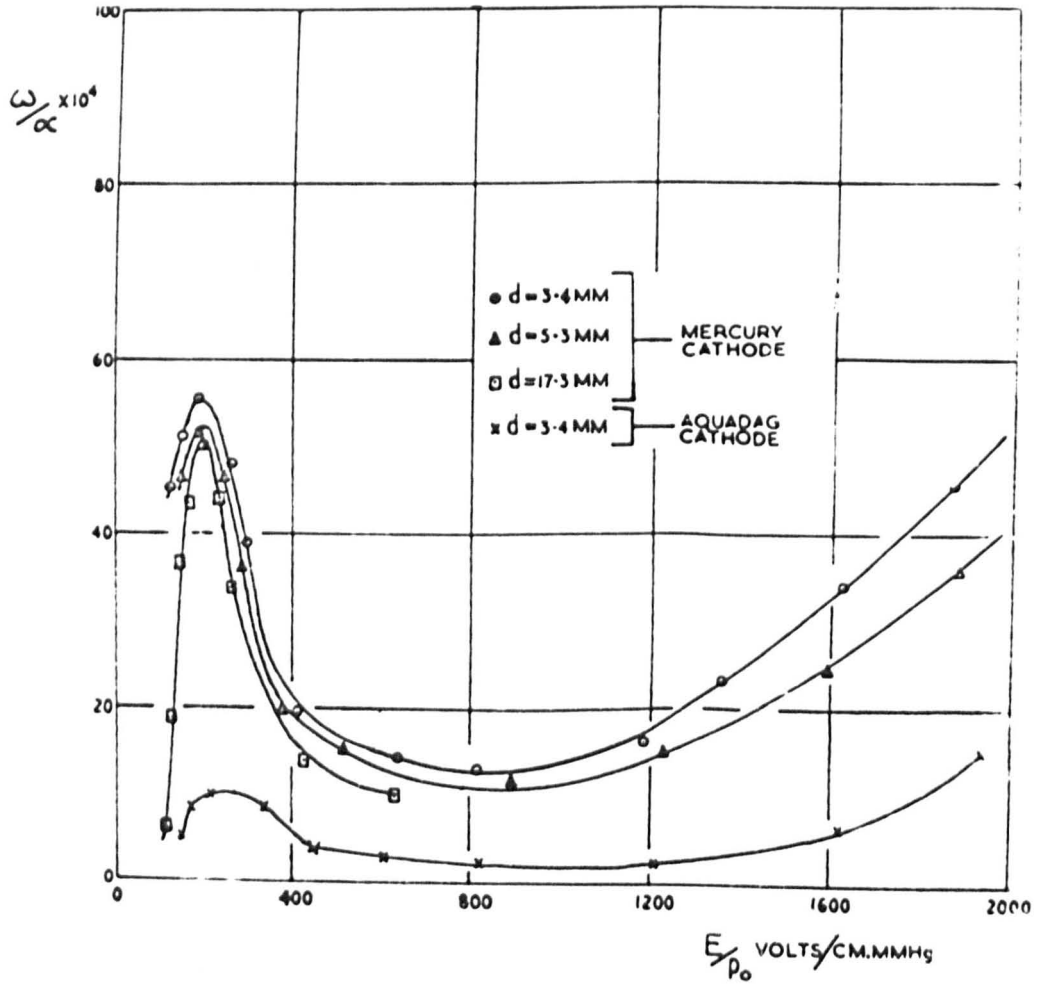

fig.16

The first investigation of any importance in a mercury gas discharge was carried out by Llewellyn-Jones (50) and soon after by Grigorovici(51). They limited their experiments to the measurements of sparking potential in mercury vapour using bulk-metal electrodes. Their work showed that surface effects were important with bulk metal electrodes, either because of amalgamation or condensation. A few years later, Badareu and Bratescu (52) obtained values of α/p as a function of E/p using iron electrodes. However their results were in doubt due to the poor vacuum conditions under which the experiment was done (residual gas pressure of 10^{-4} mm. Hg. attained in the experimental tube before distillation of the mercury).

It was not until recently that, in this laboratory, the mercury discharge parameters (first and second Townsend ionization coefficients) were measured by Smith and Overton under clean consistent conditions. The results obtained by Smith (53) demonstrated that a mercury pool can provide a clean reproducible surface of constant work function, suitable for use as a cathode under the gas discharge conditions. Using the values of α/p_o and of the sparking potentials, Smith (53) obtained curves of the second Townsend coefficient (ω/α) as a function of E/p_o, shown in fig. (16), for three electrode separations. The three curves show the same general trends with high peaks (along the ω/α -axis) at low values of E/p_o, which was attributed to the action of photons (produced by de-excitation of atoms in the resonance states

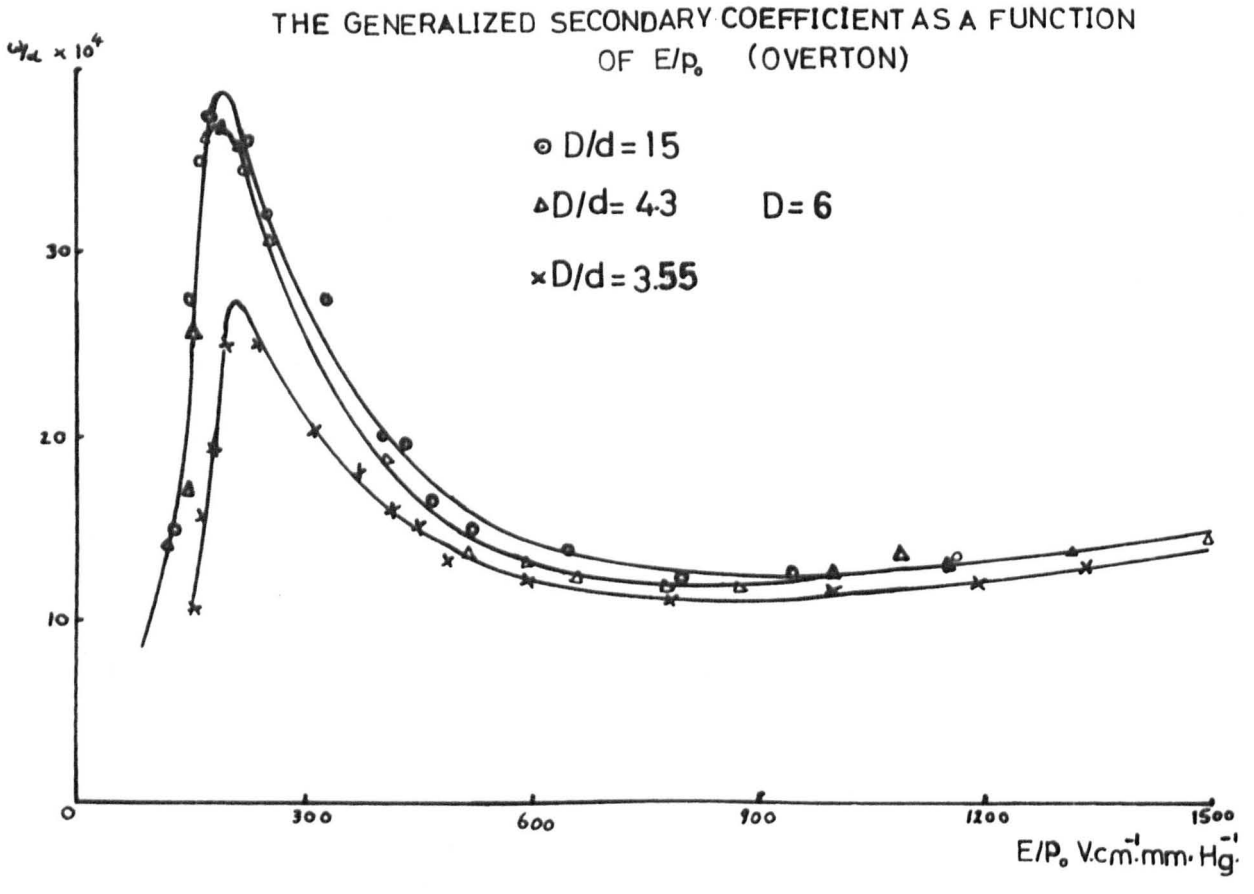
THE GENERALIZED SECONDARY COEFFICIENT AS A FUNCTION OF E/P₀ (OVERTON)
γ/α × 10⁴
⊙ D/d = 15
△ D/d = 4.3
D = 6
× D/d = 3.55
30
20
10
0
300
600
900
1200
1500
E/P₀ V.cm⁻¹.mm.Hg⁻¹

Fig. 17

$^3P_1$ and $^1P_1$) at the cathode. The increased loss of photons from the discharge volume was given as an explanation of the displacement of the curves along the ω/α- axis. Using a graphite cathode it was found that the values of ω/α were much lower than those obtained for mercury cathode because of the higher work function of the graphite.

Later on, Overton (54) using similar techniques confirmed the existence of such peaks in the curves of ω/α at low values of E/p_o shown in fig. (17). The appearance of these peaks was attributed by Overton to the increase in the densities of resonance-photons and metastable atoms. The peaks were observed in the region of E/p_o of 200 V cm^{-1}. $mm.Hg^{-1}$., where the excitation probabilities (5) to the four P-states of mercury, are maximum. The present author has observed similar peaks and also similar displacements of the curves along the ω/α -axis which is accounted for as due to the loss of the active particles as the ratio of the gap separation (d) to the electrode diameter (D), increases.

The increase of ω/α, at higher values of E/p_o (greater than 900 V cm^{-1}.$mm.Hg^{-1}$.), was attributed by Smith to the increase in the emission of secondary electrons produced by the incidence of doubly charged mercury ions (Hg^{++}) on the cathode surface. However, Kovar (55), while determining the mobility of mercury ions in mercury vapour did not detect Hg^{++} although his range of E/p_o extended as far as 1500 V cm^{-1}. $mm.Hg^{-1}$. The only fast ion detected was Hg_2^+ (with a mobility of approximately twice that of the atomic singly charged ion) which could not be

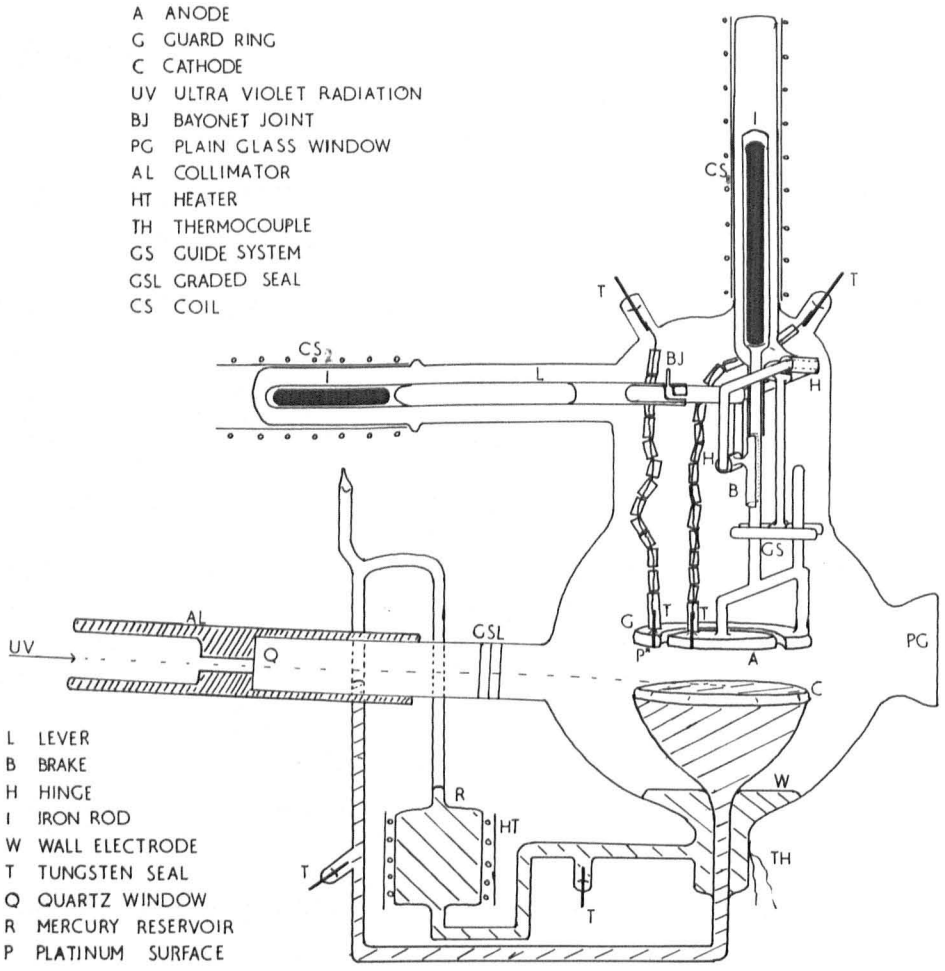
A ANODE
G GUARD RING
C CATHODE
UV ULTRA VIOLET RADIATION
BJ BAYONET JOINT
PG PLAIN GLASS WINDOW
AL COLLIMATOR
HT HEATER
TH THERMOCOUPLE
GS GUIDE SYSTEM
GSL GRADED SEAL
CS COIL
L LEVER
B BRAKE
H HINGE
I IRON ROD
W WALL ELECTRODE
T TUNGSTEN SEAL
Q QUARTZ WINDOW
R MERCURY RESERVOIR
P PLATINUM SURFACE
UV
AL
Q
GSL
CS
I
L
BJ
H
B
GS
T
G
P
A
C
PG
W
TH
R
HT

fig.18

detected above an E/p_o of about 100 V cm^{-1}. $mm.Hg^{-1}$. Taking an advantage of Kovar's measurements, Overton assumed that the emission of secondary electrons from the cathode in the range of $E/p_o > 650V\ cm^{-1}$. $mm.Hg^{-1}$., is entirely due to the incidence of the singly charged positive ions (Hg^+) on the cathode and that they cause the emission of electrons from the cathode by virtue of their potential energy.

In order to facilitate the interpretation of the curve $\omega/\alpha = f(E/p)$ and to find the relative importance of the secondary processes, Overton studied the temporal growth of ionization in mercury vapour. His experiment and results will be discussed in the next section.

3.2.2. THE WORK OF OVERTON.

A diagram of the apparatus is shown in fig. (18). The electrode system consisted of a mercury pool cathode and a glass anode. The mercury forming the cathode was contained in a conical cup attached to the base of the discharge chamber by an internal seal. A wall guard-ring was formed at the base of the chamber during the distillation process. This electrode was connected to the cathode (though electrically separate) via the reservoir R. The reservoir R was surrounded by a heating coil so that mercury could be distilled from the wall electrode to the cathode, thus maintaining the required mercury level in the cathode. The anode, 4 cm. in diameter, was surrounded by a glass guard-ring, making the total diameter of the anode assembly 6 cm. Both anode and

guard-ring were ground smooth and coated with platinum to make them electrically conducting. The anode assembly could be moved perpendicular to the cathode by an electromagnetic device (coil CS_1 and the iron rod I1 shown in the figure (1B)) and was prevented from sliding down by exerting a sufficient fractional force between a brake, B, and the rod supporting the anode. This force was applied on the brake B by activating the iron rod I2 by coil CS_2. Ultra-violet radiation from a high pressure mercury lamp was admitted through the quartz window. The apparatus was baked for 24 hours at 450°C while being pumped by the vacuum system. After sealing the experimental tube from the vacuum system pressure between 10^{-7} and 10^{-8} mm.Hg. was obtained (by using the pressure measuring ionization gauge) before mercury was finally distilled into it. 99.9% pure mercury was admitted into the system and it was twice distilled under vacuum before being finally distilled into the experimental tube. After finishing the distillation, the tube was disconnected from the vacuum system and placed in an electric oven so that vapour pressures could be achieved by regulating the temperature. The temperature was measured by thermo-couples and a maximum difference of 1°C could be detected between any two extreme points (1 metre) inside the oven. Before measuring the formative time lag, Overton (54) measured the Townsend ionization coefficients. Using currents between 10^{-11} and 10^{-8} amps, α/p_o was measured as a function of E/p_o.

For measuring the formative time lag, Overton used a pulse

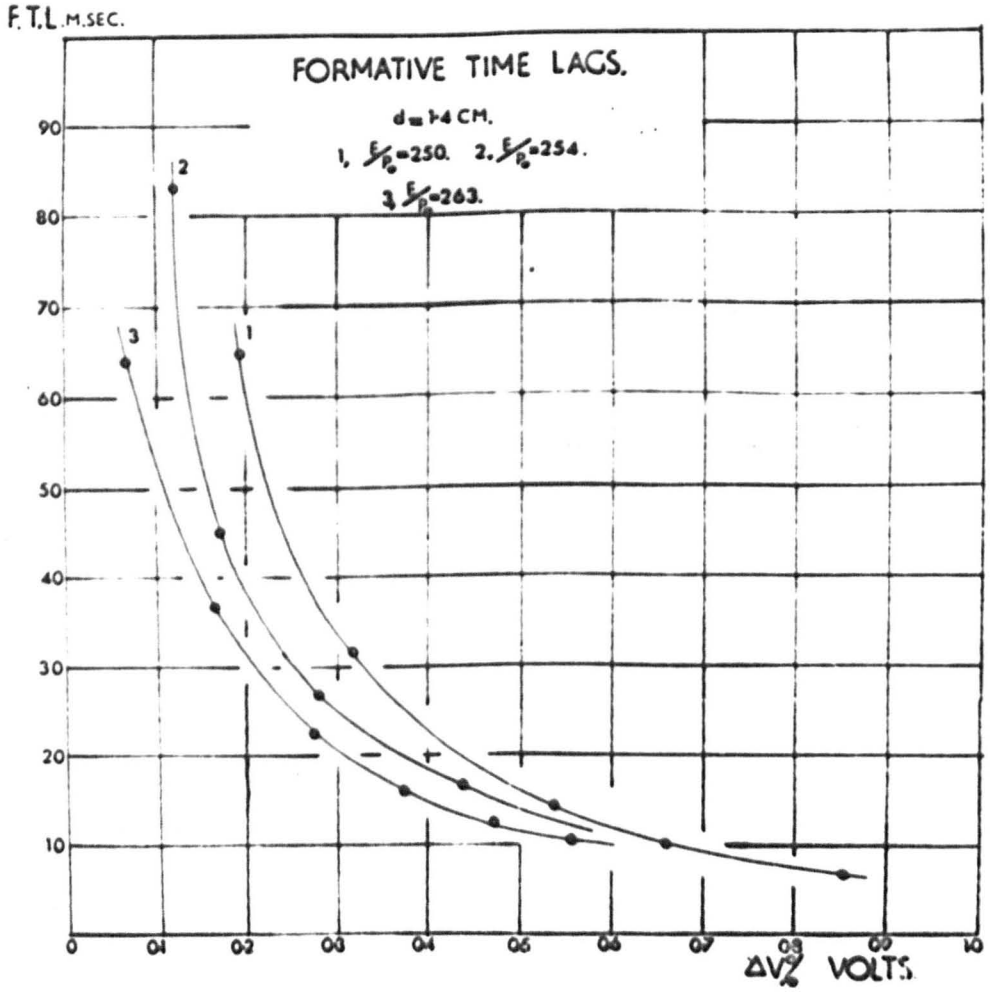
F.T.L. M.SEC.
FORMATIVE TIME LAGS.
d = 1·4 CM.
1, E/p = 250. 2. E/p = 254.
3, E/p = 263.
90
80
70
60
50
40
30
20
10
0
0·1
0·2
0·3
0·4
0·5
0·6
0·7
0·8
0·9
1·0
ΔV VOLTS

Fig. 19

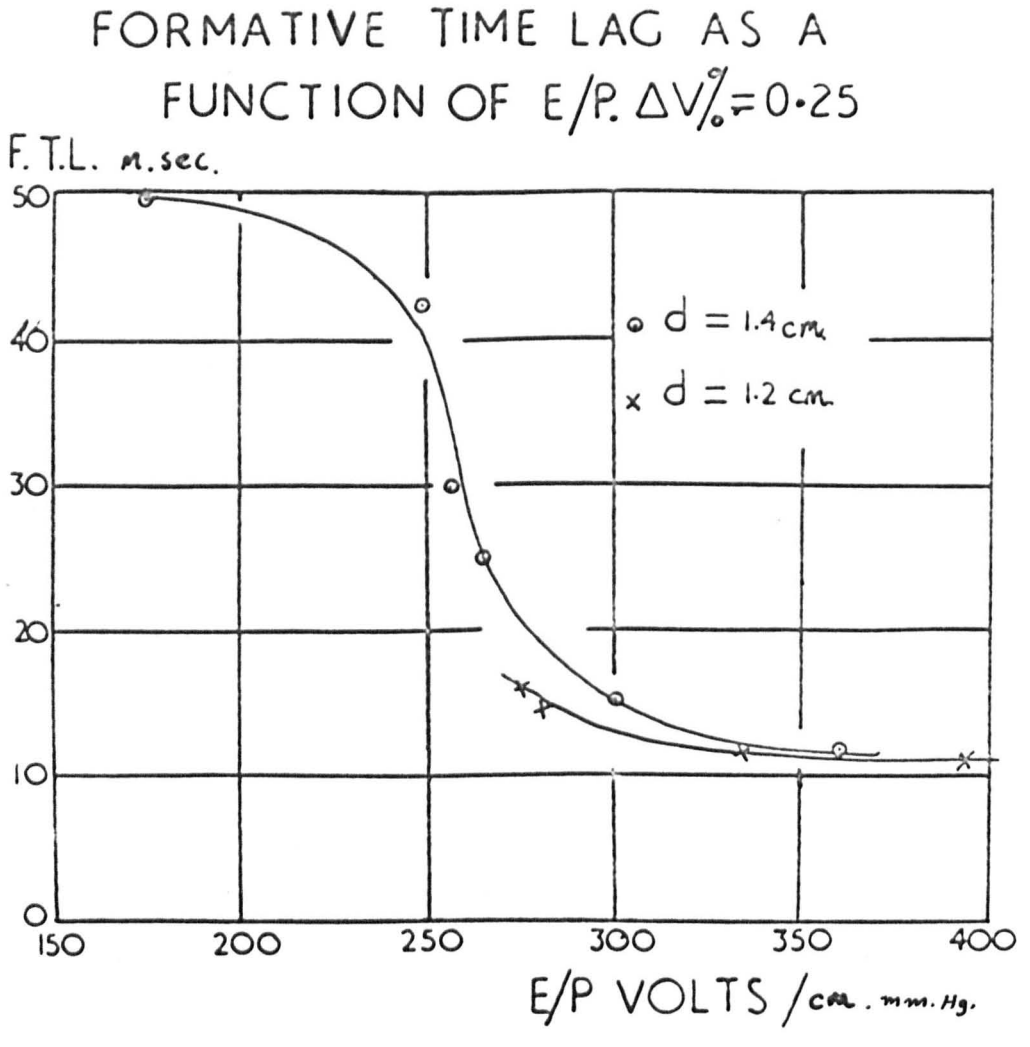
FORMATIVE TIME LAG AS A
FUNCTION OF E/P. ΔV/V = 0·25
F. T. L. m. sec.
50
40
30
20
10
0
150
200
250
300
350
400
o d = 1.4 cm.
x d = 1.2 cm.
E/P VOLTS / cm. mm. Hg.

fig.20

which consisted of the output voltage from a bank of dry batteries. This pulse was applied across the tube by means of a mercury switch which had a rise time of a micro-second. The height of the pulse (or the applied potential across the tube) was controlled by means of a potentiometer. The formative time lag was measured as the time for the current to grow from zero (i.e. from the moment of closing the mercury switch) to the value 10^{-6} amps, at which the current was found to be self maintained. The time taken for the gap to break down, and the magnitude of the current flowing, were measured by a Tektronix Type 454A oscilloscope, the probes of which were connected across the megohm resistance in the cathode circuit. The formative time lag was measured at small values of overvoltages at a particular value of E/p_o. Measurements were carried out in the range of E/p_o from 170 to 500 V cm^{-1}. $mm.Hg^{-1}$. Formative time lags were found of the order of milliseconds. Fig.(19) shows the formative time lags as a function of the percentage of overvoltage $\left[\left(\frac{V-V_s}{V_s}\right) \times 100\right]$ at different values of E/p_o. A plot of the time lag against E/p_o for a given percentage of overvoltage, showed that at values of E/p_o above 170 V.cm^{-1}.$mm.Hg^{-1}$., the breakdown mechanisms were becoming progressively faster. The time lag decreased from 50 milliseconds at an E/p_o of 170 V.cm^{-1}.$mm.Hg^{-1}$., to 12 milliseconds at an E/p_o of 400 V.cm^{-1}. $mm.Hg^{-1}$., this is shown in fig. (20.). Comparison of the two curves in fig. (20) shows that the formative time lag was becoming faster when the

fixed electrodes separation was reduced only from 1.4 cm. to 1.2 cm. Unfortunately, Overton did not take any more measurements at the last electrode separation (1.2 cm.) to show the dependence of the time lags on the electrodes separation. Such dependence is investigated by the present author and it is found that the formative time lag and thus the breakdown processes depend to a great extent on the pressure and on the discharge gap geometry, as will be seen in chapter (6).

Using Davidson theory (chapter 2), Overton (54) analysed his results on the assumption that one or all of the following secondary processes,

(a) the action of delayed resonance radiation,

(b) collision-induced-non-resonance radiation from metastable atoms,

(c) the destruction of metastable atoms at the cathode, were active at the cathode together with,

(d) the action of positive ions.

Assuming an upper limit of 2000 cm^{-1} for the absorption coefficient of the resonance radiation, and that the process of transfer of resonance radiation through mercury vapour is a diffusion process, Overton calculated the time lag when processes (a) and (d) were assumed to be active. Using Davidson's theory (2.2) the times calculated were found to be three orders of magnitude faster than the measured time lags. The next case considered was that of the combined action of metastable atoms (in the states $^3p_2$) and of positive ions at the cathode. The time

lags were calculated (using theory 2.2) for 0%, 20%, 50% and 80% positive ion contribution to ω / α . At an E/p_o of 250 $V.cm^{-1}.mm.Hg^{-1}$, metastable action alone yielded time lags approximately 200 times greater than the measured ones, whereas for 80% positive ion action, Overton found the calculated time lag to be only three times too great. The present author analysed his own results in terms of Davidson's theory (2.2) on the assumption that the two processes considered above (metastable atoms and positive ions) are the only active secondary processes at the cathode. Again as in Overton's case, no combination of the two processes could fully account for the present observed growth of ionization (i.e. formative time lags). The present analysis is discussed later in chapter (6).

Overton performed his last analysis on the assumption that only processes (b)(photons produced from the volume destruction of metastable atoms) and (d) were active. Time lags were calculated (using Davidson's theory 2.3) at four different values of overvoltages and for three different assumed life-times of the mercury metastable atoms. The assumed values of life-times were 5×10^{-3} sec., 10^{-3} sec., and 5×10^{-4} sec. Only three curves of the observed time lags were analysed at values of E/p_o of 250, 358 and 391 $V.cm^{-1}.mm.Hg^{-1}$

At an E/p_o of 250 $V.cm^{-1}.mm.Hg^{-1}$, the time lag was calculated for 0%, 20% 50% and 80% positive ion contribution for the three assumed life-times. Fairly close agreement between the calculated and the

measured time lags was obtained, for 10^{-3} sec. life-time (τ_I) and 80% positive ion contribution (γ) and for 5×10^{-4} sec. and 50% positive ion contribution. The results are summarised in the following table.

Table (3.1)

$\Delta V\%$	0.46	0.67	0.85	1.0	$\gamma\%$	τ sec.
t_{exp} (m.sec.)	15.0	11.0	8.0	7.0		
$t_{calc.}$ (m.sec.)	12.0	10.0	8.0	6.5	80	10^{-3}
$t_{calc.}$ (m.sec.)	12.0	9.0	7.5	6.0	50	5×10^{-4}
$t_{calc.}$ (m.sec.)	6.0	5.0	4.0	3.0	80	5×10^{-4}

At E/p_o of 358 $V.cm^{-1}.mm.Hg^{-1}$, Overton carried out the calculation for 20%, 40% 55% and 80% positive ion contribution in ω/α . A good agreement was found between the calculated and the experimental time lags for 55% positive ions contribution when the life-time of the metastable atoms was taken as 5×10^{-4} sec., as can be seen from table 3.2.

Table 3.2

$\Delta V\%$	0.49	0.77	1.13	1.54
α	4.452	4.464	4.488	4.512
$t_{exp.}$ (m.sec.)	7.25	4.96	3.40	2.40
$t_{calc.}$ (m.sec.)	6.0	4.97	3.84	3.0
λ	614.3	731.6	993.7	1307.9

γ = 55%, ω/α = 22×10^{-4}, p_o = 0.6 mm.Hg., d = 1.4 cm.,

E/p_o = 358, τ = 5×10^{-4} sec. λ , as defined in Chapter 2.

At E/p_o of 391 $V.cm^{-1}.mm.Hg^{-1}$., Overton performed his last calculation of the formative time lag for 20%, 40%, 60% and 80% positive ions contribution in ω/α . The best fit between the measured and the calculated time lags, was foundfor 60% positive ions contribution in ω/α as can be seen from the following table.

Table 3.3

Δ V%	0.53	0.81	1.15	1.54
α	5.279	5.298	5.320	5.345
$t_{exp.}$ (m.sec.)	6.0	4.28	3.20	2.4
$t_{calc.}$ (m.sec.)	5.0	3.72	3.01	2.38
λ	776.4	986.5	1260.3	1638.0

γ = 60%, ω/α = 20×10^{-4}, p_o = 0.63 mm.Hg., d = 1.2 cm., E/p_o = 391.,

τ = 5×10^{-4} sec.

Although a close agreement between the measured and the calculated time lags was found at E/p_o of 358 and 391 $V.cm^{-1}.mm.Hg^{-1}$., the calculated times at E/p_o of 250 $V.cm^{-1}.mm.Hg^{-1}$ show a deviation from the measured ones. The deviation is more pronounced at the smallest value of percentage of over voltage (0.46%), although the analysis was carried

out for only a small range of $\Delta V\%$, between 0.46% and 1.0%, (the present author's measurements of time lags were analysed for a range of $\Delta V\%$ between 0.2% and 2% and in some cases up to 4%). The deviation is not surprising since at all the three values of E/p_o, the nearest agreement was found for a lifetime of 5×10^{-4} sec. The average lifetime of metastable atom is governed by the destruction processes (36) which depend in most cases on the number of collisions per sec. the metastable atom undergoes. It is expected, therefore, that the average lifetime of metastable atoms will be a function of pressure (see section 2.3). The lifetime τ_1, would be expected to be smaller at E/p_o = 250 $V.cm^{-1}$. $mm.\ Hg.^{-1}$; (p_o = 0.98 mm.Hg.,) than at E/p_o of 358 and 391 $V.cm^{-1}$. $mm.Hg^{-1}$ (p_o is 0.6 and 0.63 mm.Hg., respectively). The dependence of the average lifetime of metastable atoms on the pressure is investigated by the present author and it will be discussed in Chapter (6). From the present analysis (Chapter 6), it is found that a lifetime of approximately 50 μ sec. would be expected at E/p_o = 250, which agrees with the lifetime (46.8 predicted by Aubrecht (56), of 46.8 μ sec. A lifetime of approximately 5×10^{-4} sec., would be expected by the present analysis at E/p_o of 358 and 391 $V.cm^{-1}$. $mm.Hg^{-1}$.

3.3 CONCLUSION.

As it can be seen from the previous review, apart from Bratescu's measurement of breakdown potential, the electrical properties of caesium, in the Townsend region, have not been measured yet.

In mercury however, values of the primary and secondary ionization coefficients have been established (Smith (53 and Overton (54)) and have shown that the general behaviour of mercury vapour under controlled discharge conditions is very similar to that of the rare gasses. Overton's measurements of the formative time lag have shown that slow processes are involved in the mercury discharge. His analysis has shown the importance of non-resonance radiation (produced by the volume destruction of metastable atoms) as a secondary process at the values of E/p_o mentioned above.

However, as it has been seen, further measurements of the formative time lags are needed to show its dependence on vapour pressure and gap geometry as well as to confirm Overton's measurements. Analysis of the formative time lag measurements are also required in order to identify and to assist the relative importance of the secondary processes involved in the mercury discharge at low values of E/p_o.

Vacuum system and manifold used in the mercury experiments

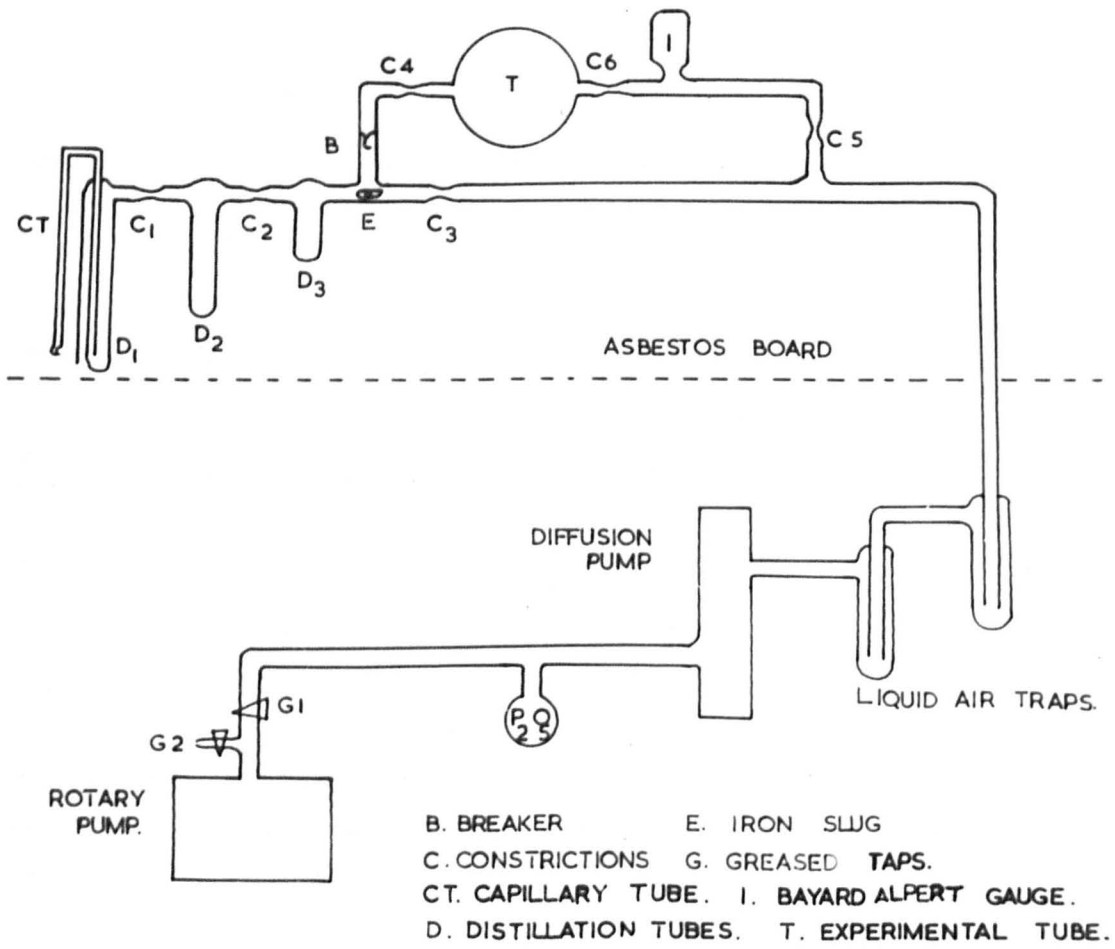

Fig. 21

CHAPTER IV

EXPERIMENTAL APPARATUS

4.1 VACUUM SYSTEM.

A line diagram of the vacuum system used to process the mercury experimental tubes, is shown in fig (21). The system, apart from the rotary pump was made of Pyrex glass. The asbestos board which separated the manifold from the pumping system acted as a support for an electric furnace. This allowed the glass (manifold) to be baked and thus enabled a good ultimate vacuum to be obtained.

The pumping system consisted of a rotary pump in series with a two stage mercury diffusion pump, separated from the latter by a flask containing phosphorous pentoxide, included to protect the rotary pump from moisture. The diffusion pump was connected to the manifold via two liquid air traps which were connected in series. The purpose of the liquid air traps was to condense any mercury on the high vacuum side and prevent it reaching the manifold.

There were two greased taps G1 and G2, which were greased with the minimum amount of "A piezon N" grease. The function of G1 was to isolate the rotary pump from the rest of the system; that of G2 to let the rotary pump up to atmospheric pressure after isolation. No greased taps were present on the high vacuum side of the pumping system.

The manifold consisted of three distillation tubes, D_1, D_2, D_3, connected together in series through constrictions C_1 and C_2. The constriction C_3 separated the distillation tubes from the pumping system. The pigstail breaker B served to isolate the experimental tube T from the distillation tubes. An Edwards ionization gauge (1 G3) was mounted between the experimental tube T, and the constriction C_6. When the constriction C_6 was closed, the ion gauge served as a measuring and pumping device. An iron rod completely surrounded by glass was placed

Vacuum system and manifold used in the caesium experiments

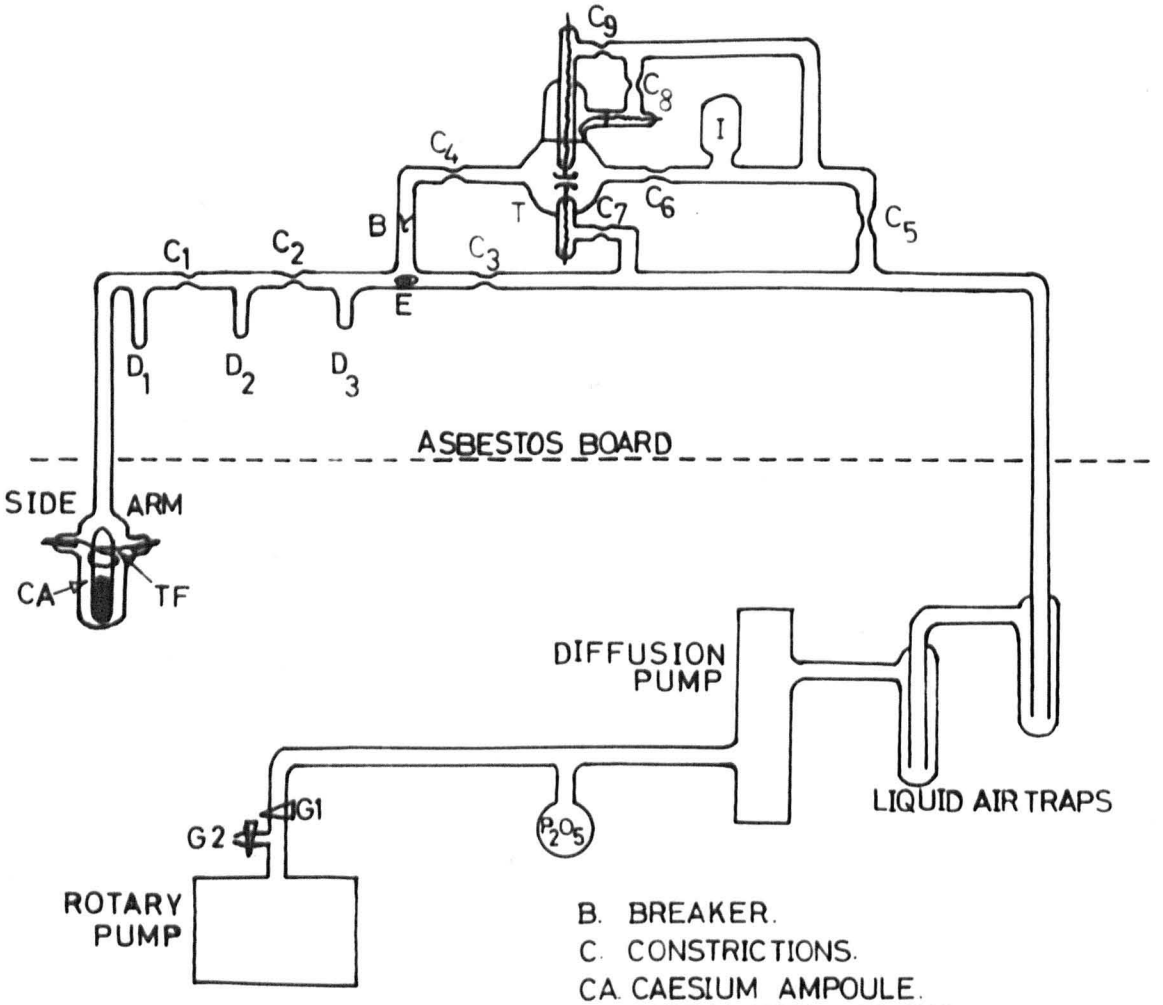

B. BREAKER.
C. CONSTRICTIONS.
CA. CAESIUM AMPOULE.
D. DISTILLATION TUBES.
E. IRON SLUG.
G. GREASED TAPS.
I BAYARD ALPERT GAUGE.
T. EXPERIMENTAL TUBE
T.F. TUNGSTEN FILAMENT.

fig.22

at E in order that the breaker might be smashed when required.

The vacuum system was modified for use with the caesium experimental tubes. A diagram of the apparatus is shown in fig(22). In this case the size of the distillation tubes was much smaller than in the previous case (by about a factor of 100). The distillation tube D_1 was connected to a side-arm, A, which was mounted underneath the asbestos board. The side-arm contained a caesium ampoule which was surrounded by a heater made of thin tungsten wire. Electrical connection to the coil was made through two thick tungsten-pyrex seals. The side-arm was baked at a lower temperature than the rest of the manifold, because the ampoule was made of low melting-point glass.

4.2. THE CAESIUM EXPERIMENTAL TUBES

4.2.1. INTRODUCTION.

Experimentally caesium (and generally the alkali metals) presents a unique set of problems. Appreciable vapour pressures of this metal can be achieved at temperature of a few hundred degrees centigrade. At these high temperatures, the experimental difficulties are caused by two main problems.

(a) Intensive reduction of the oxide film of the glass-tungsten seals (which provide the electrical connection to the electrodes) results either in developing leaks or cracking and thus a complete destruction of the seals. The destruction process takes from one to several hours (in the first tube the seals were destroyed in less than 24 hours at a temperature of 200°C).

(b) The glass becomes electrically conducting so that measurements of the Townsend ionization coefficents would become impossible (a leakage current of $\sim 10^{-4}$A. was flowing on applying 100V between the electrodes in the

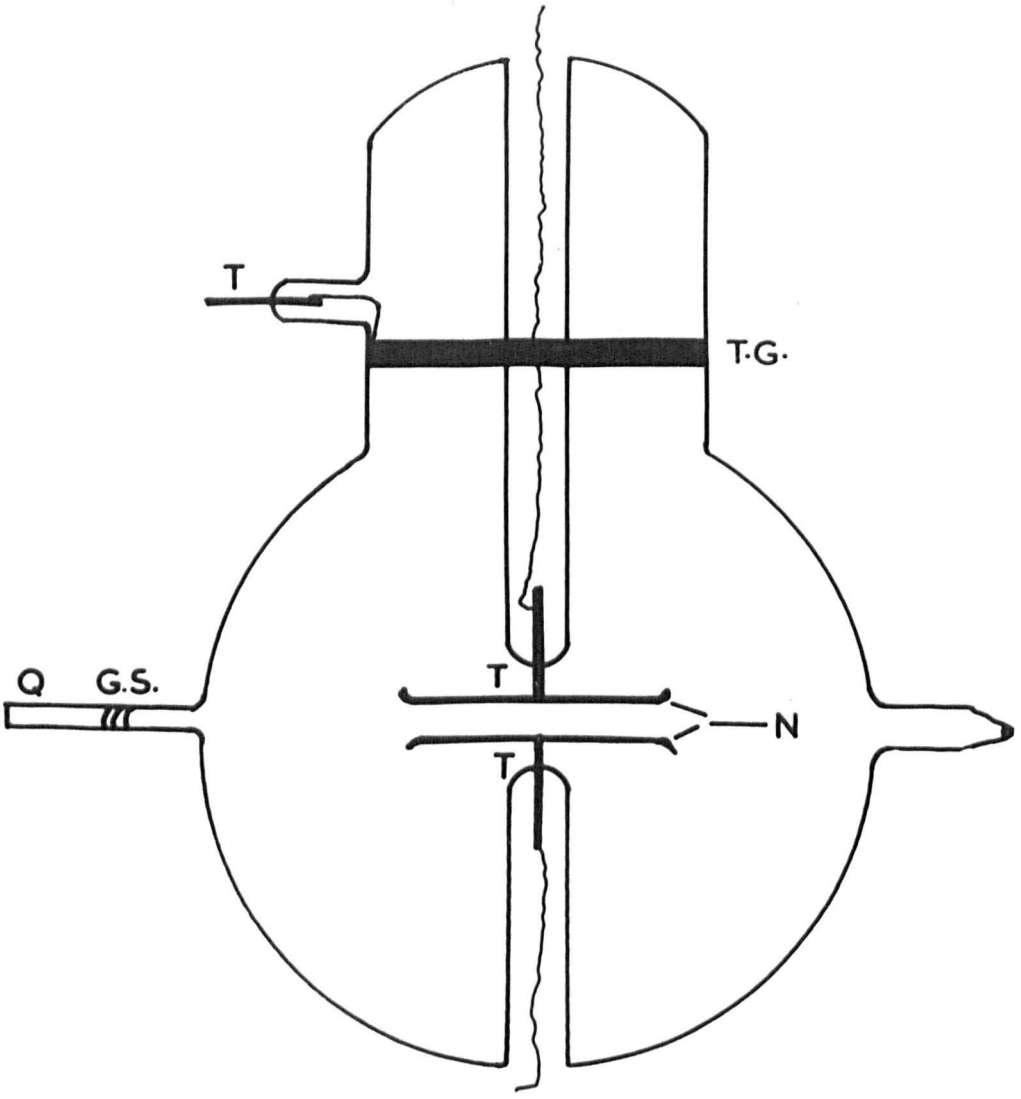

G.S. Graded seal
N. Nickel electrodes
T.G. Tracking guard ring
Q. Quartz window
T. Tungsten-Pyrex seals

The first and second Caesium tubes

Fig. 23

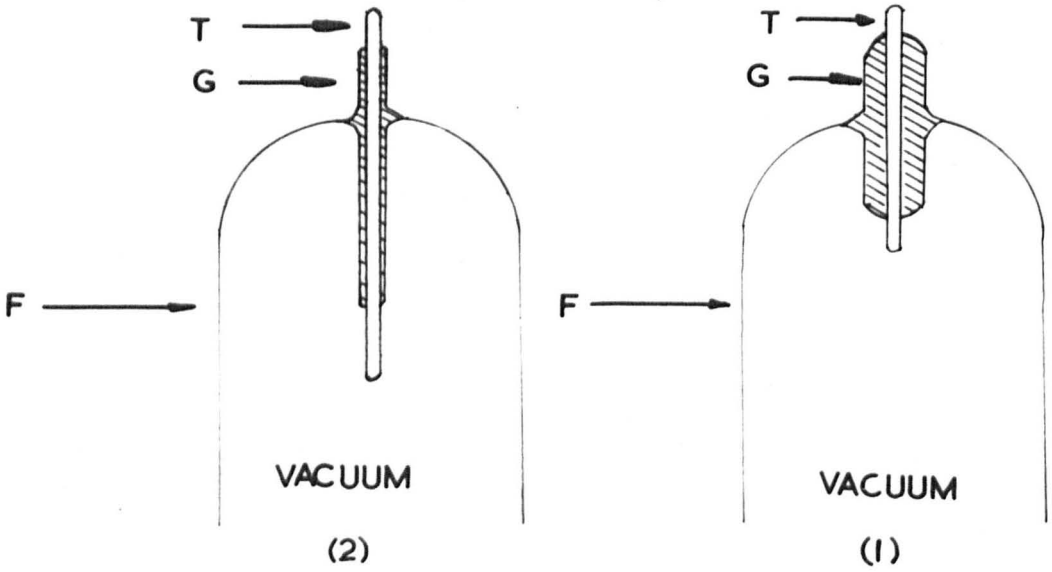

T. TUNGSTEN ROD
G. GLASS FILM
F. GLASS TUBE

Fig. 24

first and second experimental tubes).

Three different tubes were built with different designs before finally the life time of the tungsten-pyrex seals was nearly 20 days (under continuous running at temperatures above 200°C with caesium inside the experimental tubes) and the leakage current was cut down to better than 10^{-8}A.

4.2.2. THE FIRST AND SECOND CAESIUM TUBES.

The two tubes were similar in the general design, fig(23). The main body of each tube was made of a 500 c.c. pyrex boiling flask. The electrodes were made of nickel and had a Rogowski profile to reduce the field distortion and were 5 cm. in diameter. They were polished with a fine emery paper and jeweller's rouge and washed by 30% diluted nitric acid and then by a distilled water. The electrodes were joined to the central tubes by tungsten-pyrex seals which served also as their electrical connections. The separation between the electrodes was 1.23 cm. and 1.18cm. in the first and second tube respectively. Parallelism between the electrodes was within 3%. A graphite guard-ring was painted on the inside of each discharge tube in order to intercept currents travelling along the walls. Connection to each ring was made by a nickel wire joined to a tungsten-pyrex seal in the wall of each tube. The only two differences in the design of the tubes were in the qualities of the tungsten-pyrex seals and in the width of the painted rings. A diagram of the two seals used in tubes (1) and (2) are shown in fig(24). In the case of seal (1), the glass film around the tungsten rod was about 1→1.5mm. thick and was 1cm. long. In seal (2) the thickness was 0.15→0.25mm. and it was 2.5cm. long. Experiments with the first and the second tubes indicated that at a temperature above 200°C, the life time of seal (1) (and thus of the corresponding

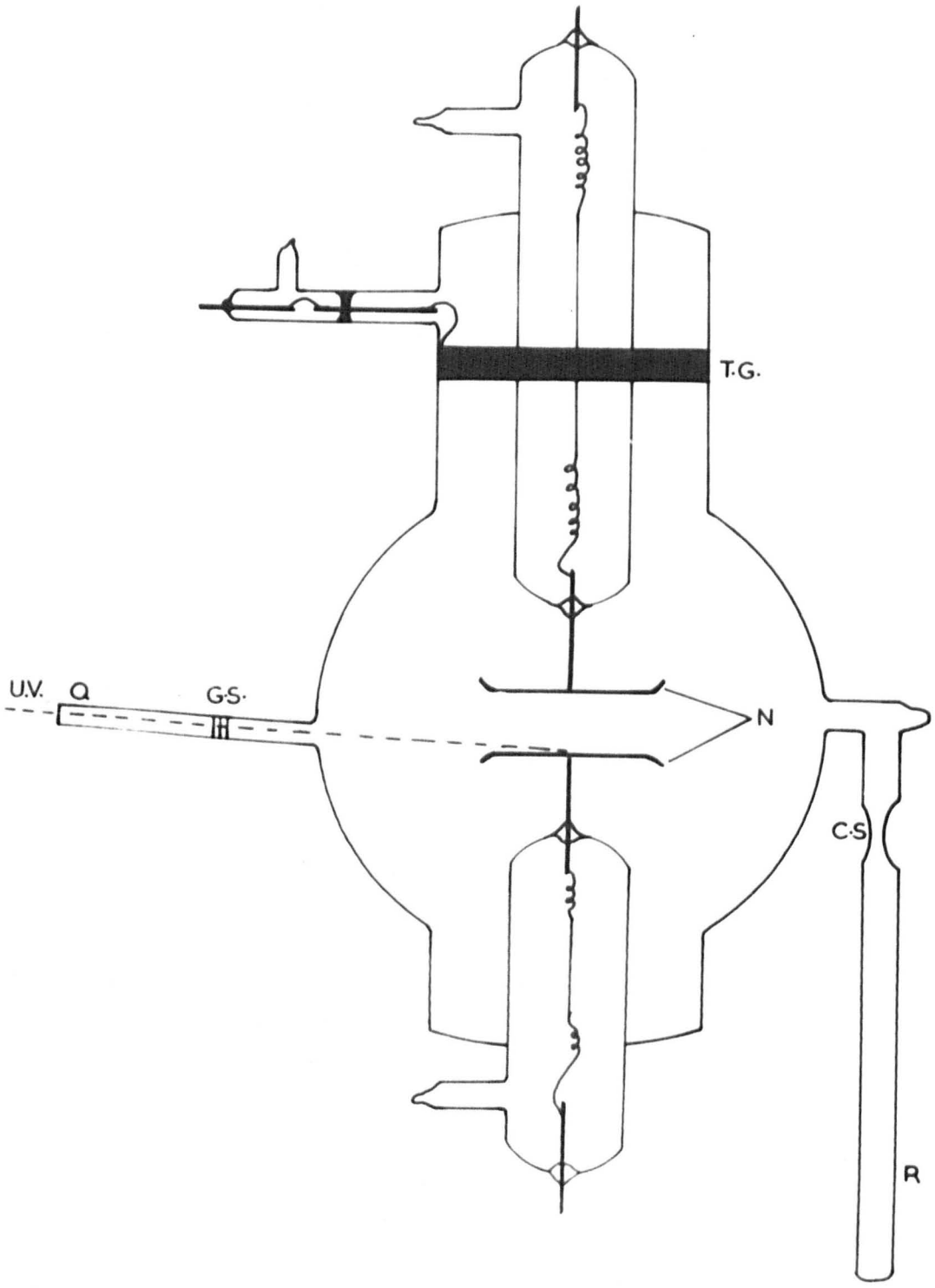

G.S. Graded seal
Q. Quartz window
U.V. Ultra violet radiation
N. Nickel electrodes
T.R. Tracking guard ring
C.S. Constriction
R. Caesium reservoir

The third caesium tube

Fig. 25

discharge tube) was less than 24 hours, while that of seal (2) was about 240 hours. The shortness of the life of seal (1) was caused by the destruction of the entire seal due to the cracks which started at the end of the thick glass film. In the case of seal (2),however, because of the thinness of the glass film, the cracks were localised and owing to the very slow entry of the caesium along the already reduced part of the seal, the reduction process in the next part of the seal was very slow, (and therefore seal (2) lasted ten times longer than seal (1). Close inspection of tube (2) revealed that the seals were not destroyed completely as in tube (1), but the air was starting penetrating inside the tube, probably due to leaks which developed through the slow reduction of the oxide layer at the other end of the seals.

In both tubes, a high leakage current (circuit in fig(34)) of about 10^{-4}A. was found to flow around the walls although the tracking (wall) guard-ring was at the same potential as the anode and the width of the painted ring in tube (2) was five times bigger than in tube (1).

4.2.3. THE THIRD CAESIUM TUBE.

As it has been seen, the seals used in the second caesium tube, proved to be quite satisfactory as it lasted for a period long enough to take enough measurements, on the other hand the leakage current was too large ($\sim 10^{-4}$A). Such high leakage current disturbs the uniform field in the discharge gap. Therefore, the third caesium experimental tube was designed with the object of cutting down the leakage current flowing around the walls, as well as extending the life-time of the tungsten-pyrex seal (and eventually the life-time of the discharge tube). A line diagram of the third caesium tube is shown in fig (25). The electrodes were constructed and treated in the same way as in the first two

caesium tubes and were 1.745 cm. apart. The body of the discharge tube was made of 7cm. diameter Pyrex glass tube which had its wall blown out around the discharge gap. The distance between the circumference of the electrodes and the walls of the discharge tube was more than 3 cm. All the tungsten-Pyrex seals used in this tube were similar to those used in the second tube. To stop air penetrating into the tubes (through the eventual development of leaks or cracks) each electrical connection to the inside of the tube electrodes was made through double (tungsten-Pyrex) seals in series with each other. The side-glass tube between the first and second seal was pumped separately through a constriction and wide bore tube which were connected straight to the main pumping system. The wall guard-ring was painted this time with a very thin layer of platinum of 3 cm. width. The liquid bright platinum (Johnson Matthey Ltd.) was fired before the nickel electrodes were welded in the tube to prevent any attachment of the fumes from the liquid on the electrodes. In an attempt to reduce the leakage current, a side-arm (glass tube) R, was attached to the main discharge tube to act as a caesium reservoir. This reservoir was kept at a lower temperature while taking the measurements. A small diameter (0.6cm.) quartz tube was attached to the discharge tube through a graded seal to facilitate irradiation of the cathode by ultra-violet light.

4.2.4. THE FOURTH, FIFTH CAESIUM TUBES.

Observations made with the third tube proved that the double seals extended the life-time of the tube to approximately a month under continuous running at caesium pressure between 0.1 and 0.5mm.Hg. which corresponds to temperatures between 207°C and 253°C. However, a high leakage current (~ 10^{-6}) was still flowing around the inside walls, even

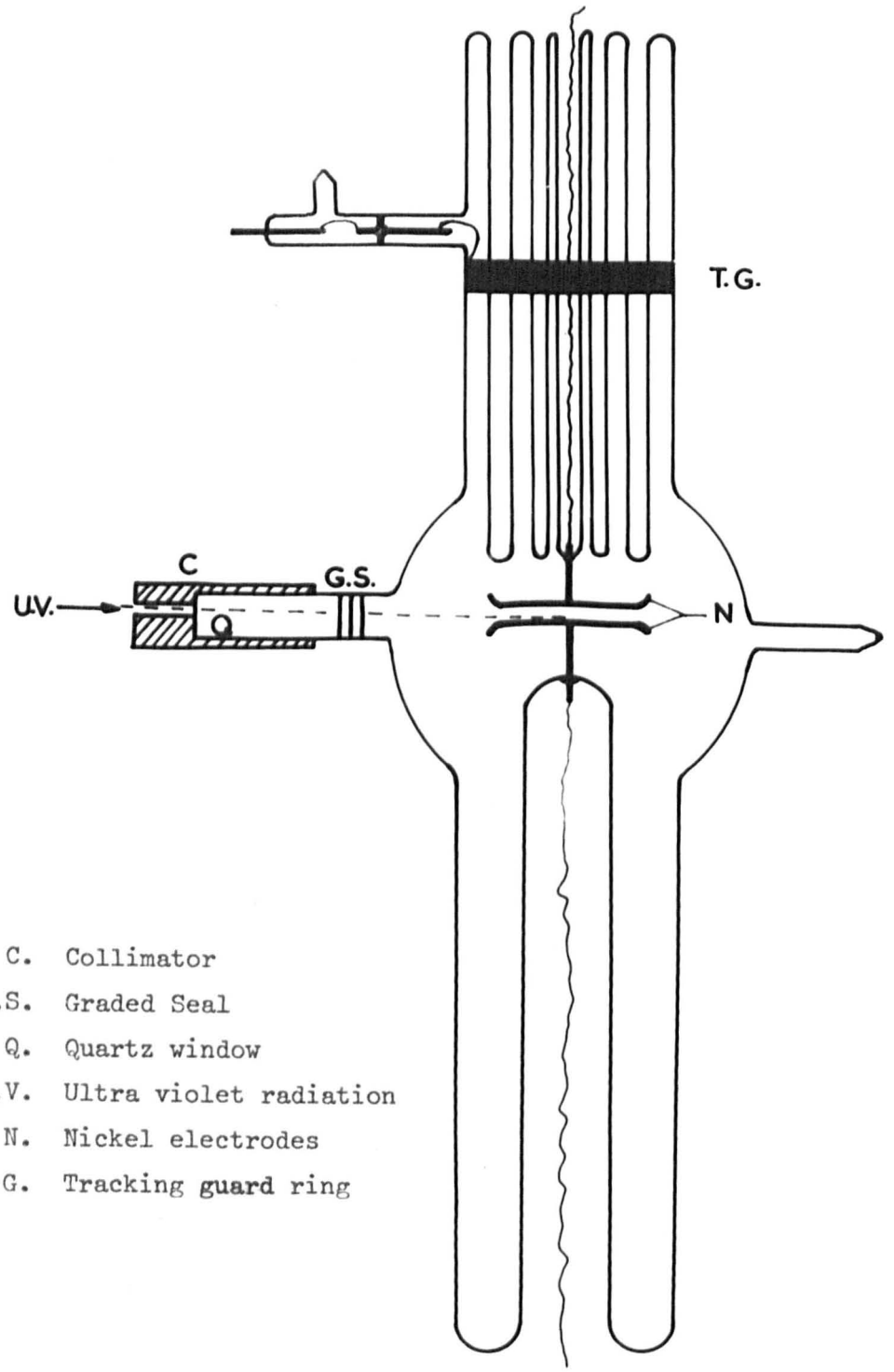

C. Collimator
G.S. Graded Seal
Q. Quartz window
U.V. Ultra violet radiation
N. Nickel electrodes
T.G. Tracking guard ring

The fourth Caesium tube

Fig 26

when the temperature of the reservoir was 150°C lower than that of the discharge tube.

The extension of the tracking path length (distance along the inside walls) betwen the two electrodes (anode and cathode), was found to be more effective in reducing the leakage current. Two different techniques were employed in the fourth and fifth tubes for the extension of the tracking path length.

A line diagram of the fourth tube is shown in fig(26). The tracking path length was extended by corrugating the surface of the top of tube upwards and downwards. The corrugated part consisted of six Pyrex tubes of diameters 0.8, 1.5, 2.5, 4, 5.5 and 7 cm., and were of medium size walls. These tubes were sealed to each other alternately at each end and were arranged to fit inside each other concentrically, so that their walls would not touch each other. Each seal was tested for leaks individually and they were annealed at a temperature of 520°C to get rid of any strains which might have developed during the sealing processes. The outside tube was joined to a 500 C.C. Pyrex flask. The electrodes were supported by central tubes which were sealed to the top and the bottom of the discharge tube. Attachment of the electrodes to the central tubes were made through tungsten-Pyrex seals (of similar kind to those used in the second tube). The length of the tube from the top to the bottom was 50 cm., and that of the corrugated part was 20 cm., which made a tracking path of about 150 cm. Unfortunately, due to the large height of the tube compared to that of the electric oven (~ 60 cm.) it was not possible to make double-seals for the electrical connections to the two electrodes.

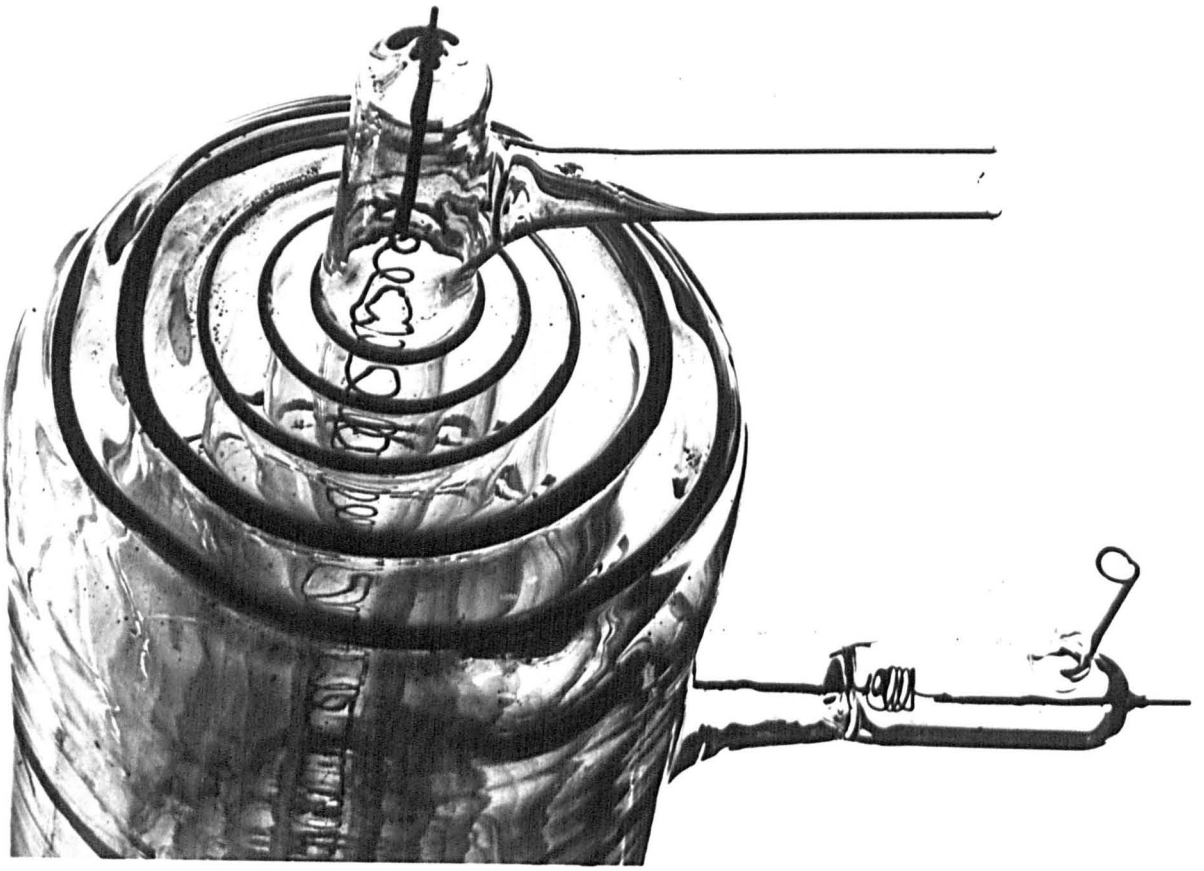

The top of the fifth caesium tube

Fig. 27

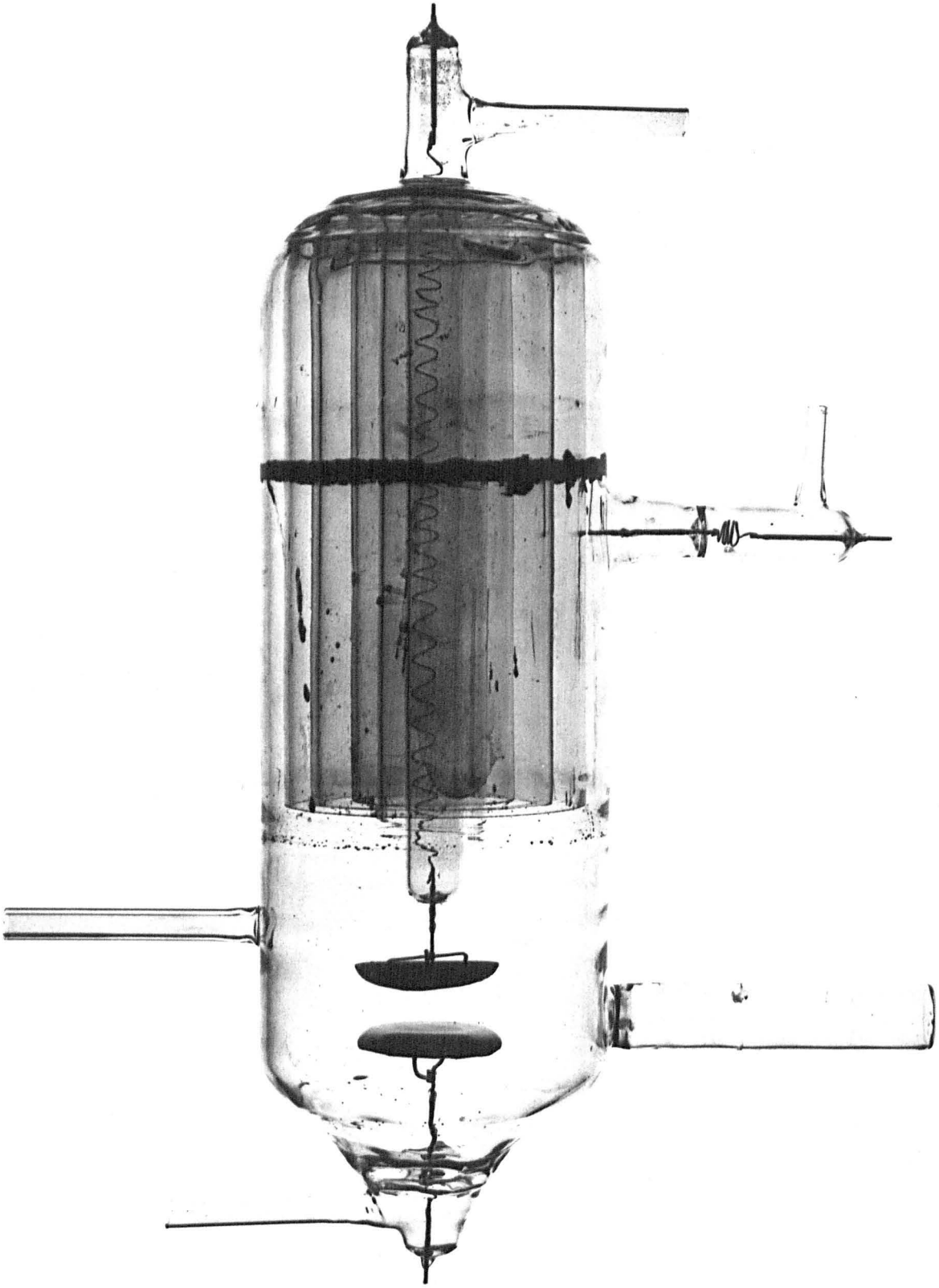

The fifth caesium tube

Fig. 28

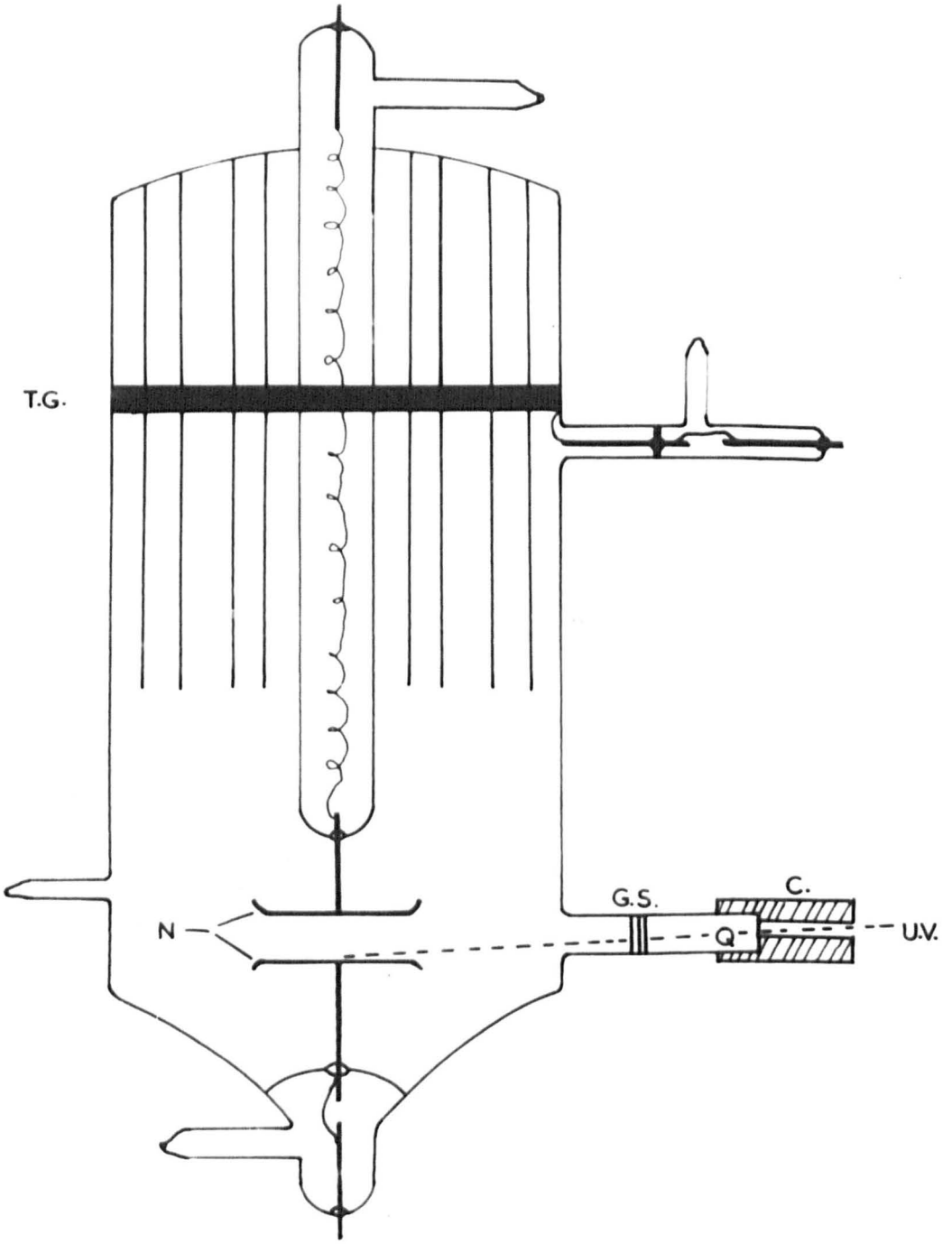

C. Collimator
G.S. Graded seal
Q. Quartz window
U.V. Ultra violet radiation
N. Nickel electrodes
T.G. Tracking guard ring

The fifth caesium tube

Fig. 29

In the fifth tubes, however,the top part was made in a simpler way. A Pyrex tube of diameter 17c.m., was sealed at one end and five tubes of different small diameters and each of length 20cm., were clamped inside it concentrically. All the five tubes were then joined to the sealed top of the outside tube by internal seals. While these seals were hot the top of the central tube was blown out and another tube was joined to it. A photograph of the top of the tube is shown in fig(27). The bottom of the outside tube had a small diameter tube joined by an internal seal in the inside and another small tube from the outside, as shown in the photograph and the line diagram im figs.(28) and (29).

The length of the whole tube was 4.5cm., and that of the attached tubes at the top was 20 cm., which constituted a tracking path length of about 230cm. Because of the shorter length of the tube (compared to fourth tube) all electrical connections to the electrodes were made through double-tungsten-Pyrex seals similar to those used in the third tube. In both tubes the wall guard-rings were made with a very thin layer of platinum, and were 1 cm. wide. Electrical connections to both guard-rings were made through the double seals. The electrodes used in these two tubes were made from nickel, and were constructed and treated in the same way as in the first two tubes. The electrode separations were 0.566 cm., and 1.65 cm., in the fourth and fifth tubes respectively. Parallelism between any pair of electrodes was within 3% accuracy. A wide diameter (1.5cm.) quartz window was attached to each tube through a graded seal for the irradiation of the cathode by ultra-violet radiation. Collimation of the radiation was achieved by an appropriately machined cylinder(of small diameter 0.3cm.) made of Copper, mounted over each

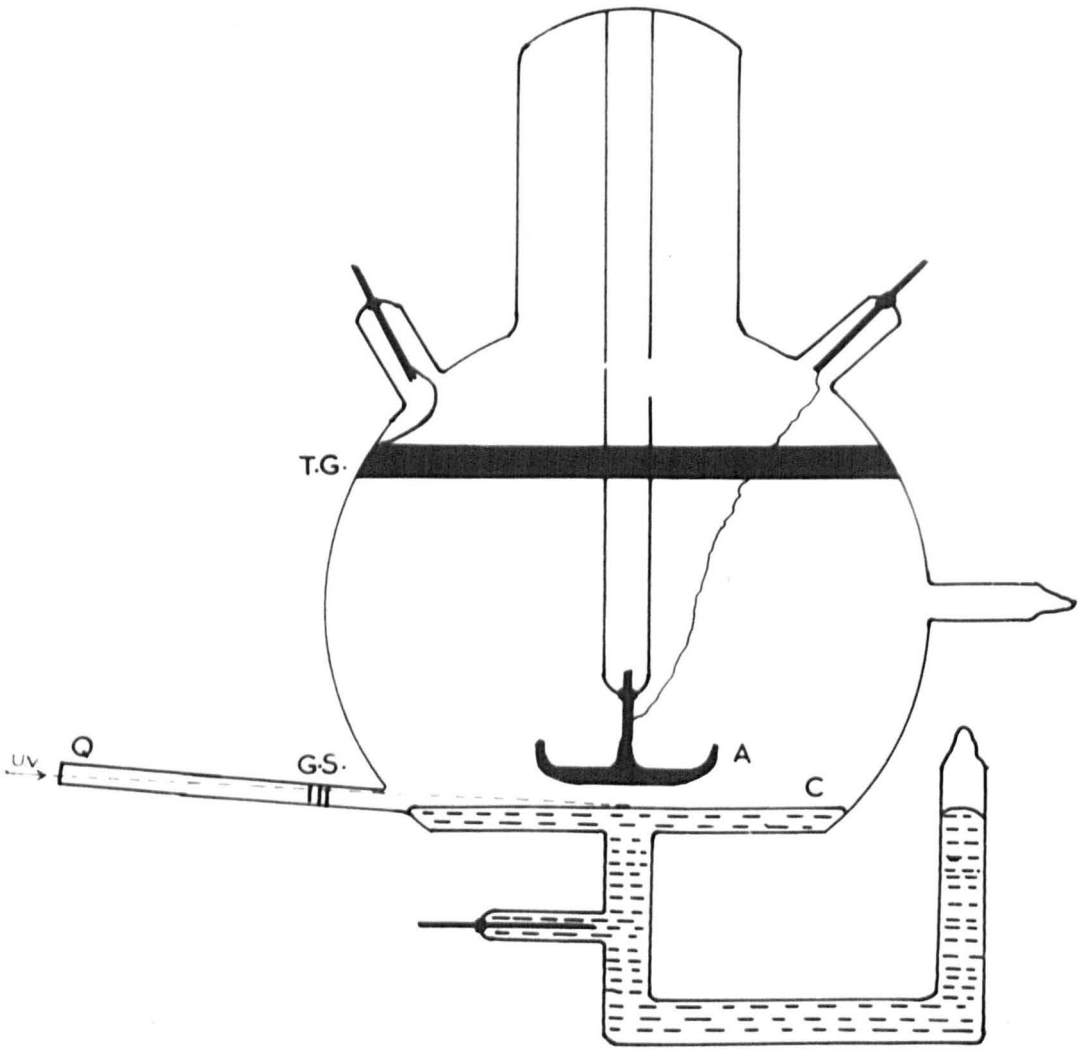

A.	Anode	T.G.	Tracking Guard ring
C.	Liquid mercury cathode	Q.	Quartz window
G.S.	Graded seal	U.V.	Ultra violet radiation

The first mercury tube

Fig. 30

quartz window.

Each experimental caesium tube was connected to the distillation system via a breaker and a length of narrow bore tubing which could be easily collapsed and sealed after the caesium had been distilled into the tube. The main body of each discharge tube and the side-tubes (which contained the double seals) were joined to the pumping system via a wide bore tube which had constrictions.

4.3. THE MERCURY EXPERIMENTAL TUBES.

4.3.1. THE FIRST MERCURY TUBE.

A line diagram of the tube is shown in fig(30). The tube was made of a rounded flask with a flat bottom. The electrode system consisted of a mercury pool cathode and a stainless steel anode, which had a Rogowski profile. The neck of the flask, unfortunately limited the anode diameter to 4 cm. The anode was ground smooth using successively finer grades of emery paper, then polished by using a mixture of jeweller's rouge and Brasso. It was finally washed by tetrachloroethylene and distilled water successively. The anode was supported at the centre of the tube by a small diameter (1 cm.) glass tube sealed to a tungsten rod which was spot welded to the anode. The glass tube was fixed in position by means of an internal seal at the top of the neck of the tube. Care was taken to ensure approximate parallelism between the anode and the flat bottom of the tube, while sealing the anode to the central tube. A fine nickel wire was attached to the tungsten rod (which was spot welded to the anode) and to a tungsten seal in the walls of the tube to provide the electrical connection to the anode. Connection to the mercury pool was provided through a tungsten-Pyrex seal in the base of the tube.

A graphite ring was painted on the inside of the discharge chamber in order to intercept currents flowing along the walls of the tube. Electrical connection to the ring was made by a nickel wire joined to a tungsten seal in the wall of the tube. A quartz window was joined to the tube through a graded seal and positioned at such an angle that Ultra-violet radiation transmitted through it would strike the cathode at almost grazing incidence and provide an efficient source of photo-electrons. The quartz window had a diameter of about 0.3 cm. The distance between the periphery of the anode and the walls of the tube was approximately 3cm., which was approximately five times bigger than the electrode separation.

The tube was connected to the distillation apparatus via a breaker and a length of a narrow bore tube (C_4) which could easily be collapsed after the mercury had been distilled into the tube. A tube of wider bore containing a constriction (C_6) served as a pumping arm. The experimental tube could be removed from the manifold after sealing the constrictions. A thermo-couple was strapped to the outer wall of the base of the discharge chamber so that the temperature of the mercury pool could be determined.

4.3.2. THE SECOND MERCURY TUBE.

Preliminary measurements show that at an E/po < 250 V.cm.$^{-1}$ mm.Hg.$^{-1}$, the formative time lag was not dependent only on the gap geometry (i.e. ratio of the electrodes diameter D to the electrode separation, d) but also on the pressure. Therefore, in the design of the second mercury tube, electrodes of large diameters with small variable separation distances were used. This design enabled the formative time lag to be measured for higher ratios of D/d and for a wide range of pressures. A photograph of the tube, during mercury distillation, is shown in fig(31), and a line

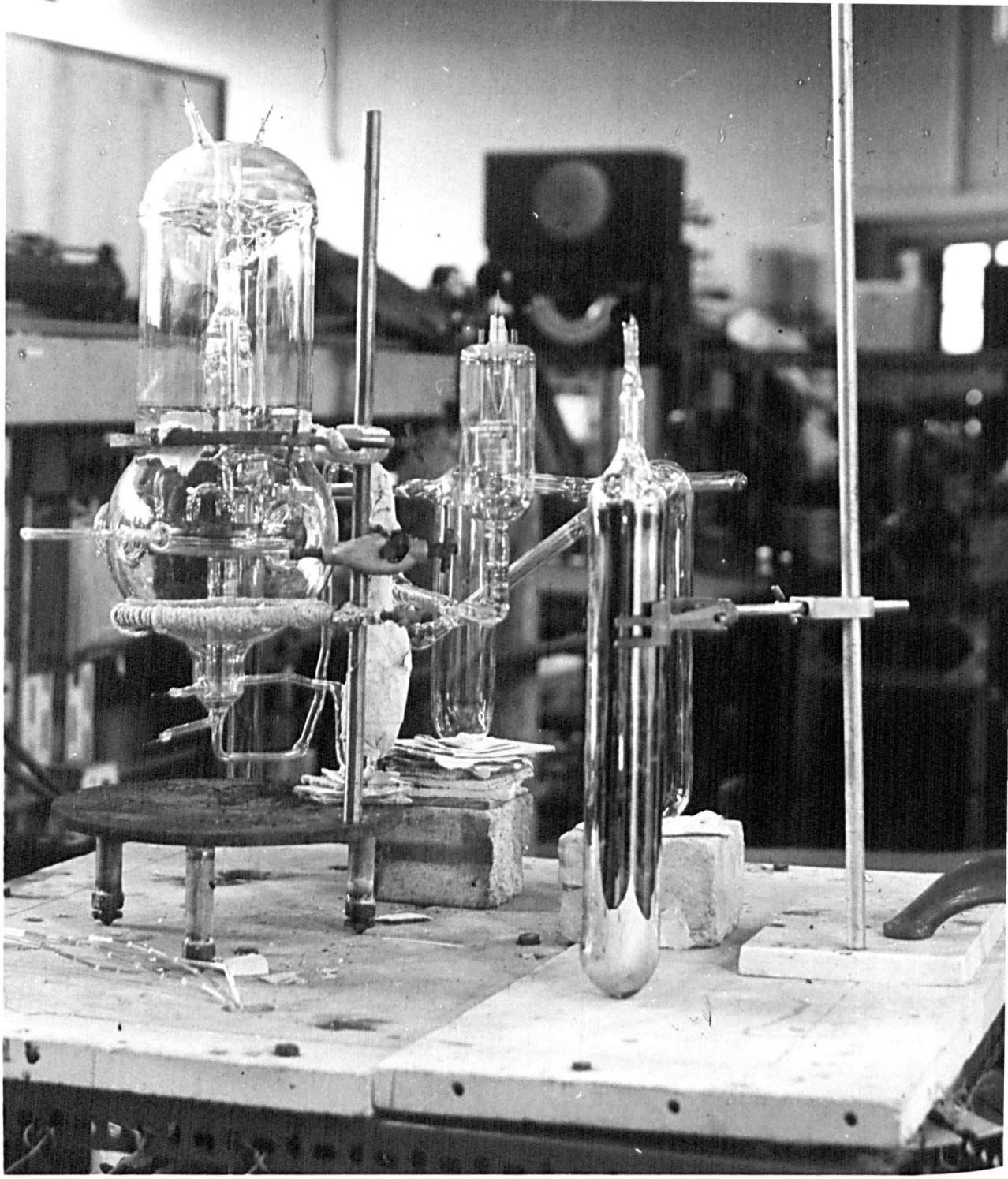

Photograph of the second mercury tube

Fig. 31

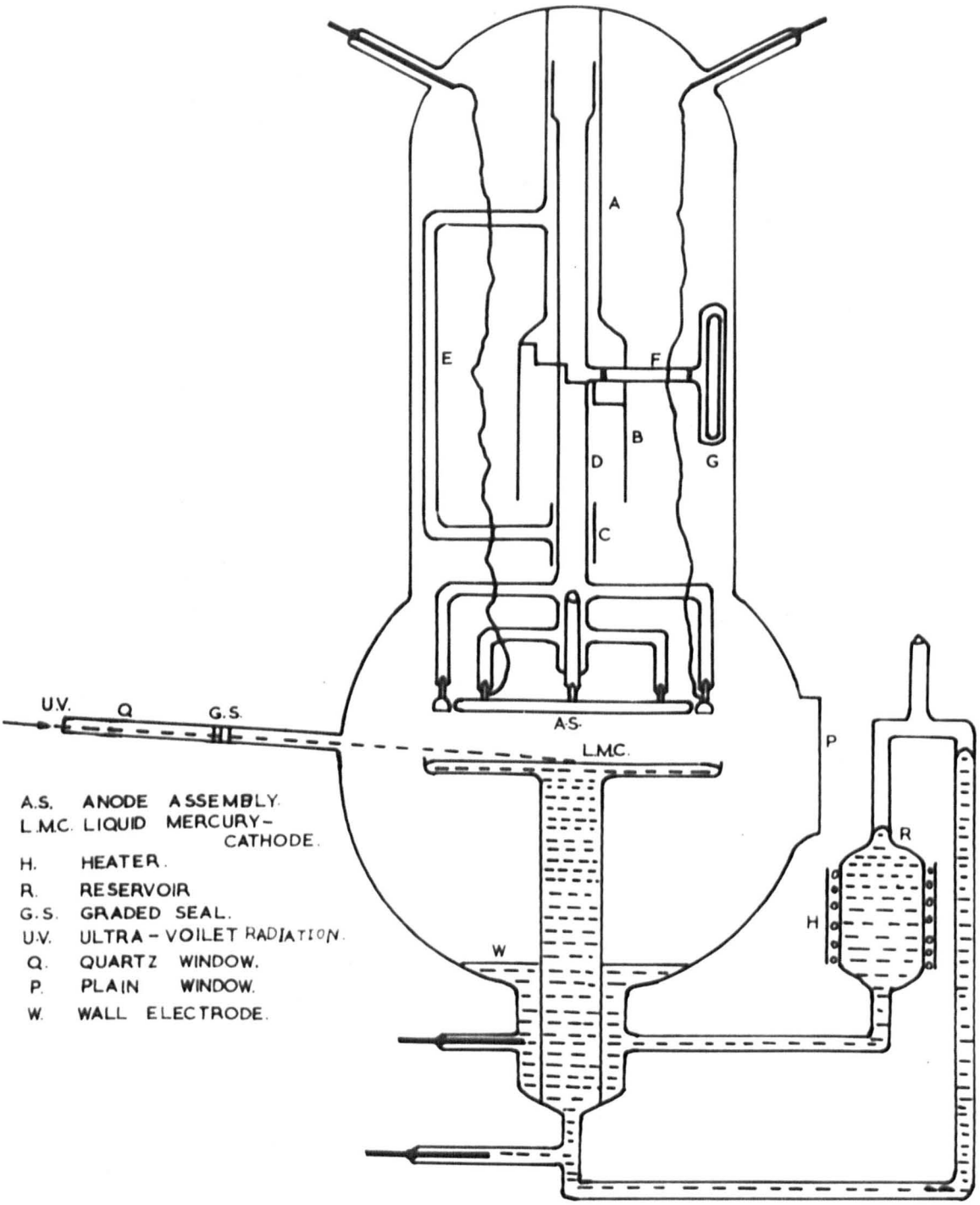

The second mercury tube

Fig. 32

diagram of the same tube is shown in fig (32). The main body of the discharge tube was made of pyrex flask of diameter 17cm. The neck of the flask was made of pyrex tube of diameter 11.8cm. The electrode system consisted of a mercury pool cathode and of anode disk and guard-ring. The diameter of the anode was 8.7cm., and that of the anode and guard-ring, 0.5cm. wide ,taken together, was 10cm. Both electrodes were made of antimagnetic stainless steel (grade EN58E), and were ground smooth and polished by Beck and Moss Ltd. (Faraday Works, Hanley, Stoke-on-Trent, England). The maximum deviation from flatness at any region on the surface of the electrodes was not greater than 0.005cm. The anode and guard-ring were each supported by four glass branches coming out from a central tube, D. Each electrode was attached to these branches in the following way. Four blind holes were drilled at equal intervals round the back surfaces of the electrodes. Into each of these eight holes was screwed a piece of stainless steel studding which had been welded at the top to a tungsten rod. The electrodes were adjusted symmetrically on a flat surface, then all the tungsten rods were sealed into the glass branches of the central tube. In order to prevent the electrodes being strained during this process every two tungsten rods that were diametrically opposite were sealed at the same time. After the eight seals had been completed they were all annealed together. During the sealing process, the electrodes were covered with asbestos to prevent them being oxidised by over-heating. The anode assembly was held in the central plane by passing the central tube, D, through two close-fitting tubes A and C. The close-fitting tube C was held in position by joining its widened end to a tube E which was joined at its other end to the other close-fitting tube A. Due to the small diameter of the central tube, D, it was joined at its top to another bigger diameter tube which just fitted inside the close-

fitting tube, A. The close-fitting tube, A, was connected to the top of the main body of the discharge tube by an internal seal. Tube A was widened at its other end and joined to a large diameter tube, B, which had half of its upper top sloped and serrated. The central tube, and thus the anode assembly, was held in the vertical position by joining the central tube at right angles to a glass rod, F, which rested on one of the notches. Joined to the glass rod was a metal rod enclosed in a glass tube, G, so that a magnet could be used to select different notches to hold the glass rod, F, and thus the height of the anode assembly above the mercury pool could be altered.

The mercury forming the cathode was contained in a flat bottomed cup of diameter 11cm. A flat surface was necessary so that the mercury cathode to be formed could have the largest possible surface area with the minimum amount of distilled mercury. The cup was attached to the base of the discharge tube by an internal seal. A wall guard-ring was formed at the base of the discharge tube during the distillation process. This electrode (wall guard-ring) was connected to the cathode (though electrically separate) via the reservoir, R. This was surrounded by a heating coil so that mercury could be distilled from the wall electrode to the cathode thus maintaining the required cathode level. This method of maintaining the correct amount of mercury in the cathode was simple and convenient as no mechanical disturbance of the tube was required and the level could be restored without moving the electric furnace.

A small diameter (0.3cm.) quartz window was attached to the discharge chamber at such angle that irradiation of the centre of the cathode could be achieved at grazing incidence by Ultra-violet radiation.

Electrical contacts to the electrodes were made by tungsten seals and nickel tape. Observations of the electrode separation were made through two plain glass windows, which were built at right angles to each other. The tube was connected to the vacuum system in the same way as in the first experiment.

4.4. THE ELECTRIC OVEN.

The electric oven used in these studies is the one used by Smith (53) and Overton (54). It was an air oven, which consisted of two enclosures, one inside the other. The inner enclosure consisted of a cube of side 2'-3" and was constructed from ½" thick steel plate. The outer container was a cube of side 4' made from hard asbestos and lined on its outer faces with polished aluminium sheet to reduce heat losses. The amount of air space between the inner faces of the outer box and outer faces of the inner box was about 6" all around. Three heating elements were mounted on each of the inner faces of the outer box. These elements were mounted obliquely across each face to assist the even distribution of heat. These heaters were connected to the mains through 8A Variac transformers gauged together so that they could be operated simultaneously. The transformers enabled the temperature of the oven to be adjusted to any desired value up to a maximum of 300°C. Four calibrated copper-constanton thermo-couples were used to test the oven for temperature gradients. These were mounted at different parts and at different heights inside the inner box. The maximum difference in temperature that could be detected between the extremes of the oven was 2°C. This meant that the variation in temperature in the centre, in the region of the experimental tube, was about 0.2°C.

Illumination, inspection of the inter-electrodes separation, and irradiation of the cathode by Ultra-violet, were made through windows 2" in diameter which were drilled in the centre of each lateral face of each container. Leads to the thermo-couples and to various electrical connections to the experimental tubes were taken out through the base of the oven through glass tubes and attached to coaxial sockets on a panel fixed to the main frame. In the case of the anode and cathode leads, the glass tubing was encased in copper conduit piping and fixed rigidly in position. This reduced vibration and the production of small charges by friction. The inner steel box and the copper pipes were earthed, and thus provided an efficient electrostatic screen. In this way measurement of currents of the order of 10^{-11}A were possible.

In the case of the third caesium experimental tube, a small oven was attached to the big oven through its base to regulate the temperature of the side-arm which contained the caesium reservoir. This small oven consisted of copper pipe of bigger inner diameter than the outer diameter of the side-arm tube. The lower end of the pipe was closed and the other was screwed to the base of the big oven.

A heater wire was wrapped regularly around the outer surface of the copper pipe, which ensured even heat distribution around the side-arm. The heater was electrically isolated from the copper tube by thin sheets of mica and was driven by a stabilized power supply of 2.5 KW output. The temperature of the reservoir was measured by a thermo-couple strapped to the walls of the side-arm.

4.5 THE VOLTAGE SOURCE.

The D.C. voltages were obtained from a bank of dry cells connected

VOLTAGE SOURCE

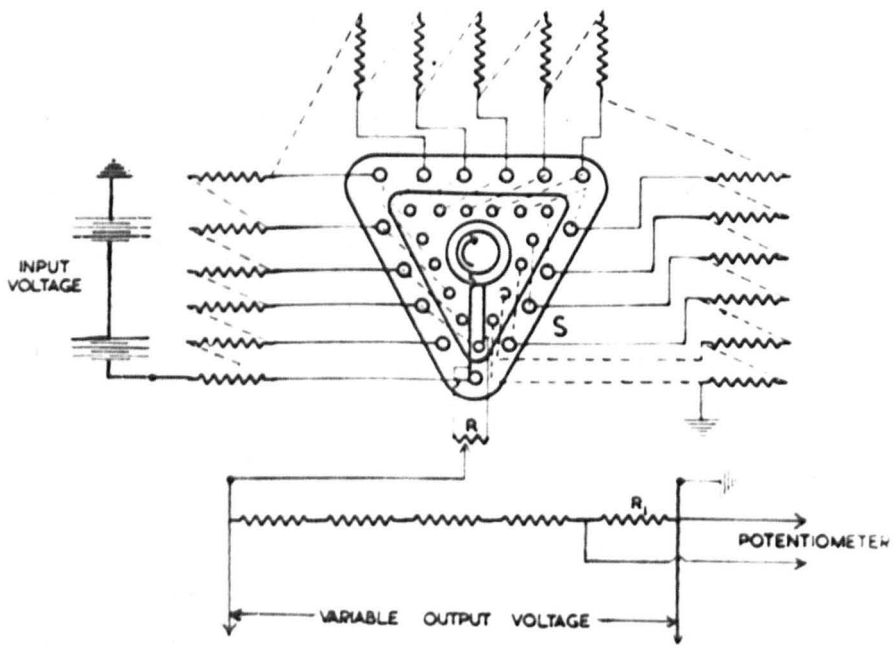

Fig. 33

in series through a chain of 500 kr resistors. These resistors were wired to a double bank selector switch, S, (fig. 33), enabling various voltages to be tapped. A 250 k Ω wire-wound potentiometer, R, was connected across the output of the switch. The centre terminal of this potentiometer was used as the high tension output, enabling the voltage to be varied by less than 0.1v.

The output voltage was measured by applying it across a chain of calibrated resistances, each of the order of a megohm. This chain was wired in series with a calibrated wire-wound 15 k Ω resistor, R_1, and the voltage drop across this resistor measured with a potentiometer. The multiplication of this voltage by the appropriate factor gave the value of the output voltage. The apparatus described above was used in the measurement of breakdown ptoentials, first ionization coefficents and formative time-lags. The techniques used in obtaining these measurements will be described in the following chapter.

CHAPTER V

EXPERIMENTAL PROCEDURE

5.1 VACUUM TECHNIQUES.

All grease and dust particles were removed from glassware before it was assembled by washing it thoroughly, first in 30% diluted nitric acid and then in distilled water. After the assembly, the system was evacuated to a pressure of 10^{-3} mm.Hg. by means of the rotary backing pump, and was tested for leaks by using a "Tesvac" high frequency leak detector. Once it was established that the system was free of leaks large enough to be detected by this method, the mercury pump was switched on, and liquid nitrogen was added to the liquid air traps to condense any mercury vapour and thus prevent it from reaching the manifold.

The Bayard-Alpert gauge was outgassed in two stages, firstly the filament alone by resistive heating and then the grid and the collector together were outgassed by electron bombardment from the filament. The maximum currents used in the two stages were those values quoted in the manufacture catalogue. The manifold was then covered with a large electric oven and baked at 450°C for about one day with continuous pumping. In the caesium vacuum system the side-arm was baked alone at 250°C by an electric "Isotape" heater. The pressure at this stage was about 8×10^{-7} mm.Hg. Hydrogen from a cylinder was then introduced into the system through a rubber tube between the cylinder gauge head and tap (G2). A glow discharge was initiated by applying 700 D.C. V. between the electrodes of the experimental tubes. The current passing between the electrodes was limited to a value of 10^{-3}A., by using a variable resistor (of about 1 megohm) in series with the cathode. After passing the discharge for a period of half-hour, the polarity of the electrodes was reversed, and the

discharge was passed again for nearly the same period. This was done in an attempt to remove any oxidized surfaces on the electrodes, by bombarding them with hydrogen positive ions. In the mercury tubes, only the anode system was bombarded by passing the discharge between the anode system and one of the tungsten-Pyrex seals at the bottom of the tubes. The system was then pumped down (after closing tap (G2) and the electrodes of the experimental tubes were then outgassed by means of an eddy current heater. Unfortunately, the output power of the heater was not sufficient to raise the temperature of the electrodes to a red heat. In case of the caesium tubes, extra care was taken to protect the tungsten-Pyrex seals from destruction by excessive heating. After the electrodes had been outgassed, the Bayrad-Alpert gauge was again treated as previously described and the manifold was then immediately baked at 450°C for 20 hours. While the system was being baked, the liquid air trap (nearest to the manifold) was taken away and the trap (as well as the glass tube connecting it to the manifold) was baked at a temperature of 250°C for 4 hours, by the use of electric "Isotape" heater. This was done to get rid of any condensed mercury in this trap and to make sure that the whole manifold was baked up to the glass tube separating the two traps. After finishing outgassing this part of the vacuum system, the trap was refilled with liquid nitrogen. The temperature of the electric oven was then lowered to 100°C and the Bayard-Alpert gauge was outgassed again and the manifold was then rebaked (at 450°C) for another two days. At all times, it was made sure that sufficient liquid nitrogen was present in the cold traps. An ultimate pressure of approximately 5.10^{-8} mm.Hg. was obtained in all experimental tubes.

The experimental tubes were then isolated from the pumping system by

collapsing the constriction C_5 . Because of the considerable amount of gas released from the glass while being heated, each constriction was collapsed-in extremely slowly in order to allow sufficient time for the pump to remove this gas. Constrictions C_7, C_8 and C_9 which were leading to the side tubes (containing the double seals) of the case of the third, fourth and fifth caesium experimental tubes, were then sealed in the same way as constriction C_5. The Bayard-Alpert gauge was used to test the experimental tubes alone for leaks. The constriction C_5 (and C_7, C_8 C_9 in the case of the caesium tubes) was replaced if any leaks were found. After it was indicated that the tubes were leak-free, the gauge was then used to pump the experimental tubes for about a week (and for three weeks in the case of the second mercury experimental tube) during the distillation processes. An ultimate pressure better than 10^{-8} mm.Hg. was obtained in all experimental tubes.

5.2 DISTILLATION OF THE MERCURY.

Distillation of the mercury was carried out while the distillation tubes were being pumped continuously with the pumping system. The mercury used in the experiments had a purity of not less than 99.8%. It was introduced into the first distillation tube by breaking the fine tip of the capillary tube underneath the mercury surface and drawing the liquid mercury into the tube under the action of the vacuum. The purpose of the capillary tubing was to reduce the speed and violence of the entry of the mercury into the distillation tube and so to prevent the apparatus from shattering. After sufficient mercury had been admitted, the capillary tube was softened and sealed. Distillation to the second tube was achieved by means of electric "Isotape" heater surrounding the first distillation tube. The electric tape was driven by a Variac transformer which enabled the

selection of a convenient slow distillation rate. After about two-thirds of the mercury had been distilled, constriction C_1 was closed.

During the distillation process, the mercury was thoroughly outgassed, and a large amount of air liberated was probably adsorbed on to the surface of the glass. Therefore, before proceeding with the second distillation, the region of the manifold between constriction C_1 and C_3 was baked at high temperature (450°C) by using the electric "Isotape" heater, and then the second distillation into the third tube was carried out in the same way as in the first distillation. After two thirds of the mercury had been distilled into the third tube, the constriction C_2 was closed.

Again the part of the manifold between the third distillation tube and constriction C_3 was baked at 450°C. The constriction C_3 was then slowly closed thus isolating the twice distilled mercury from the pumps. The Bayard-Alpert gauge was removed from the experimental tube by slowly collapsing constriction C_6 and the pig's tail breaker B was then smashed by means of the glass encased iron rod. The final distillation of the mercury into the experimental tubes was completed in the same way as in the previous distillations. After enough mercury had been distilled, the experimental tubes were then removed from the manifold by sealing the constriction C_4.

The distillation tubes were made progressively smaller so that the volume above the mercury surface in the third tube was small compared to the volume of the experimental tubes. The volumes differed by a large factor (300), so that any residual air pressure of 5×10^{-7} mm.Hg. in the final distillation tube would not then increase the residual pressure in the experimental tubes by an appreciable amount.

The experimental tubes were mounted on a tripod table in the inner enclos-

ure of the oven in such a way that the electrodes and the quartz windows could be seen through the windows of the enclosures. After the electrical connections had been made, the electrodes were checked for parallelism by measuring the electrode separation at two positions at right angles, by means of a cathetometer. Parallelism was obtained by tilting the mercury cathode surface in the desired direction by adjusting the appropriate supports of the tripod. The oven was switched on and the Variacs were then set to give the required operating temperature.

5.3 DISTILLATION OF THE CAESIUM.

After the isolation of the experimental tubes by sealing the constriction C_5, the distillation tubes were still continuously pumped through the constriction C_3. Before the distillation of the caesium the tungsten coil heater (surrounding the caesium ampoule) was outgassed by resistive heating. While outgassing the coil, the distillation apparatus was baked at high temperature (450°C) by the electric "Isotape". The caesium ampoule was then broken by flashing high current through the tungsten coil. The distillation was carried out in the same way as for the mercury. The volume of the distillation tubes were much smaller than those used for mercury, each distillation tube was about 5 cm. long and 1 cm. diameter. Only about 2 grams of the original 5 grams in the caesium ampoule were finally distilled into each experimental tube. The caesium ampoule was supplied by Koch Light Laboratories Ltd. A caesium purity of 99.98% was claimed. After finishing the distillation, the experimental tubes were disconnected from the manifold by sealing constriction C_4, and were mounted inside the oven so that the electrodes and the quartz windows could be seen through the windows of the oven enclosures. The oven was then switched on and the variacs were set up to

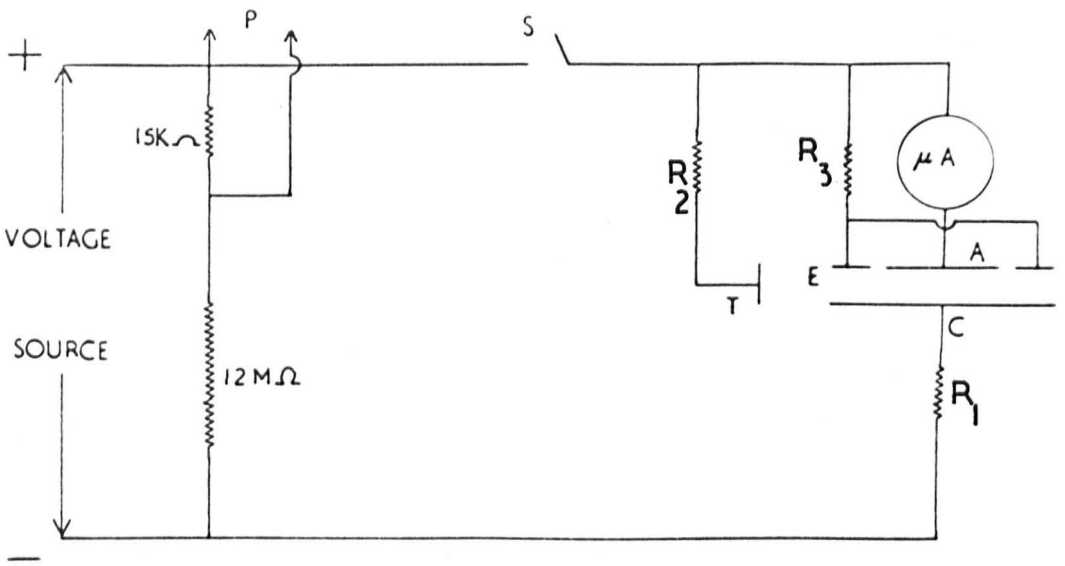

P POTENTIOMETER A ANODE
E ELECTROSTATIC GUARD RING
T TRACKING GUARD RING
C CATHODE S TAPPING KEY

Circuit for the Determination of Breakdown Potentials.

fig.34

give the required temperatures.

5.04 MEASUREMENTS OF THE BREAKDOWN POTENTIALS.

The circuit used in the determination of the breakdown potential is shown in fig(34). The resistances R_1, R_2 and R_3 were included to limit the currents flowing in the cathode, the wall guard-ring and the electrostatic guard-ring circuits respectively. The resistance R_3 (10 MΩ) was included only in the second experimental tube, since no electrostatic guard-rings were included in other tubes. The resistance R_1 and R_2 had different values in the case of the mercury and caesium experiments. In mercury experiments R_1 and R_2 were each of the order of 10 MΩ , while in caesium experiments R_1 was 10 MΩ and R_2 was 1 MΩ . This was done in an attempt to draw most of the leakage current (in the caesium experiments) through the wall electrode. It was hoped that the leakage currents flowing in the wall guard-ring would not distort the field between the electrodes. This was ensured in the design of the tubes by keeping the walls of the discharge tubes as far as possible from the electrodes.

The technique used to determine the breakdown potential of a given gap was to increase the applied potential (at the critical stages) in steps of about 0.5V and applying it across the gap by closing the tapping key, S, for about 10 seconds. The breakdown potential was taken as the potential just sufficient to maintain the discharge without the external radiation. The currents flowing under these conditions were observed to be of the order of 3×10^{-6}A in the caesium experiments and 1.5×10^{-7}A in the mercury experiments. The currents were measured by a Cambridge spot galvonometer, which had a maximum sensitivity of 10^{-8}A per scale division. Paschen curves were obtained by varying the vapour pressure inside the

CIRCUIT USED FOR THE DETERMINATION OF FIRST COEFFICIENTS

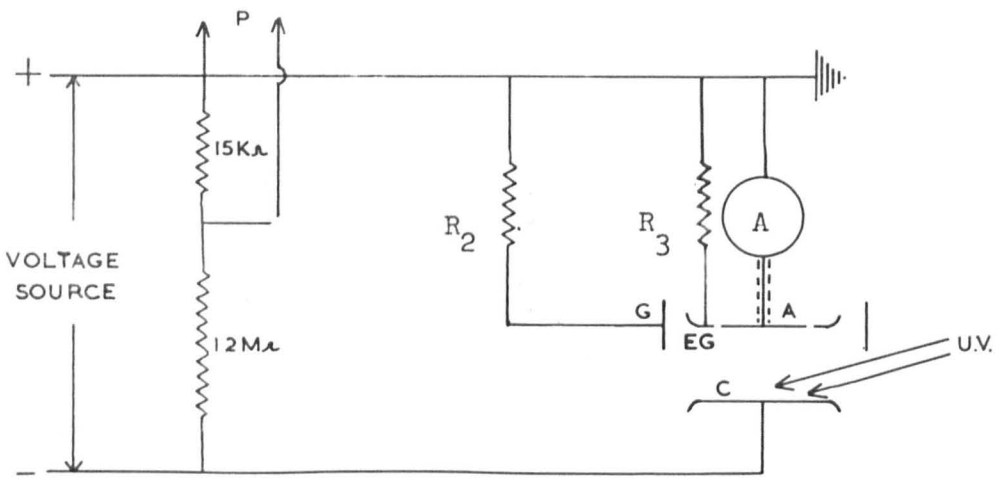

A ANODE
C CATHODE P POTENTIOMETER
G TRACKING GUARD-RING
EG ELECTROSTATIC GUARD-RING

Fig. 35

tubes, which was achieved by varying the temperature inside the oven. The temperature of the vapour, taken as that of the cathode, was determined by the calibrated thermo-couple strapped to the walls of the tube adjacent to the cathode. No measurements were taken until identical readings between this thermo-couple and the others measuring the air temperature of the enclosure of the oven were observed. This condition meant that there was no temperature gradient between the inside and the outside of the experimental tubes. This condition was confirmed by identical breakdown potentials measured half an hour apart. When it was certain that the temperature measured was that of the vapour, the electrode separation was measured with a cathetometer and the breakdown potential taken. The pressure, reduced to the vapour pressure at $0^{o}C.$, was then determined from a graph of pressure and thermal e.m.f. which was plotted from two graphs of pressure against temperature (58, 59) and of thermal e.m.f. against temperature (60). The measurement of breakdown potentials was facilitated by the irradiation of the cathode by Ultra-violet radiation from a high pressure mercury lamp. Smith (53) had demonstrated the suitability of such a lamp for these experiments.

5.5. MEASUREMENT OF THE FIRST IONIZATION COEFFICIENTS.

The circuit used in the determination of the first ionization coefficients is shown in fig (35). In the mercury experiments the resistance R_2 and R_3 were each $10^{10}\ \Omega$, while in caesium experiments R_2 was 1 $M\Omega$. Because the electrodes were at a fixed electrode separation, in most of the tubes, only the values of the coefficient η ($= \alpha/_E$) were obtained by plotting $\log I$ as a function of the applied voltage for different values of E/p_o.

The technique of measuring the gas (gap) currents was the same in all caesium and mercury experiments. The temperature of the oven was regulated to give a convenient vapour pressure inside the experimental tubes. When an agreement between the readings of the thermo-couple strapped to the tube and those measuring the air temperature was reached, the vapour pressure and the electrode separation were then determined in the same way as described in the last section. The electrode separation, d, and the reduced pressure p_o were then used to calculate the voltages required to give the chosen values of E/p_o. Each calculated value of voltage was then applied across the tube, by setting the potentiometer to the required value and increasing the voltage until no deflection was observed on the galvanometer of the instrument. After measuring the corresponding currents, the temperature of the oven was then regulated to give a different vapour pressure and the above process was repeated. Due to the appreciable leakage currents flowing on the walls of the tubes (especially in the case of the caesium experiments) the gas current was taken as the difference between the measured currents with and without Ultra-violet radiation. The current was measured by a Keithly microammeter (type 610) in the mercury experiments and by a Keithly picoammeter (type 1409) in the caesium experiments.

5.6 THE TECHNIQUE OF MEASUREMENT OF FORMATIVE TIME-LAGS.

Formative time lags are measured by applying a step voltage across the discharge gap. The rise time of the step must be short in comparison with the time-lag to be measured. This requirement is less difficult to meet for mercury than for some other gases, such as hydrogen, where the time-lags are much shorter, of the order of microseconds. The

Circuit for the measurement of the formative time lag

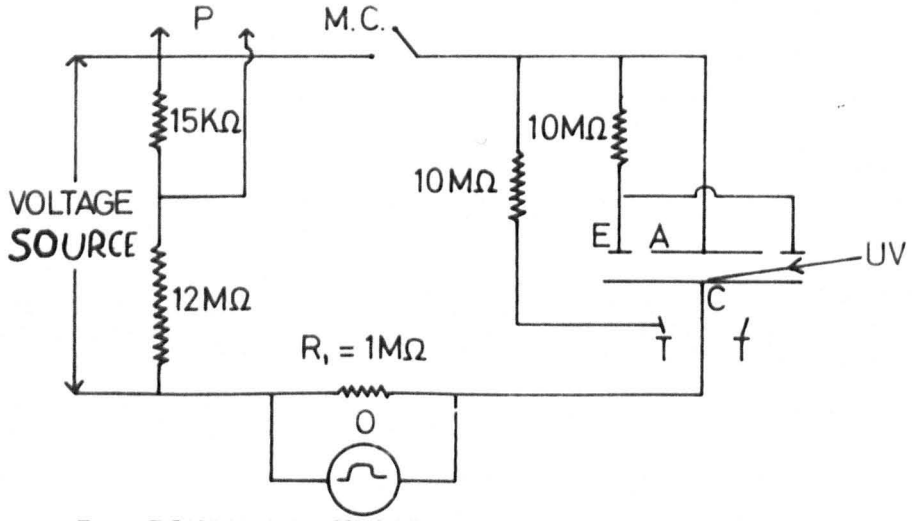

P POTENTIOMETER, M.C. MERCURY SWITCH,
E ELECTROSTATIC GUARD RING,
A ANODE, C CATHODE,
UV ULTRA VIOLET RADIATION,
O OSCILLOSCOPE,
T TRACKING GUARD RING

Fig. 36

formative time-lag for mercury is of the order of 10m.sec. at 0.25 per cent overvoltage, therefore a step voltage with a rise time of a few micro-seconds will fulfil this requirement for mercury. The other requirements for this step voltage are that, it must last for a longer period than the time interval needed for the gap to breakdown and must be continuously and finely variable up to about 600V. These requirements are fulfilled by the circuit shown in fig (36) which has been used in the present measurements of the formative time-lags in mercury vapour. The step voltage consisted of the output voltage from a bank of dry batteries. The step voltage was applied by means of a liquid mercury switch, M.S., which had a rise time of a micro-second, and it also enabled the voltage applied across the gap to be sustained for any required period so long as MS was closed. The time taken for the gap to breakdown (the formative time-lag) and the magnitude of the current flowing were measured by a Tektronix Type 545A oscilloscope, the probes of which were connected across the resistance, R_1, in the cathode circuit. The voltage drop across the resistance was used to trigger the time base of the oscilloscope. Quickly changing currents less than 10^{-6}A could easily be observed by this method. The time constant of the whole circuit was less than 5 micro-seconds. After the pressure and electrode separation had been measured, the onset of breakdown (self-sustained current) was observed with a micro-ammeter and the oscilloscope. The values obtained by these two methods were identical, and for later measurements the oscilloscope only was used. The magnitude (height) of the step voltage (equal to the breakdown potential plus required percentage of this amount) was measured by the potentiometer before the mercury switch was closed. The time taken for the gap to break down after closing the switch was measured by the oscilloscope.

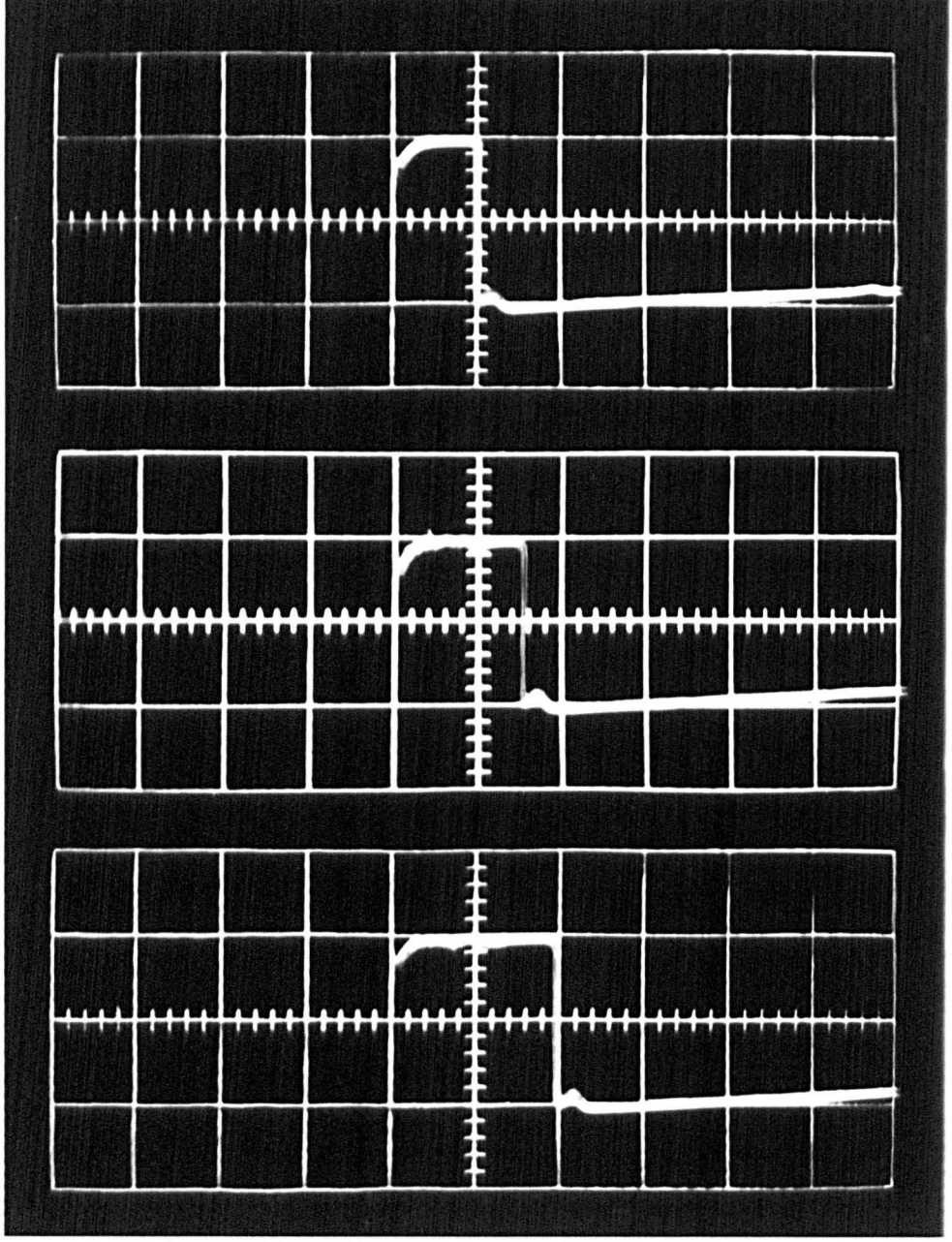

Variation of the time-lags with the period between the discharge at E_s/p_o = 160Vcm^{-1}mm.Hg^{-1} and ΔV = 1.5%

Time/cm = 1.m.sec
Volts/cm = 10volts

1. After 1 sec from the previous discharge
2. After 3 sec from the previous discharge
3. After 7 sec from the previous discharge

Fig. 37

Some of these measurements were obtained by photographing the oscilloscope trace.

At voltages near the breakdown potential of the gap, the formative time-lag becomes sensitive to small voltage changes. An increase in the overvoltage from 0.05% to 0.5% might lead to over 50% reduction in the formative time-lag from its original value at 0.05%. At 400V.this change in percent overvoltage corresponds to a voltage change of 1.8V. Since at these small overvoltages, very stable high voltage supply and high accuracy voltage measurements are needed, no measurements of the time-lag were taken below 0.1% overvoltage. In the present measurements, this percentage of overvoltage (0.1) corresponded to over 0.3V. Formative time-lags are usually plotted as a function of over-voltage at a constant E_s/p_o (where $E_s = \frac{Vs}{d}$, V_s is the breakdown potential and d is the electrode separation, and p_o is the reduced pressure). The maximum overvoltage was limited to less than 4%, so that E_s/p_o could be taken as sensibly constant. However in the analysis of the results, using Davidson's theory, no calculation of the time-lags were performed above 2% overvoltage, since the generalized secondary ionization coefficient (ω/α) is assumed to be constant at each E_s/p_o.

In order to improve the accuracy of the reading of the length of the oscilloscope trace, the average of several readings at each value of overvoltage was taken. However it was noticed that the interval between successive measurements at the same percentage of overvoltage, can sometimes effect the formative time-lag. If the interval was too short the formative time-lag used to reduce from 2 m.sec. to 1 m.sec. as shown in the oscilloscope trace shown in fig (37). This reduction in the time-lag could be produced by two effects.

(a) If the charged particles from the discharge could reach the tube walls and remain there for some time after the discharge had ceased.

(b) Some of the active particles (atoms excited in metastable states from previous discharge might still be present in the discharge gap. Accumulation of charged particles on the inside walls of the discharge tube can be distort the electric field between the electrodes, and therefore the time-lags. However, since the walls of tubes were connected to the anode and were kept away from the discharge region, it is likely then that it was the presence of the active particles which caused this reduction. It was found that consistent formative time-lag measurements were obtained when at least 5 seconds interval was allowed between each discharge.

The method adopted (with both of the two experimental tubes) was to measure a set of five successive time-lags for a given overvoltage with a standard interval of ten seconds between each discharge. The applied voltage, equal to the breakdown potential plus the required overvoltage was measured before and after each set of time-lags. The breakdown potential was measured after every set of time-lag measurements, since a small variation in the breakdown potential could result in a large error in the overvoltage setting and thus in the time-lags as well. In the first experimental tube formative time-lags measurements at different E_s/p_o, were obtained by varying the vapour pressure. In the second experimental tube, however, this was achieved by varying the pressure and the electrode separation.

Statistical time-lags was eliminated (or reduced to very short times) by irradiation of the cathode by Ultra-Violet from a high pressure mercury lamp (Smith). Photo-electric currents of 5×10^{-11}A and 2.5×10^{-12}A were obtained in the first and second experimental tubes respectively. These photo-electric currents corresponded to statistical time-lags of the order of 3.2×10^{-9}sec and 6.4×10^{-8}sec, which are negligible compared to the

measured time-lags (>1m.sec.). The results of these measurements together with those on the breakdown potential and first ionization coefficients in caesium and mercury will be presented and discussed in the following chapter.

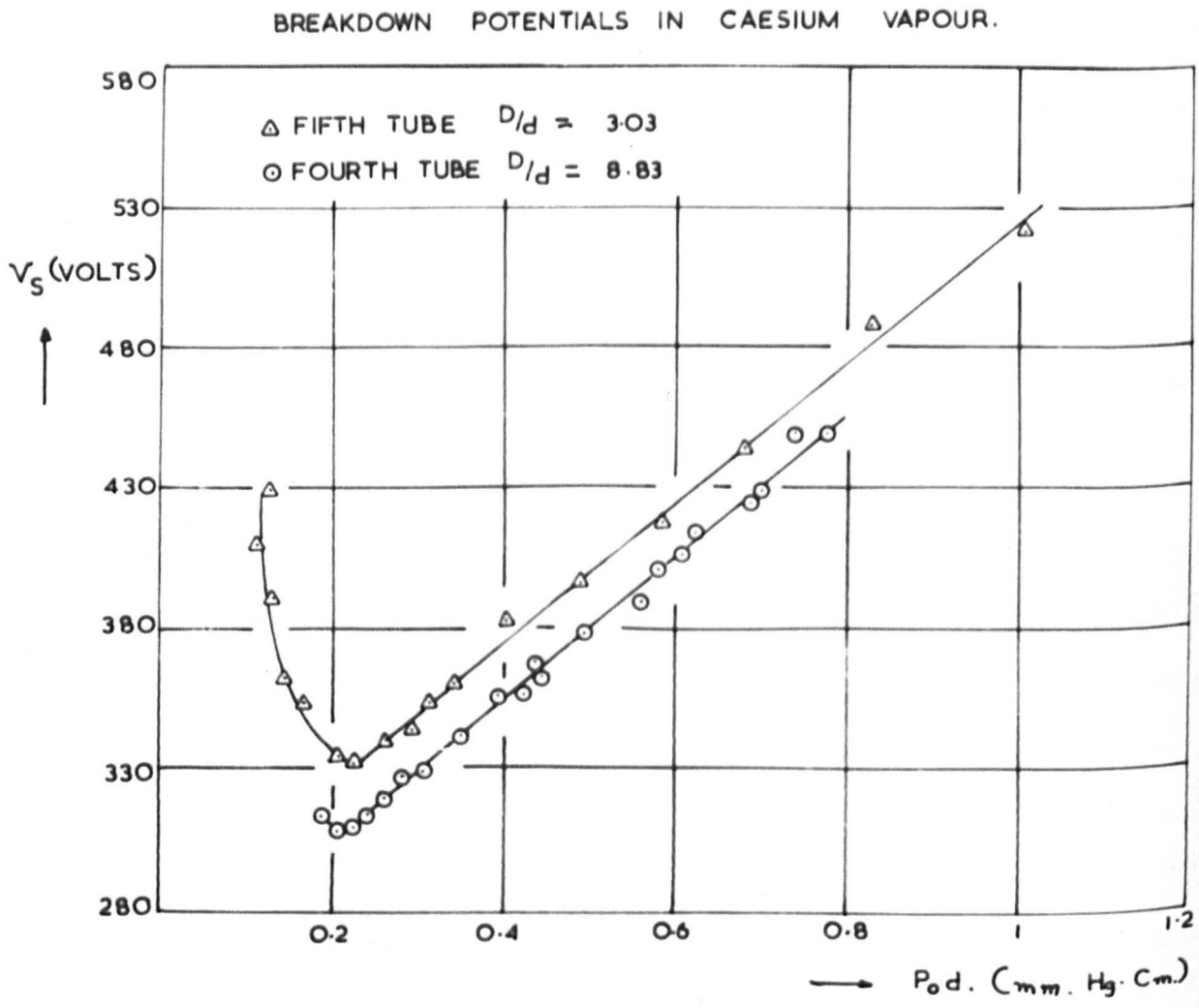
BREAKDOWN POTENTIALS IN CAESIUM VAPOUR.
△ FIFTH TUBE D/d = 3·03
⊙ FOURTH TUBE D/d = 8·83
580
530
480
430
380
330
280
Vs (VOLTS)
0·2
0·4
0·6
0·8
1
1·2
Pod. (mm. Hg. Cm.)

Fig. 38

CHAPTER VI

DISCUSSION OF THE RESULTS

6.1. CAESIUM RESULTS.

6.1.1. INTRODUCTION.

The first three experimental tubes are interesting only in so much as they provided information which resulted in the improvement in experimental technique and in the design of subsequent experimental tubes. The useful results were only obtained from the fourth and fifth experimental tubes.

These experiments were concerned with obtaining accurate breakdown potential measurements in caesium vapour. Preliminary values of the Townsend first ionization coefficient were also obtained from both tubes. These results will now be presented and discussed together with the results of the breakdown potentials obtained by Bratescu (section 3.1).

6.1.2. THE BREAKDOWN POTENTIALS.

Measurements of the breakdown potentials as a function of the product $p_o d$ were taken during the rise and fall of temperature. In order to obtain more accurate results measurements were subsequently taken only after the thermo-couple on the tube gave the same thermal e.m.f. as those in the surrounding air. The results obtained in this way with the fourth and fifth experimental tubes are shown in fig (38). Unfortunately, no measurements could be obtained at high values of $p_o d$. It is found from the first three experimental tubes, that caesium vapour attacks the quartz windows at high temperature ($\sim 270^{\circ}C$) and forms a brown layer on the inside walls (presumably an oxide layer) and thus stops the function of the quartz windows. Due to the limited life-time of fourth tube, it was not

possible to obtain any measurements at low values of $p_o d$. The leakage currents were nearly of the same order of magnitude as the gap current. It can be seen from the two curves in fig(38) that for any given value of $p_o d$ over the range plotted the breakdown potential is lower for smaller electrode separations. The breakdown potentials obtained from the fourth experimental tube are about 20V lower than the breakdown potential obtained from the fifth tube. The vacuum and caesium distillation techniques were similar and the same ultimate pressure, of better than 10^{-8}mm.Hg.,was obtained in both of the experimental tubes before distillation. The higher voltages , in the case of the fifth experimental tubes, could not be due to any differences in these techniques. McCallum and Klatzow(61), working in argon and neon, demonstrated that the breakdown potential depended on the ratio D/d, (D, electrode diameter and d electrode separation) and to some extent on the distance between the walls of the tube and the electrodes. The effect was investigated by measuring photo-electric currents between the electrodes. The variation of breakdown potential with D : d was explained by the investigators as being caused by the loss of electrons by diffusion from the discharge region. The loss would be greater for an apparatus of which the ratio D/d is small than for one in which the ratio is large, and consequently it would be expected that the breakdown potential would be greater in the former apparatus although the value of pd is the same.

Dependance of the breakdown potential on the ratio D/d would be expected also when metastable atoms and photons (29) are important in the breakdown mechanism. A loss of these active particles from a discharge volume for which D/d is small, can only be compensated by an increase in the

applied potential for the breakdown to occur. If it is assumed that the nickel electrodes, used in the present investigation, attained the work function of caesium ((≈1.9eV) (49), the most important photons which are likely to contribute in the caesium breakdown mechanism are those omitted in the transition (fig(13)) $6^2P_{1/2,3/2}$ to $8^2D_{3/2,5/2}$ of energy ~2 eV. However, since the excitation function of caesium excited states are not available in the literature, it is difficult to estimate the importance of the above transition or any other transitions in a caesium discharge.

Comparison of the present results of breakdown potential with those obtained by Bratescu given in fig (15), shows that breakdown potentials obtained from the fourth tube are much lower than those obtained by Bratescu over the whole range of p_od. The difference in the breakdown potential varies from 53V at p_od of 0.23mm.Hg.cm. to 65V p_od of 0.8 mm.Hg. cm. Such a big difference can be referred to many factors. The ratio of D/d can be one of the factors for such high breakdown potentials in Bratescu's case, since a value of D/d of 1.41 was used in his apparatus compared to D/d of 8.83 which was used in the fourth tube. In his paper, Bratescu reported that the ultimate pressure in his apparatus was that similar to the one reported in one of his previous papers (48) of 10^{-5}mm.Hg. Such high pressure can markedly change the breakdown characteristics through a change of the gaseous ionization processes and change of the cathode work function by reaction of caesium with oxygen, which exists in fairly large quantities at the above residual air pressure. Smith (53) has shown that an air impurity with a partial pressure of 10^{-4}mm.Hg. was sufficient to raise the breakdown potential in mercury vapour by 40V.

In an attempt to limit the leakage currents flowing on the inside

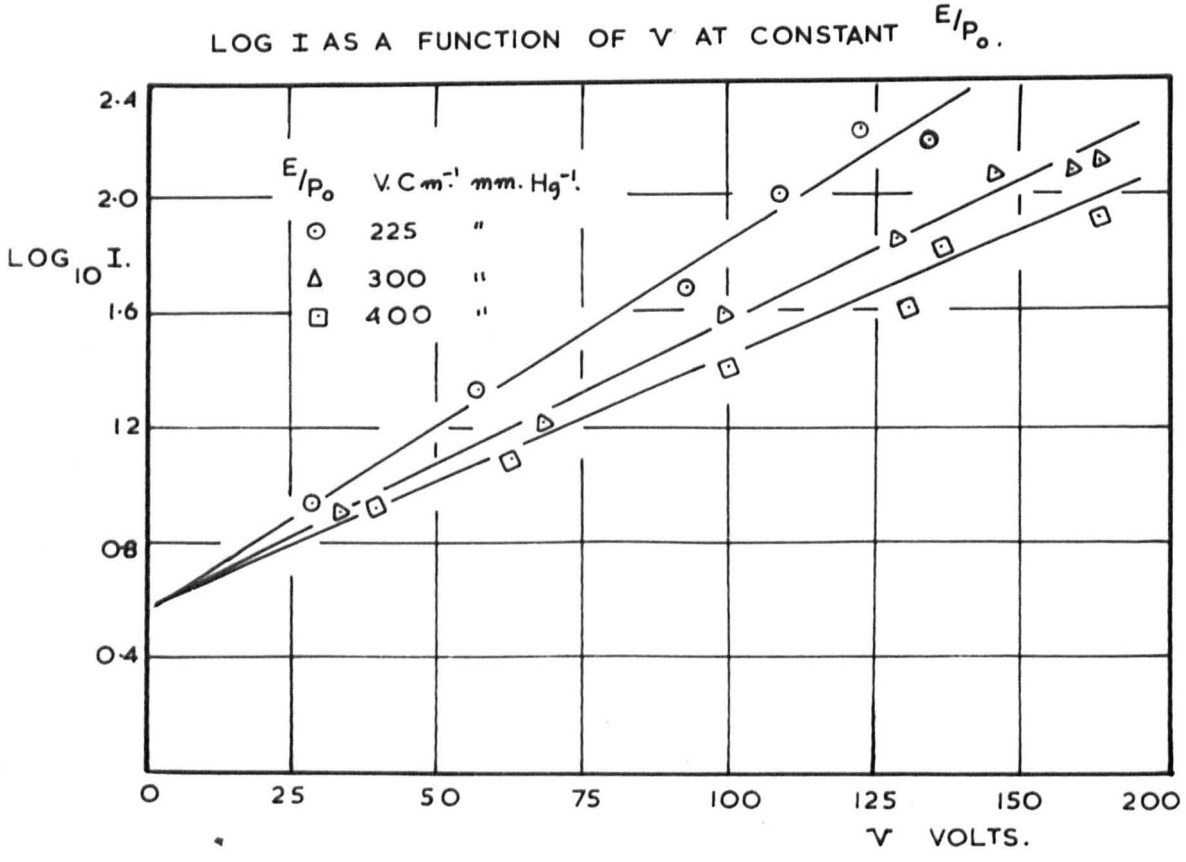
LOG I AS A FUNCTION OF V AT CONSTANT E/Po.
LOG10 I.
2·4
2·0
1·6
12
08
0·4
E/Po V.Cm⁻¹ mm.Hg⁻¹.
225 "
300 "
400 "
0
25
50
75
100
125
150
200
V VOLTS.

Fig. 39

walls of the discharge tube (section 3.1.2), Bratescu only kept the caesium reservoir at lower temperature (≈120°C) than the rest of the main discharge tube. From the present author's experience from the third experimental tube (section 4.2.3) it is found that such method is ineffective in limiting the leakage currents to the required values of less than the gap currents. A leakage current of the order of 10^{-5}A was observed when only 300V was applied across the electrodes and the caesium reservoir was kept at temperatures of 150°C lower than the main body of the third discharge tube. Such high leakage currents can disturb the uniform field between the electrodes, especially in Bratescu's case where the walls were only 0.6cm. away from the discharge gap compared to 3cm.and 6cm. in the present fourth and fifth experimental tubes. The influence of the disturbance of the field in the discharge gap was observed in a mercury discharge by Smith and Overton where they found it lowered the breakdown potentials. From the above discussion it is difficult to assess the contribution of each of the above factors to the high breakdown potentials of Bratescu's experiment, however the main one was probably the poor ultimate pressure obtained in his apparatus.

6.1.3 FIRST IONIZATION COEFFICIENTS.

Due to the high leakage currents flowing on the inside walls of the experimental tubes (despite the wall guard-rings being at the same potential as the anode), currents of the order of 10^{-9} to 10^{-8} were used in the measurements of the first ionization coefficients. Graphs of $\log_{10} I$ against the applied voltage, V, were plotted for constant values of E/p_o. Three of the curves obtained are shown in fig(39). From each of the slopes of these curves, values of $\eta (= \alpha / E)$ were obtained for a range of E/p_o from 50 to 600V.cm^{-1}.$mm.Hg^{-1}$. Continuation of measurements was prevented

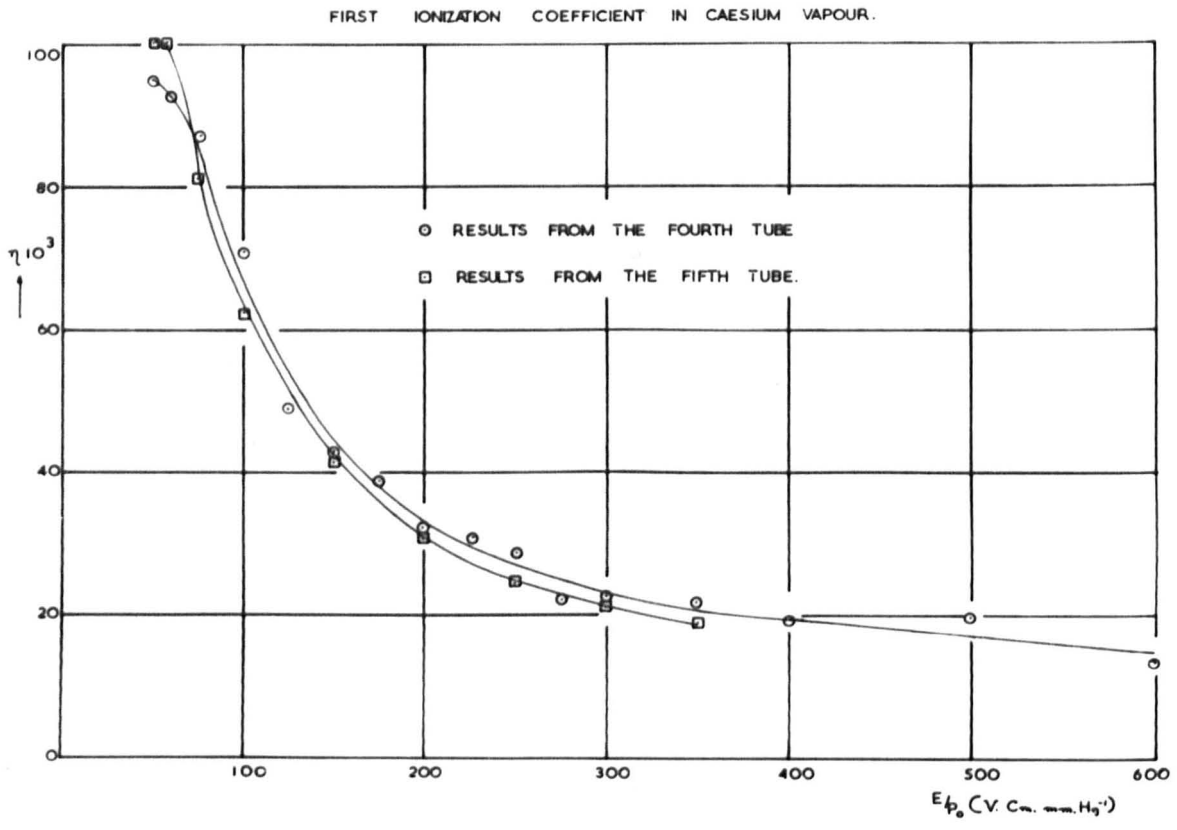
FIRST IONIZATION COEFFICIENT IN CAESIUM VAPOUR.
RESULTS FROM THE FOURTH TUBE
RESULTS FROM THE FIFTH TUBE.
η 10³
100
80
60
40
20
0
100
200
300
400
500
600
Ep₀ (V. Cm. mm. Hg⁻¹)

Fig. 40

by the high leakage currents ($>10^{-8}$A) beyond this range of E/p_o. Values of $\eta(\alpha/E)$ as function of E/p_o obtained from the fourth and fifth experimental tubes are shown in fig (40). Since no previous measurements of $\eta(=\alpha/E)$ have ever been published in the literature for alkaline metals, it is difficult to estimate the accuracy of present results because the currents were limited in the range 10^{-9} to 10^{-8}A and the leakage currents were as high as the gap current. Therefore it must be emphasised that the present measurements of the first ionization coefficients are only preliminary and an error as much as 15% to 20% is involved in their determination.

However, using these values of $\eta(=\alpha/E)$ an estimate of the generalized secondary ionization coefficient ω/α can be obtained from the curves (fig(38)) using the Townsend breakdown criterion

$$1 - (\omega/\alpha)(e^{\eta Vs}-1)=0$$

Due to the limited range of p_od at which the breakdown potentials were measured and the range of E/p_o in which η was obtained, only values of ω/α, in the range of E/p_o between 520 to 600V.cm^{-1}.mm.Hg^{-1}., were calculated. These values of ω/α calculated by using the breakdown potential obtained from the fourth and fifth experimental tubes are given in the following table (6.1.1)

Table (6.1.1)

E/p_o (V.cm^{-1}.mm.Hg^{-1})	ω/α (fourth tube)	ω/α (fifth tube)
525		1.3×10^{-4}
570	5.7×10^{-4}	4.3×10^{-4}
583	7.1×10^{-4}	5.0×10^{-4}
600	13.8×10^{-4}	8.3×10^{-4}

It must be mentioned here that this method of calculating ω/α is not very accurate because the function is somewhat sensitive to errors in $\eta (= \alpha/E)$, therefore the above values given in table (6.1.1) only give an estimate of ω/α as mentioned before.

6.1.4 CONCLUSIONS AND SUGGESTIONS FOR FUTURE WORK.

In view of the difficulties involved in working with caesium vapour in glass, a new technique has been developed by which the life-time of the experimental tubes can be as long as a month under continuous running at high temperatures (250°C). Also it is found from the experience gained from this work that the most effective way of reducing the leakage current flowing on the inside walls of the experimental tubes, is by extending the tracking path length between the electrodes. Using this technique, the breakdown potentials in uniform field and an estimate of the first and second ionization coefficients were obtained.

Since a deposit of about two monolayer of caesium on a cathode of any ordinary metal (49) changes its work function to that of the pure caesium, therefore it is assumed that the work function of nickel cathodes used in the present experiments corresponded to that of pure caesium i.e. about 1.9eV. The minimum breakdown potential in caesium vapour was found at $p_o d$ of 0.22 mm.Hg.cm. and had a value of 308V and 332V from the fourth and fifth experimental tubes respectively. The difference in the breakdown potentials obtained from these two tubes can be referred to dependance on the gap geometry. The high breakdown potentials obtained by Bratescu can be referred to many factors, however the most important factor is the high air

impurity that existed in his apparatus.

Due to the errors involved in determining $\eta (= \alpha/E)$, its values and those of ω/α obtained in the present studies give only an estimate of the order of magnitude of these coefficients.

Using the technique developed here, the leakage current could still be reduced by extending the tracking path length, and therefore more accurate values of the first ionization coefficient could be determined for a wider range of E/p_o. In order to avoid working at high temperatures above $\approx 250^{\circ}C$ for the measurements of the breakdown potentials at high values of $p_o d$, a bigger electrode separation and diameter could be used, provided that there is enough clearance between the electrodes and the walls of the apparatus. In this way values of the generalized secondary ionization coefficient could then be determined for a wider range of E/p_o, which could help in identifying the secondary ionization processes in caesium.

6.2. PRESENTATION AND DISCUSSION OF THE MERCURY RESULTS.

6.2.1. INTRODUCTION

In order to evaluate the magnitude of the individual active secondary ionization processes by using Davidson's equations (chapter 2) at any given value of E_s/p_o, it is necessary to know the primary ionization coefficient, α , the total secondary ionization coefficient, ω/α the drift velocities of the electrons and the ions, W_- and W_+, and the life-time of the different excited states, τ . The secondary ionization coefficient ω/α at a particular value of E_s/p_o can be found from the measured values of α and the static breakdown potential V_s by using the Townsend criterion for breakdown, $1 = \omega/\alpha \quad (e^{\alpha d}-1)$, (section 1.13). However because of the exponential function of α in this criterion, any error in the magnitude of α (due either to measurement's inaccuracy or impurities in the gas sample) leads to large errors in calculating ω/α and thus also in the formative time-lag calculations. Therefore a successful application of Davidson's theory requires the determination of all these quantities under the same conditions for the particular gas sample under investigation. However measurement of all these quantities under the same conditions would make the design of the experimental tube very complicated.

In the present studies of the temporal growth of ionization in mercury vapour, α , V_s and hence ω/α were the only quantities determined under the same conditions in which the formative time lag was measured. The values of these quantities obtained in the present studies will be presented and compared with those obtained by previous workers, before discussing the time-lag results.

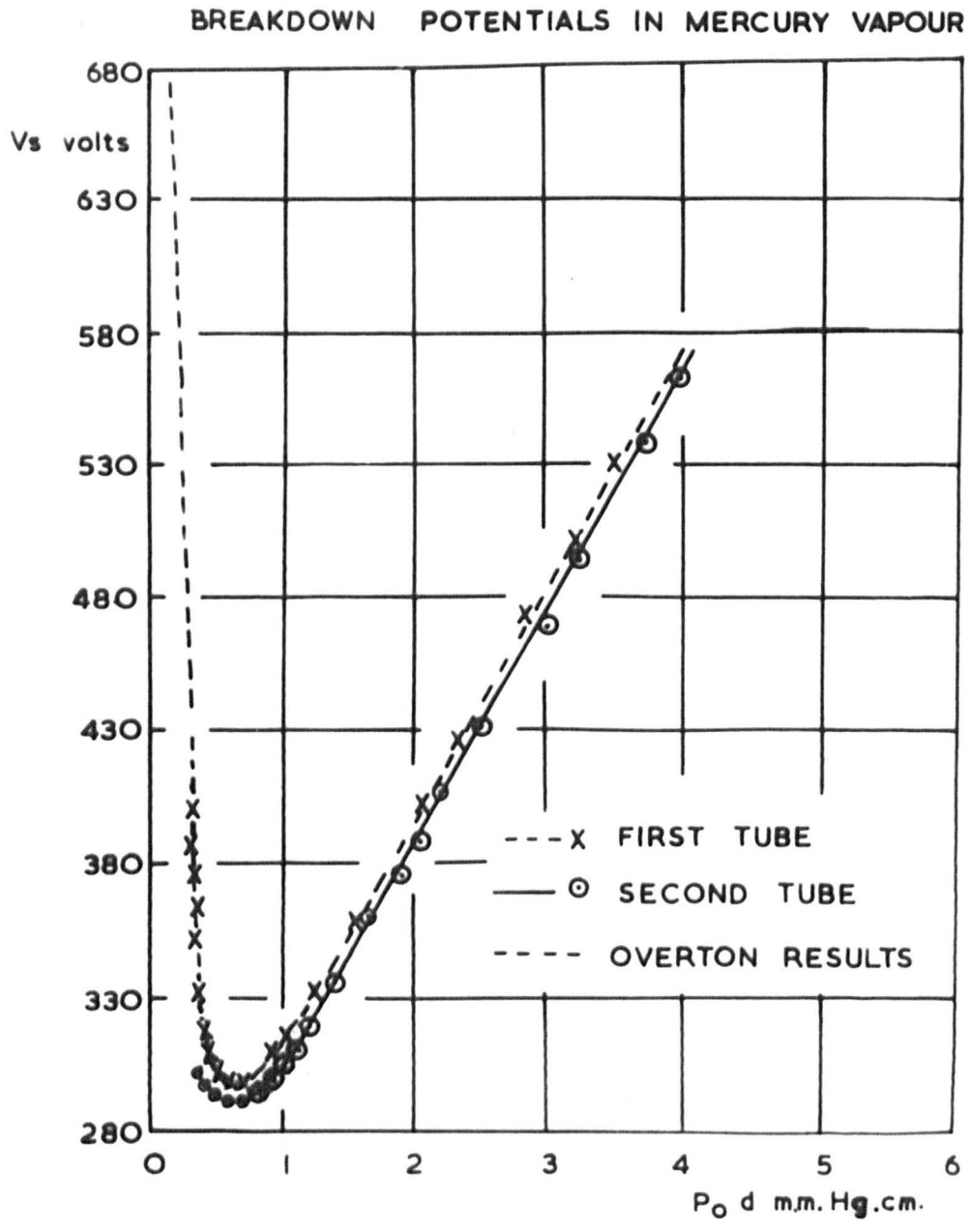
BREAKDOWN POTENTIALS IN MERCURY VAPOUR
Vs volts
680
630
580
530
480
430
380
330
280
0
1
2
3
4
5
6
Po d m.m. Hg.cm.
---X FIRST TUBE
—⊙ SECOND TUBE
---- OVERTON RESULTS

fig. 41

6.2.1. BREAKDOWN POTENTIALS AND IONIZATION COEFFICIENT IN MERCURY.

6.2.1.1. THE BREAKDOWN POTENTIALS.

The breakdown potentials as function of the product $p_o d$, fig. (41), were obtained by varying the pressure at fixed electrode separations. All measurements were taken only after agreement between all the thermocouples was obtained. The self sustained currents were taken as 8×10^{-6} A and 2.5×10^{-7} A in the first and second experimental tubes respectively. The Paschen curves obtained by Overton (54) are shown also on the same graph in fig (41), in order to facilitate its comparison with the present results. It can be seen that for any given value of $p_o d$, the breakdown potentials obtained from the second tube is lower than those obtained from the first tube and by Overton. A difference of about 6v.can be clearly seen, at any value of $p_o d$. This difference can not be referred to the purity of the mercury since similar techniques in the handling of mercury were used, and ultimate pressure better than 10^{-8} mm. Hg., was reached in both measurements. However, this can be referred to the superior gap geometry (D/d) used in the second experimental tube. The breakdown potential as it has been seen in section (6.1) depends on the ratio of D/d, (61), since the excited atoms and photons are expected to take part in the breakdown mechanism in mercury (section 6.2.3). A lower breakdown potential is associated with a large ratio of D/d (15 in the second tube), while a higher breakdown potential is associated with small D/d (6.55 in the first tube and 6.66 in Overton's results) to compensate for the loss of the excited atoms and photons. From their observation of variation of the breakdown potential at the minimum, Overton and Smith (29) have concluded that the minimum breakdown potential V_{sm} is a linear function of electrode

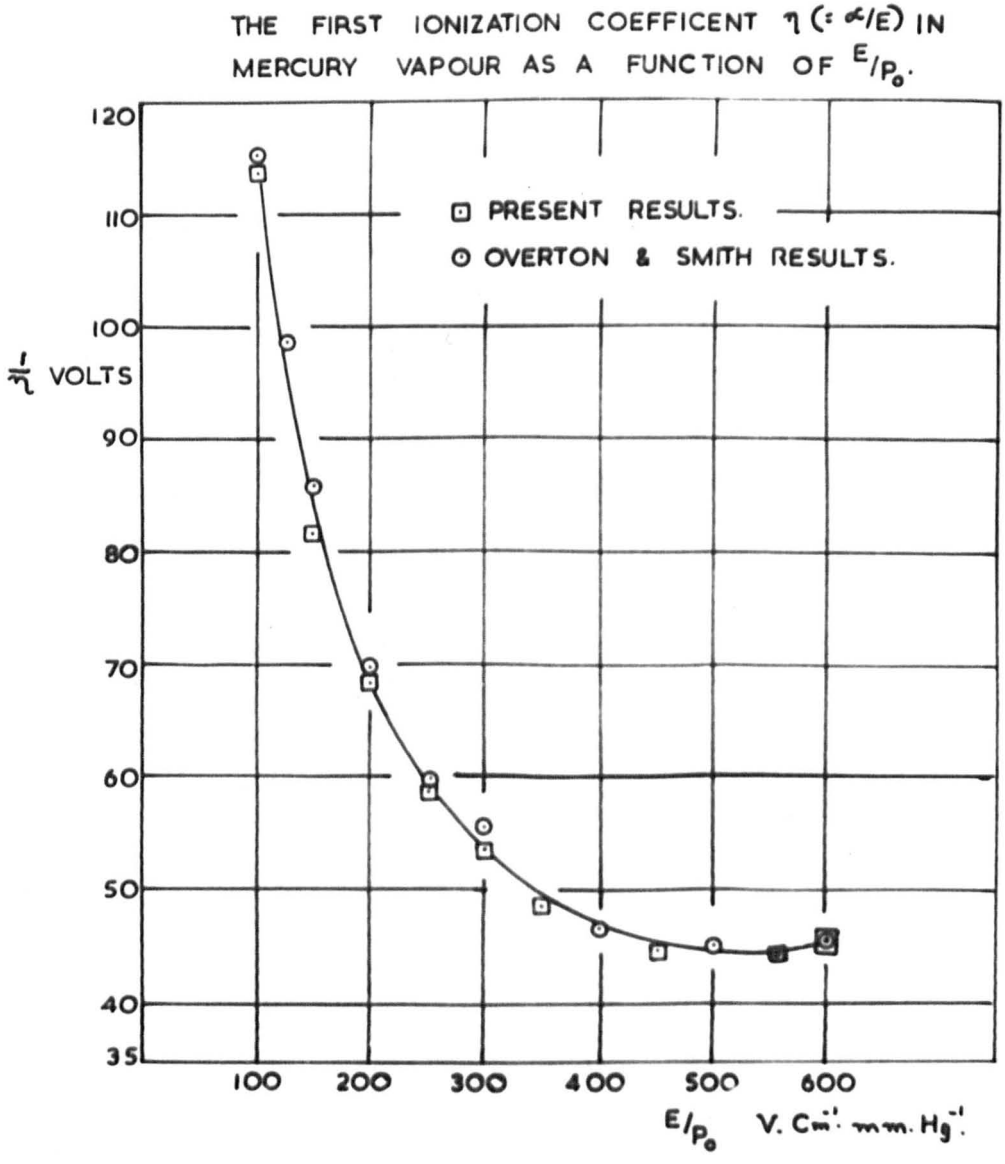
THE FIRST IONIZATION COEFFICENT η (= α/E) IN MERCURY VAPOUR AS A FUNCTION OF E/P₀.
PRESENT RESULTS.
OVERTON & SMITH RESULTS.
η VOLTS
120
110
100
90
80
70
60
50
40
35
100
200
300
400
500
600
E/P₀ V. Cm⁻¹. mm. Hg⁻¹.

Fig. 42

separation. This relation is of the form $V_{sm} = 285 + 5d$ where V_{sm} is in volts and d in cm. A Minimum breakdown potentials are 290 and 288V at electrode separations of 0.65 and 0.72 in the first and second experimental tubes respectively. Using the above formula minimum breakdown potentials of 288.25 and 288.6V would be expected for the above two electrode separations. From comparing the above results, it was concluded that the work function of the liquid mercury cathode used in the present studies was the same as in the previous experiment and it proved also that a surface of constant work function can be obtained by a properly prepared mercury pool cathode.

6.2.1.2 THE FIRST IONIZATION COEFFICIENT.

Using currents between 10^{-1}A and 10^{-8}A, values of η as a function of E/p_o were obtained from both experimental tubes. The method consisted of plotting $\log_e I$ as a function of voltage for different values of E/p_o by varying the pressure and a fixed electrode separation. In this way values of $\eta(\alpha/E)$ were obtained by measuring the slopes of curves, for a range of E/p_o from 100 to 600v cm^{-1}. $mm.Hg^{-1}$. When the Davies-Milne analysis (62), appendix I, for the correction of secondary effects, was applied to the present results, it was found that the correction factor was less than 10^{-4} in η over the whole range of E/p_o investigated. The present values of $1/\eta$, as well as those of Smith (53) and Overton (54), plotted as a function of E/p_o are shown in fig.(42). The minimum value of $1/\eta$ ($= E/\alpha$) given by Stoletow constant, represents the minimum amount of electron energy needed to produce an ion pair in the gas concerned. The value of $1/\eta$ at the minimum are 44.5 as determined by Smith and Overton and 44.6 as determined by the present author. Since $\eta(= \alpha/E)$ is a sensitive function of the gas purity, thus from the agreements between

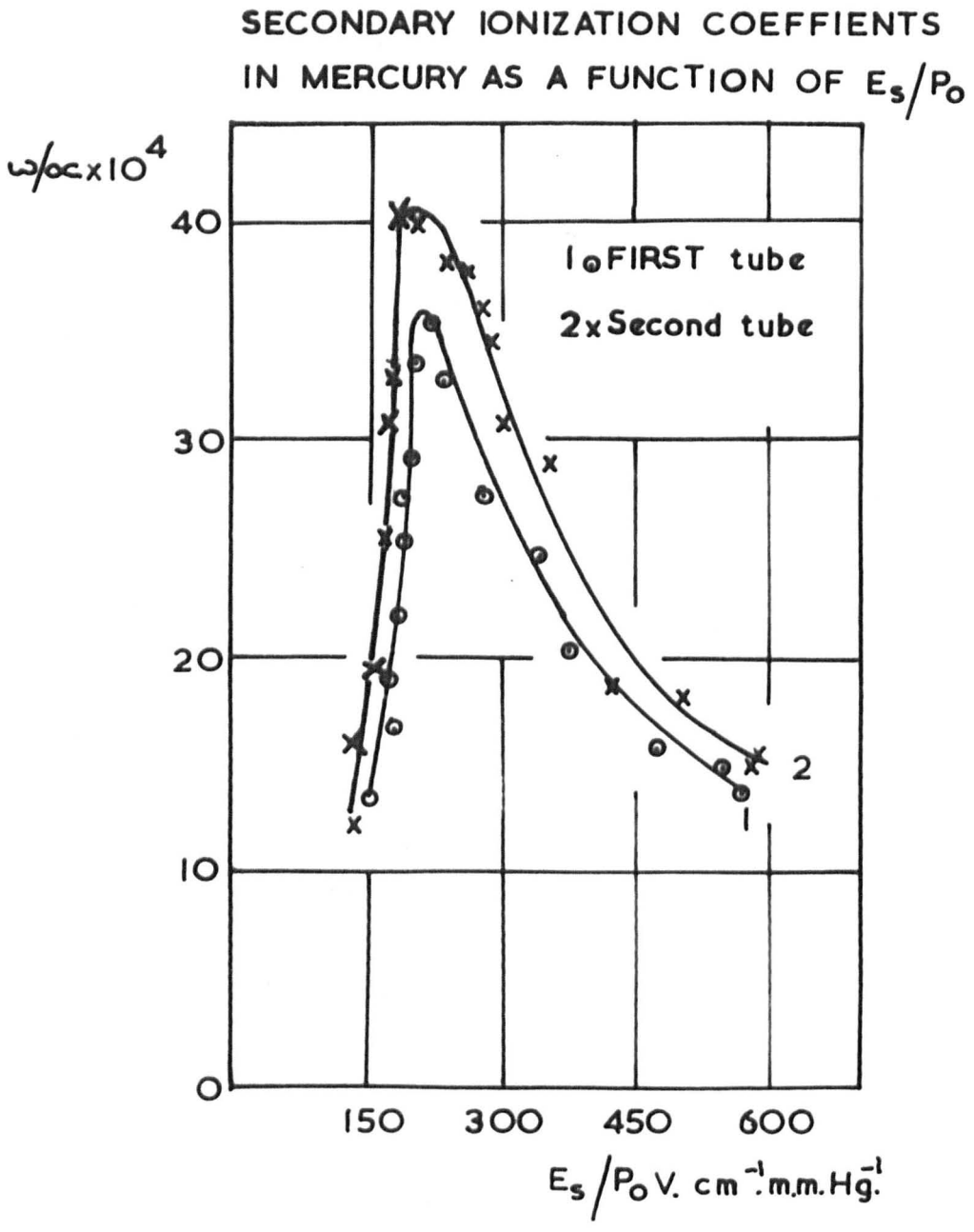
SECONDARY IONIZATION COEFFIENTS
IN MERCURY AS A FUNCTION OF E_s/P_o
$\omega/\alpha c \times 10^4$
40
30
20
10
0
1 o FIRST tube
2 x Second tube
2
1
150
300
450
600
E_s/P_o V. cm^{-1}. m.m. Hg^{-1}.

fig. 43

the present results of $\frac{1}{\eta}$ with those of previous workers fig(42), it is fair to conclude that the mercury used in the present investigation had the same purity as in Overton's case (27). Therefore from the results of the breakdown potentials and the first ionization coefficients, it is concluded that the formative time-lag measurements of the present author and of Overton, have been measured for similar mercury samples and for the similar cathode surfaces. Thus any difference in the formative time-lags of Overton and the present author cannot be referred to change in the gas purities or in the work functions of the cathodes.

6.2.1.3. THE TOTAL SECONDARY IONIZATION COEFFICIENTS.

Values of the generalized (total) secondary ionization coefficient ω/α were calculated from the values of the first ionization coefficient η together with the breakdown potential V_s, using the Townsend breakdown criterion, $1 - \omega/\alpha \quad (e^{\eta V_s} - 1) = 1$ Fig(43) shows the coefficient ω/α as a function of E/p_o obtained from the first (curve 1) and second (curve 2) experimental tubes. The values of ω/α were calculated only in the range of E/p_o between 100 and 600v $cm^{-1}.mm.Hg^{-1}$ since measurements of η did not exceed the above high value of E/p_o. The feature of these two curves bear a close resemblance to those obtained by Overton and Smith (section 3.2) both in order of magnitude and the general shape. The most striking features are the appearance of large peaks in the order of an E/p_o of $200v.cm^{-1}.mm.Hg^{-1}$ and the displacement of the ω/α for different ratio of D/d. Since at low E/p_o the ratio of exciting to ionizing collisions is large, the increase in ω/α at low E/p_o is most likely to be the result of the contribution of the increased numbers of photons and metastable atoms produced. The displacement of

ω/α is a reflection of the dependance of V_s on D/d, where at small D/d the number of active particles lost from the discharge gap is higher than when D/d is large. Smith (53) has found that, ω/α depends not only on the D/d but also on the individual values p_o and d. At the same value of E/p_o and for the same ratio of D/d, higher values of ω/α are associated with increase in p_o and decrease in d, which is mostly caused by the increased number of exciting collisions as the pressure is increased. This fact, as well as the previous one, can be of considerable significance where photon and excited atom action at the cathode is important as in the case of mercury vapour discharges.

The excited atoms which are important in producing the secondary electron emission from the cathode in a mercury discharge are the four P states. The probabilities of excitation to these states are shown in fig(4), the 2^3P_o and 2^3P_2 states being metastable, the $2\ ^3P_1$ and $2\ ^1P_1$ levels are the resonance levels. It can be seen that these excited states are most efficiently produced at an electron energy of about 11v. If it is assumed that the mean electron energy is given by $\bar{\varepsilon} = \frac{1}{42} E/p_o + 6$ (54), then a peak in ω/α would be expected at E/p_o of approximately $200 v.cm^{-1}.mm.Hg^{-1}$ This in fact can be seen to be the case.

Since the life-time of the resonance states are too short ($\approx 10^{-7}$ sec.) then they would not be expected to diffuse to the cathode to cause secondary emission, on the other hand the resonance photons emitted by these states can do so. Metastable atoms, because of the relatively long life-time, can either act directly at the cathode, or by their emitted non-resonance radiation. It is dififcult to estimate the relative contributions of the photons and metastable atoms to ω/α . The numbers of normal excited atoms (and hence photons) produced will be somewhat

greater than the numbers of metastable atoms because of the high probability of formation of the $2\ ^1P_1$ state and because of its high energy (=6.7eV.) The $2\ ^3P_1$ state has got a lower excitation probability and very low excitation energy of 4.86eV. when compared to the work function of the mercury cathode (4.5 eV). From their excitation probability 2^1P_1 state should be of increasing importance at high values of E/p_o, while the 2^3P_1 state at low values of E/p_o, if they are to contribute to

However the efficiency of electron emission by the metastable atoms can be quite high. Sonkin (63) has shown that the incidence of the $2\ ^3p_o$ mercury metastable state atom on to a tungsten surface covered with a layer of mercury and oxygen, can give a secondary emission coefficient of the order of 10^{-2}. Tehoretical calculations by Grievitch and Yavorsky (64) for the $2\ ^3P_o$ mercury metastable atom incident on to a mercury surface, indicate that the secondary coefficient can be as high as 0.75. This value is considerably higher than the maximum value of 0.004 obtained in the present study. This very high value is even more surprising since the potential energy of the $2\ ^3p_o$ state of 4.66 eV is only slightly higher than the work function of the mercury surface of 4.5 eV. However, von-Engel has shown high cross-section of 5×10^{-14} cm.^{2} for the destruction of $2\ ^3P_o$ metastable atoms in the reaction (18).

$$Hg^*(2^3p_o) + Hg^*(2^3p_1) \rightarrow Hg_2^* \rightarrow Hg_2^+ + e$$

and if one considers the very low excitation probability (of less than 10^{-16} cm.^{2}) to this state it is therefore unlikely that $2\ ^3p_o$ metastable atoms will contribute to ω/α . It is probable that $2\ ^3p_2$ mercury metastable atom will play a more impcrtant part in the secondary electron emission because of its higher probability of formation and its higher

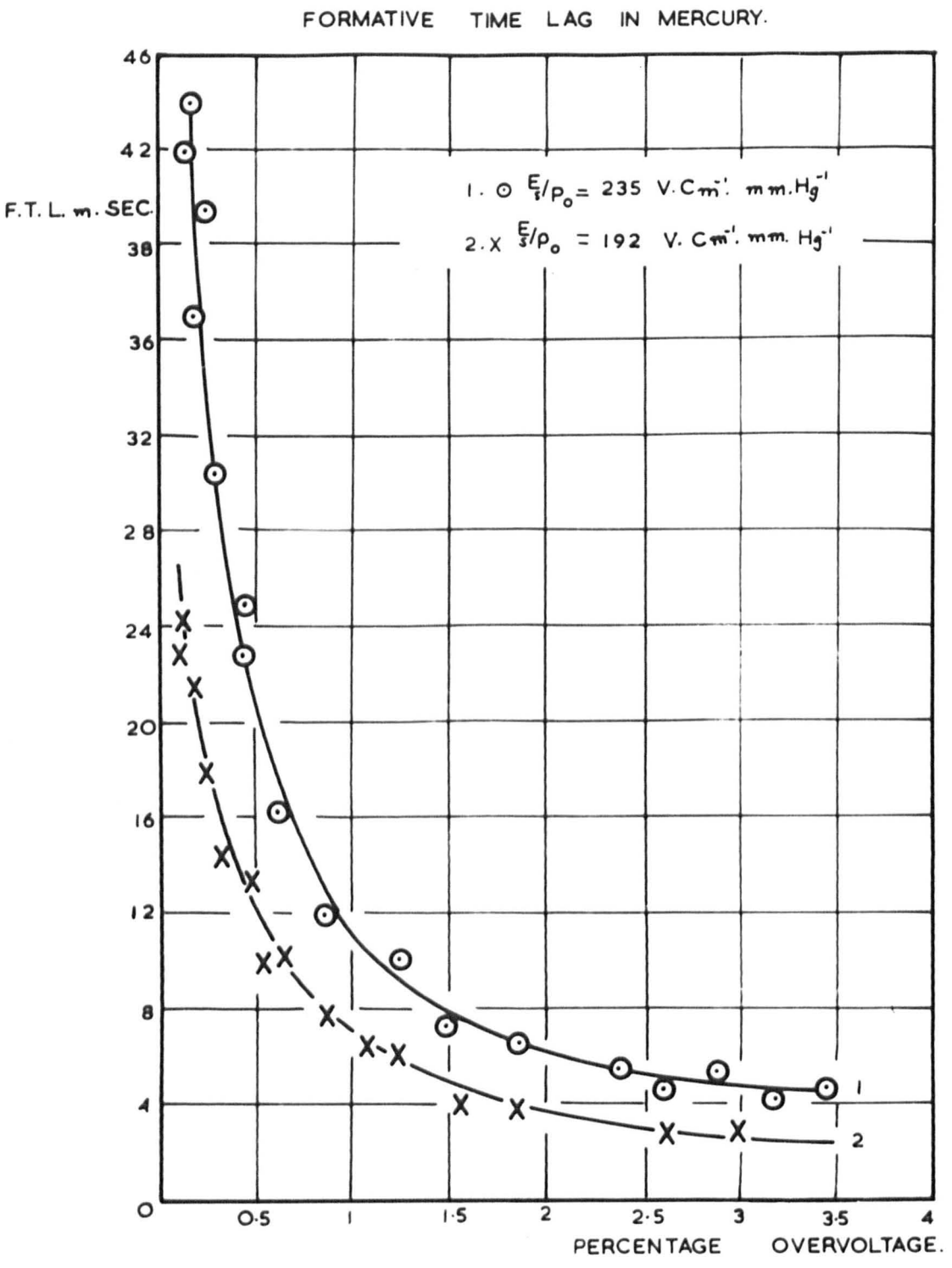
FORMATIVE TIME LAG IN MERCURY.
F.T.L. m. SEC.
1. ⊙ E_s/p_o = 235 V.Cm⁻¹. mm.Hg⁻¹
2. X E_s/p_o = 192 V. Cm⁻¹. mm. Hg⁻¹
46
42
38
36
32
28
24
20
16
12
8
4
0
0·5
1
1·5
2
2·5
3
3·5
4
PERCENTAGE OVERVOLTAGE.
1
2

Fig. 44

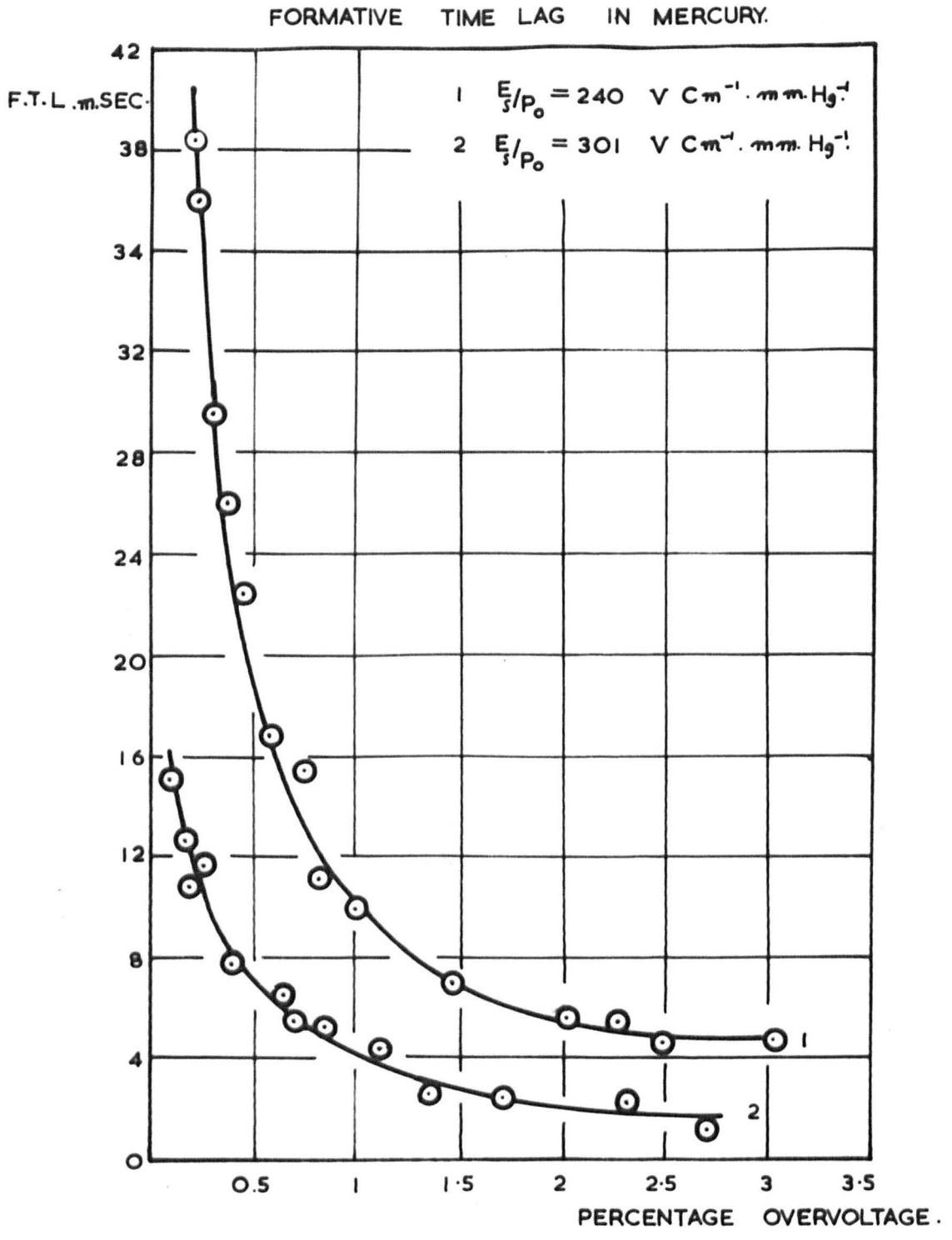
FORMATIVE TIME LAG IN MERCURY.
F.T.L. m.SEC.
42
38
34
32
28
24
20
16
12
8
4
0
1 E_s/P_o = 240 V Cm^{-1}. mm. Hg^{-1}.
2 E_s/P_o = 301 V Cm^{-1}. mm. Hg^{-1}.
0.5
1
1·5
2
2·5
3
3·5
PERCENTAGE OVERVOLTAGE.
1
2

Fig. 45

FORMATIVE TIME-LAG AS A FUNCTION OF

E_s/P_o, $\Delta V\% = 0{\cdot}25$ (OBTAINED FROM THE FIRST TUBE)

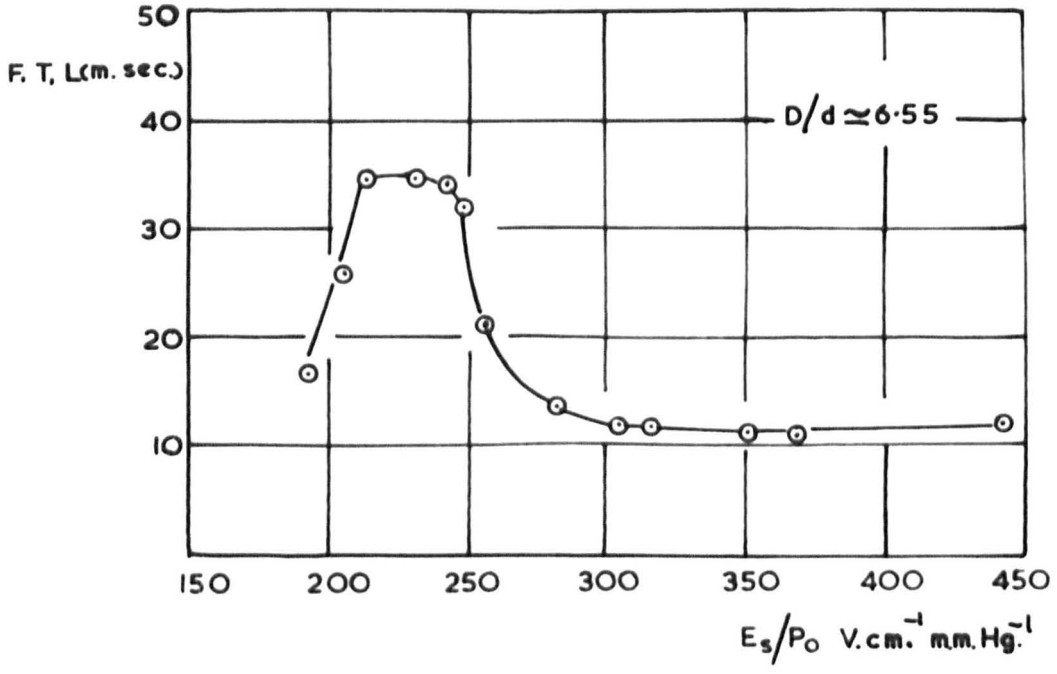

fig. 46

potential energy of 5.43eV.

From the above discussion, it appears that photons from the normal excited states $2\,^1P_1$ and $2\,^3P_1$ as well as 2^3P_o metastable atoms can contribute in the generalized secondary ionization coefficent. In order to show the relative importance of these states, the formative time-lag was studied and analysed by using Davidson theory, chapter 2. The results of the measurements of the formative time lag is presented and discussed in section (6.2.2),while the analysis is presented in section (6.2.3).

6.2.2. FORMATIVE TIME-LAG IN MERCURY VAPOUR.

Measurements of formative time lags obtained from the first experimental tube, covered a range of E_s/p_o ($E_s = \frac{V_s}{d}$, V_s is the sparking potential and d is the electrode separation) from 192 to 1020v $cm^{-1}.mm.Hg^{-1}$. Four typical curves of the formative time-lag as a function of the percent overvoltage are shown in figs(44) and (45). A plot of the formative time-lags against E/p_o for a given percent overvoltage indicated that in the region of E_s/p_o above 480v $cm^{-1}.mm.Hg^{-1}$ the growth rate is getting slower as E_s/p_o increases. It increases from 11 m.sec at an E_s/p_o of 480v.cm^{-1}. $mm.Hg^{-1}$ to 60 m.sec. at an E_s/p_o 1020 v.$cm^{-1}.mm.Hg^{-1}$ for 0.25% over-voltage. Since these measurements correspond to values of E_s/p_o on the left-hand side of the Paschen curve (E_s/p_o at the minimum breakdown potential is about 465v.$cm^{-1}.mm.Hg^{-1}$) it is to be expected that the secondary electron emission is caused by positive ions, because the excitation probability is very very low. In fact the time-lag in this region of E/p_o has only one significance, that it represents the time taken by the positive ions to reach the cathode from their point of formation (almost near the anode). In the region of E_s/p_o between 210 and 480v.$cm^{-1}.mm.Hg^{-1}$ and for 0.25% overvoltage

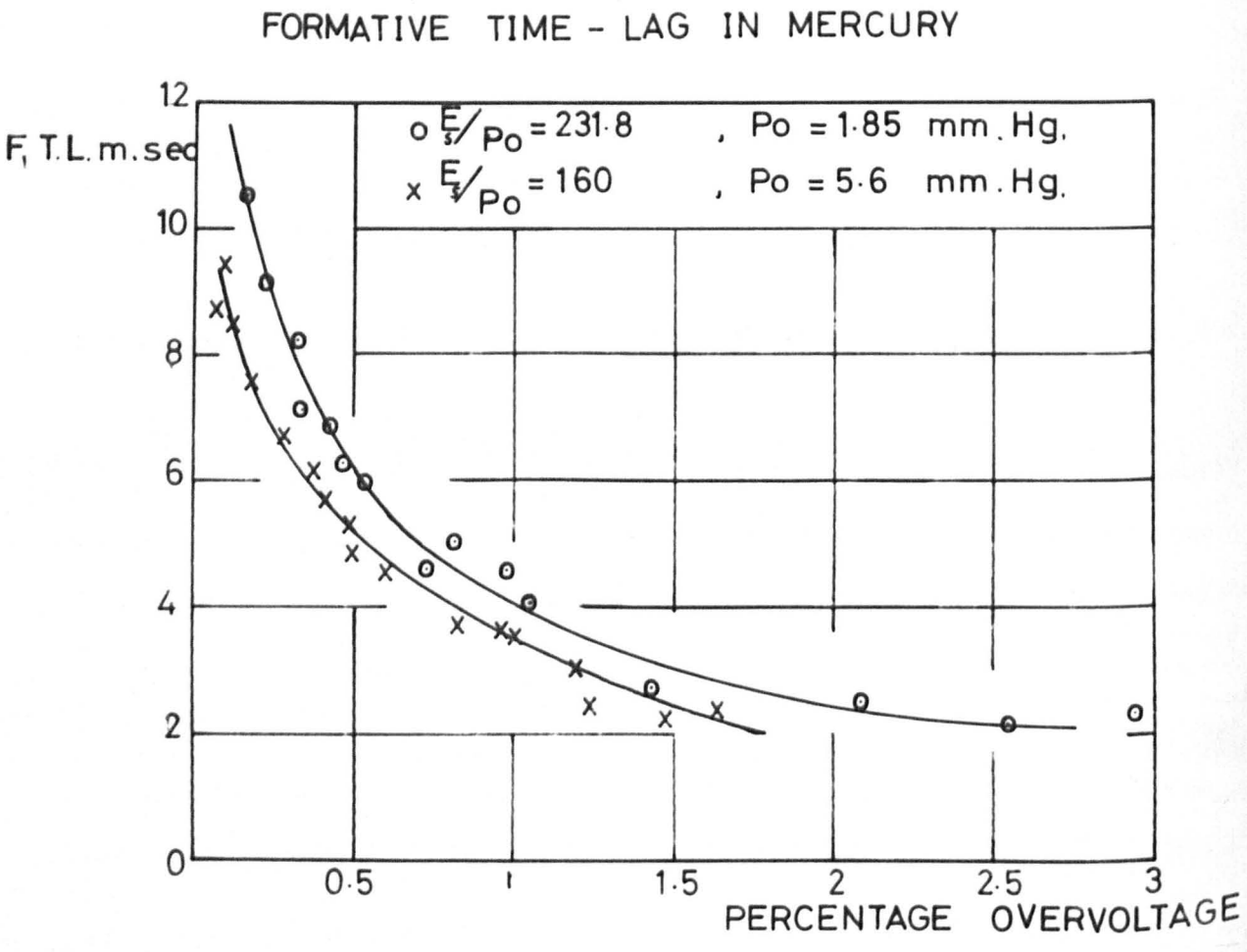
FORMATIVE TIME - LAG IN MERCURY
F, T.L. m.sec
o E/Po = 231·8 , Po = 1·85 mm. Hg.
x E/Po = 160 , Po = 5·6 mm. Hg.
12
10
8
6
4
2
0
0·5
1
1·5
2
2·5
3
PERCENTAGE OVERVOLTAGE

Fig. 47

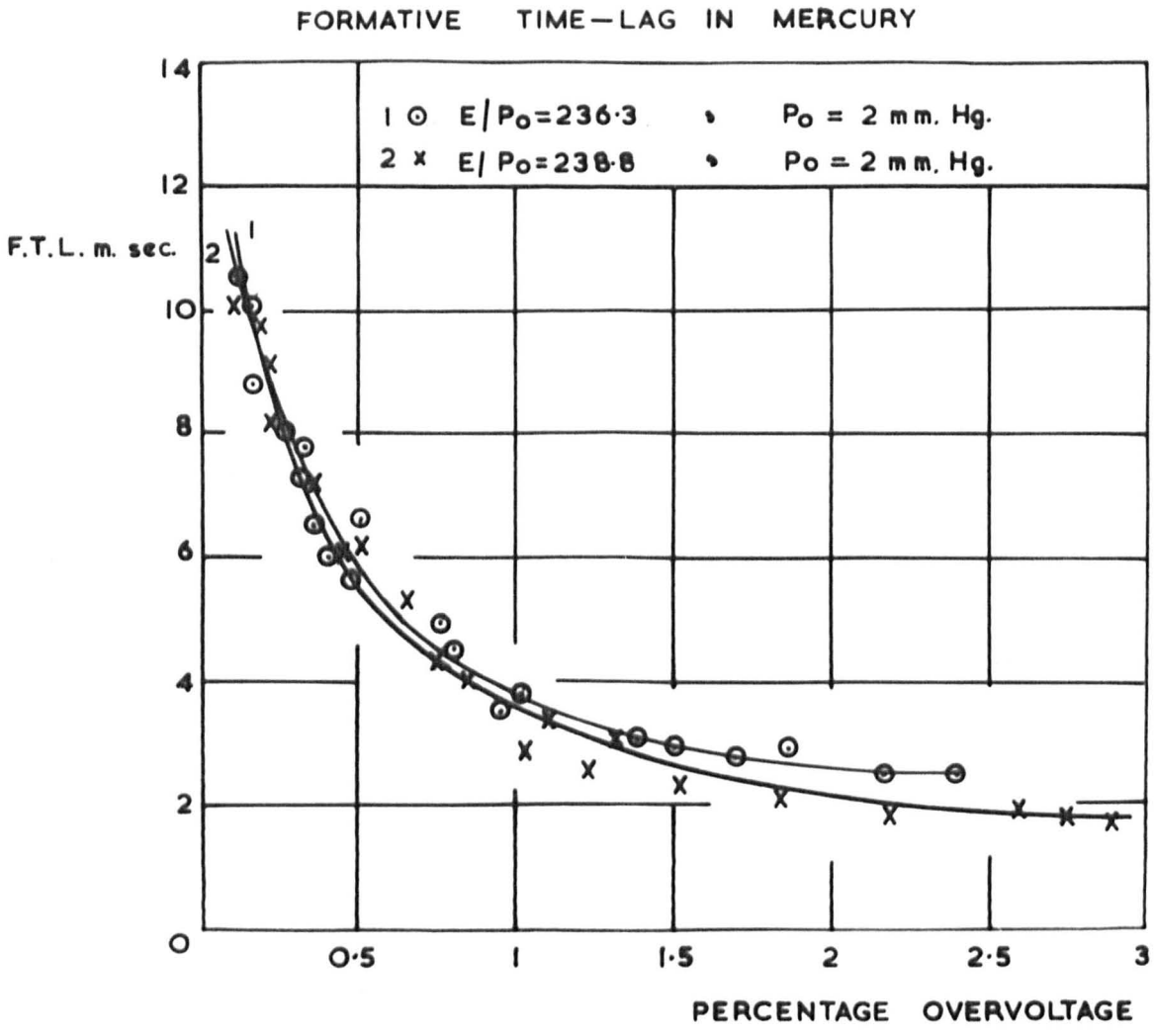
FORMATIVE TIME—LAG IN MERCURY
1 ⊙ E/Po=236·3 Po = 2 mm. Hg.
2 × E/Po=238·8 Po = 2 mm. Hg.
F.T.L. m. sec.
14
12
10
8
6
4
2
0
0·5
1
1·5
2
2·5
3
PERCENTAGE OVERVOLTAGE

fig.48

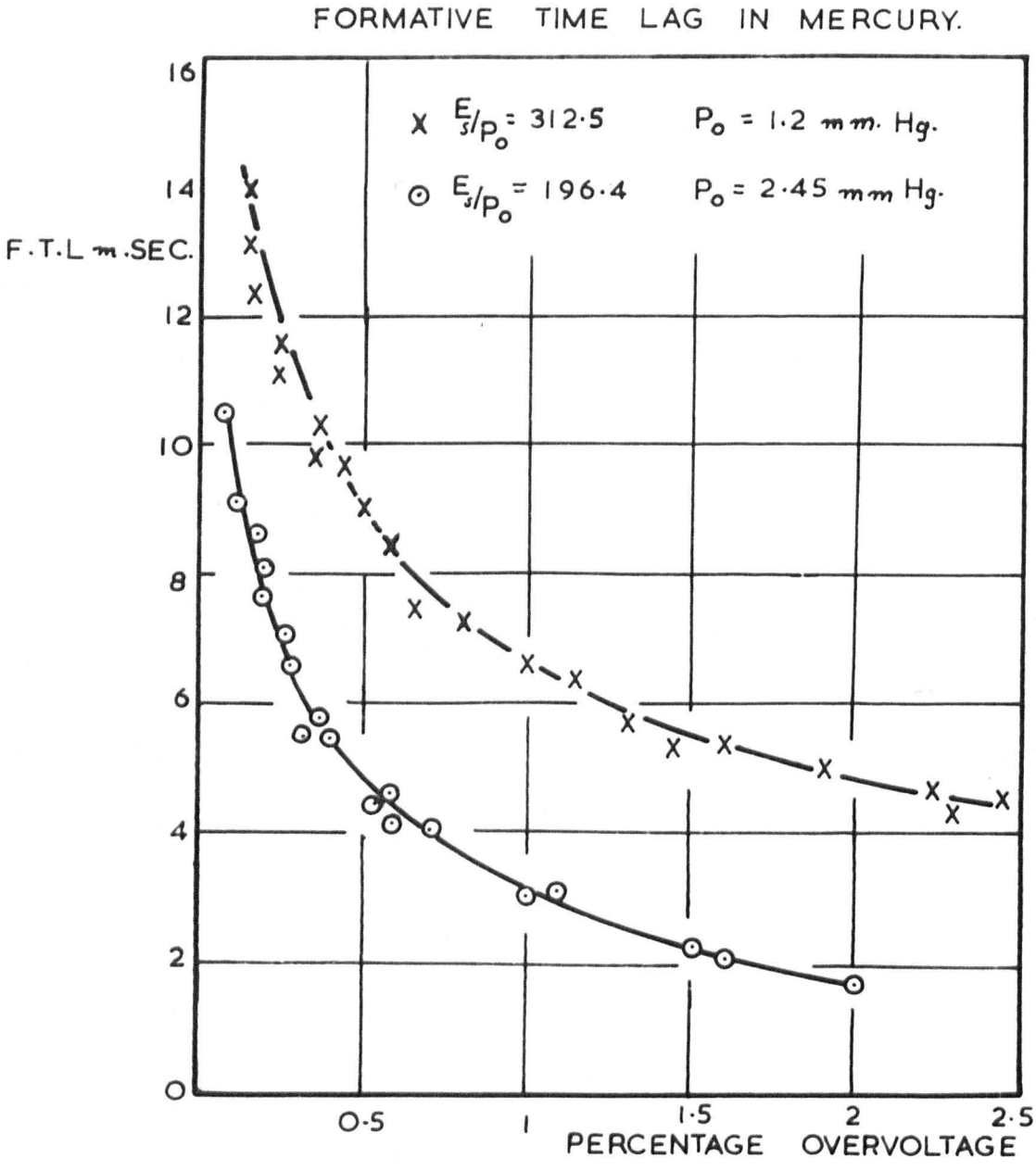
FORMATIVE TIME LAG IN MERCURY.
X E_s/P_o = 312·5 P_o = 1·2 mm. Hg.
⊙ E_s/P_o = 196·4 P_o = 2·45 mm Hg.
F·T·L m.SEC.
16
14
12
10
8
6
4
2
0
0·5
1
1·5
2
2·5
PERCENTAGE OVERVOLTAGE

Fig. 49

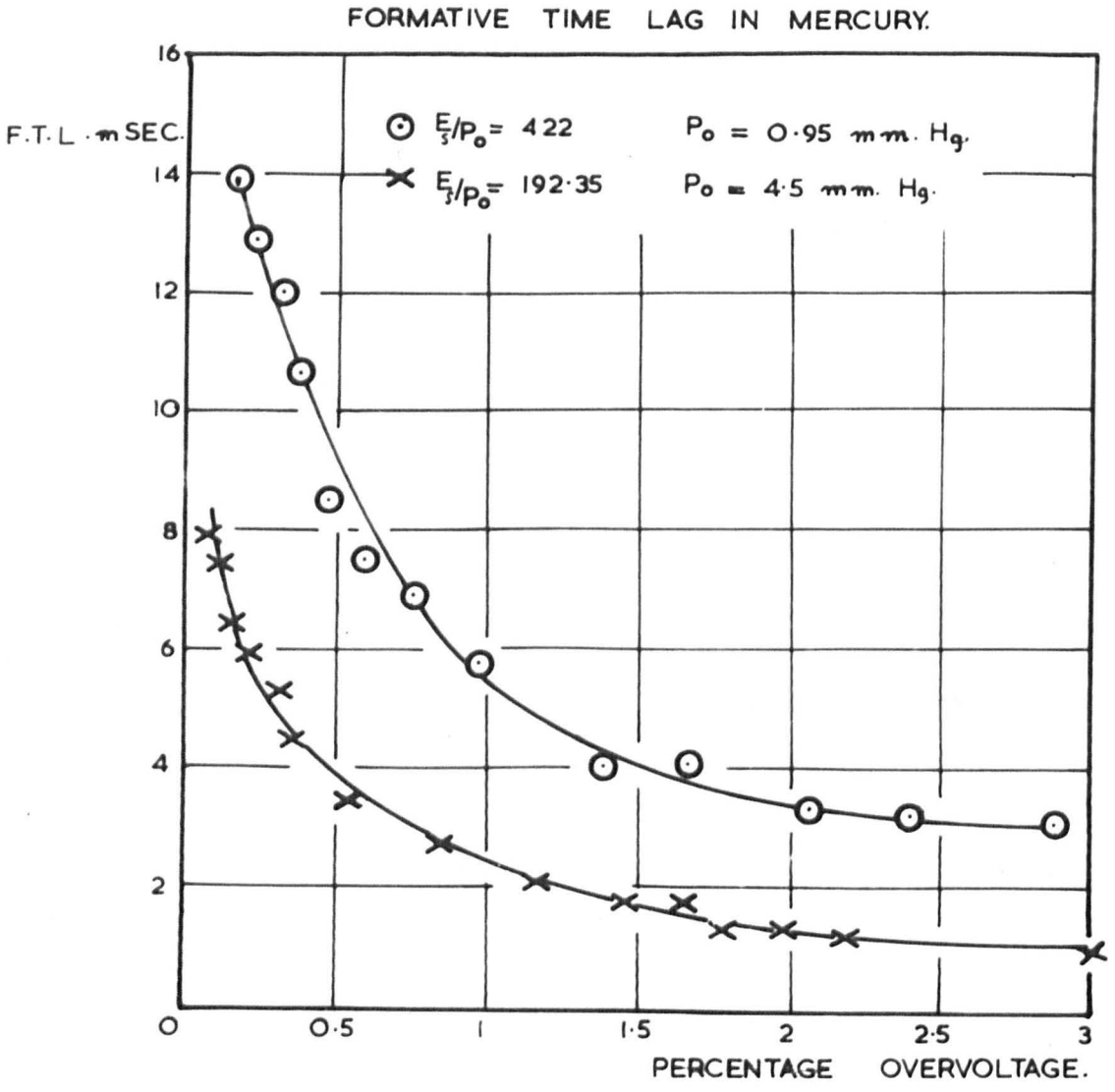
FORMATIVE TIME LAG IN MERCURY.
F.T.L. m SEC.
16
14
12
10
8
6
4
2
0
E_s/P_o = 422
P_o = 0·95 mm. Hg.
E_s/P_o = 192·35
P_o = 4·5 mm. Hg.
0·5
1
1·5
2
2·5
3
PERCENTAGE OVERVOLTAGE.

Fig. 50

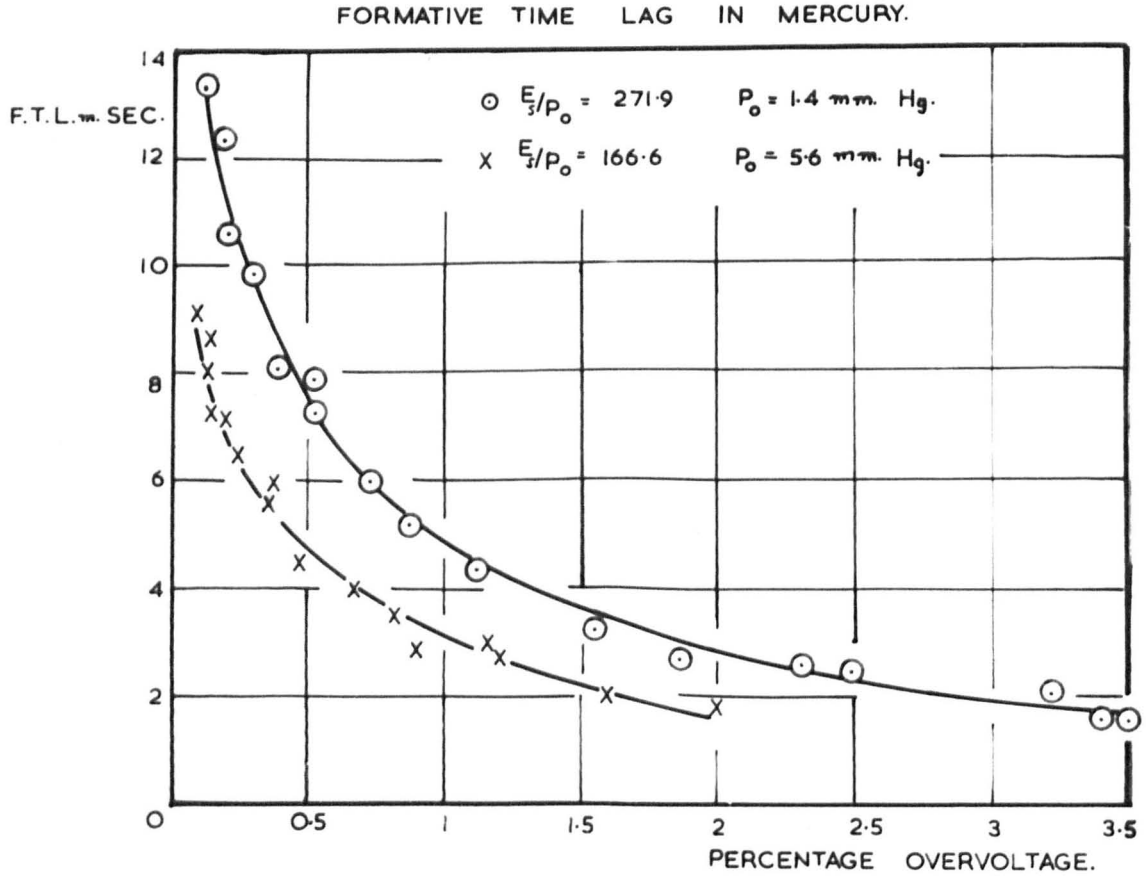
FORMATIVE TIME LAG IN MERCURY.
F.T.L. m. SEC.
14
12
10
8
6
4
2
0
⊙ E_s/P_o = 271·9 P_o = 1·4 mm. Hg.
X E_s/P_o = 166·6 P_o = 5·6 mm. Hg.
0·5
1
1·5
2
2·5
3
3·5
PERCENTAGE OVERVOLTAGE.

Fig. 51

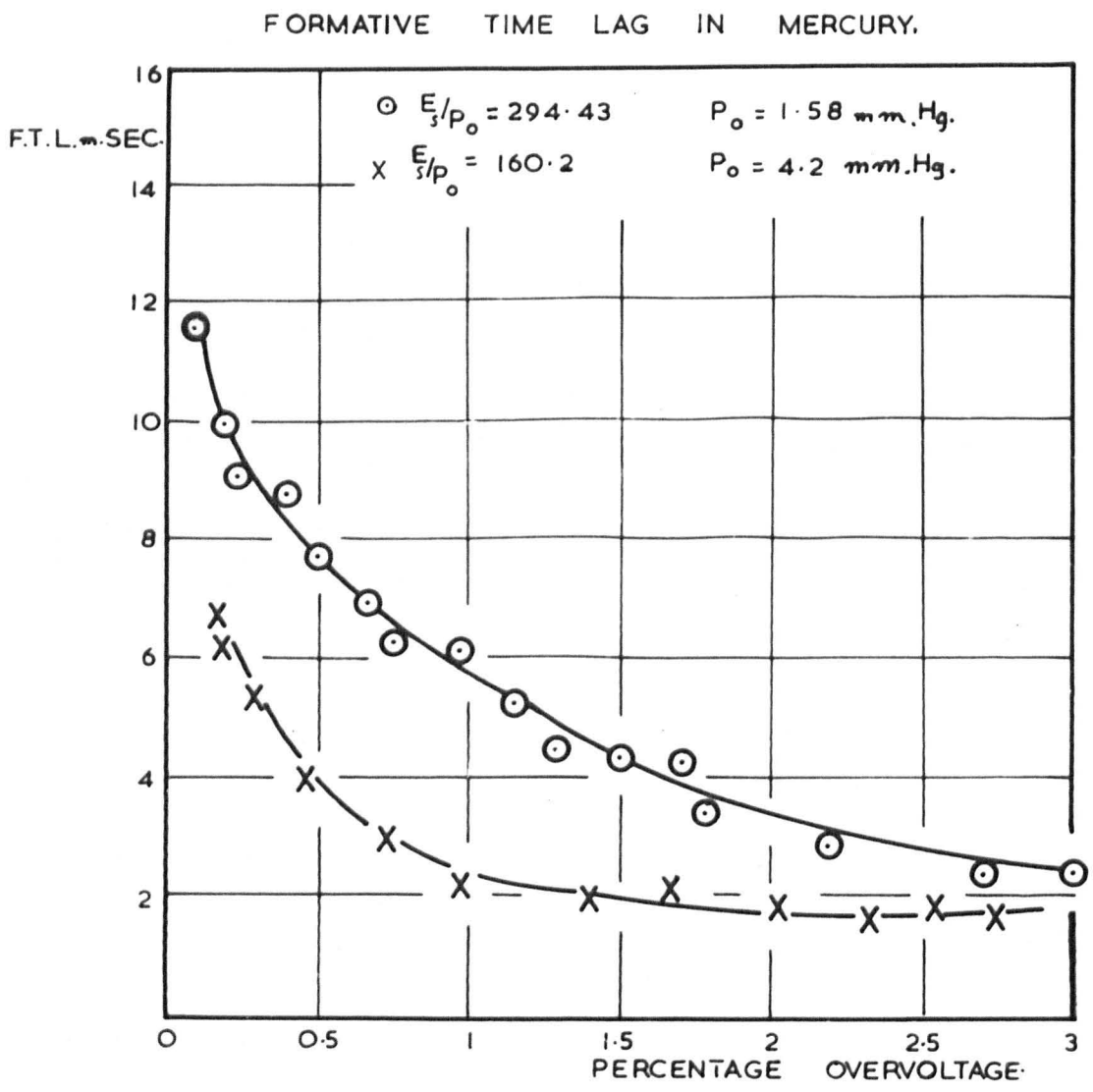
FORMATIVE TIME LAG IN MERCURY.
F.T.L.m.SEC.
16
14
12
10
8
6
4
2
⊙ E_s/P_o = 294·43
X E_s/P_o = 160·2
P_o = 1·58 mm.Hg.
P_o = 4·2 mm.Hg.
0
0·5
1
1·5
2
2·5
3
PERCENTAGE OVERVOLTAGE.

Fig. 52

fig(46), the present time-lags show similar characteristics to the growth times obtained by Overton, fig(20). The most important of these characteristics is the dependance of the growth times on the ratio D/d. At a particular value of E/p_o lower growth times are associated with higher ratio of D/d. For example, at an E/p_o of 275v.cm^{-1}.mm.Hg^{-1}., the present measured time-lag is 13 m.sec. for D/d of 6.55, while the times obtained by Overton are of the order of 20 m.sec. and 16 m.sec. for D/d of 4.3 and 5 respectively. This point will be discussed again with respect to the results obtained from the second experimental tube. In the region of E/p_o below 210v.cm^{-1}.mm.Hg^{-1}., contrary to the previous results which still show an increase in the time-lag, the present measured growth times show that the breakdown process is becoming faster. The speeding up of the breakdown process in this region of E_s/p_o is most likely due to the increase in the population of the slow components (the photons and metastable atoms) as it has been seen in the last section. Unfortunately, due to the fixed electrode separation in this experimental tube, it was not possible to obtain another set of measurements of the formative time-lags at another electrode separation. In order to investigate thoroughly the dependance of the growth times on the ratio of D/d, the second experimental tube was designed with much bigger electrode diameter (10cm.) and with a variable electrode separation system as described in section (4.3.2). Curves of time-lag as a function of percent overvoltage obtained from the second tube are shown in figs.(47) to (52). The measured times covered a range of E_s/p_o from 138 to 422v.cm^{-1}.mm.Hg^{-1}., and of d from 0.42 to 0.95 cm. and of p_o from 0.9 to 5.8 mm.Hg. As it has been seen, the liquid mercury cathode was contained in a glass cup in the centre of the tube. Change of the

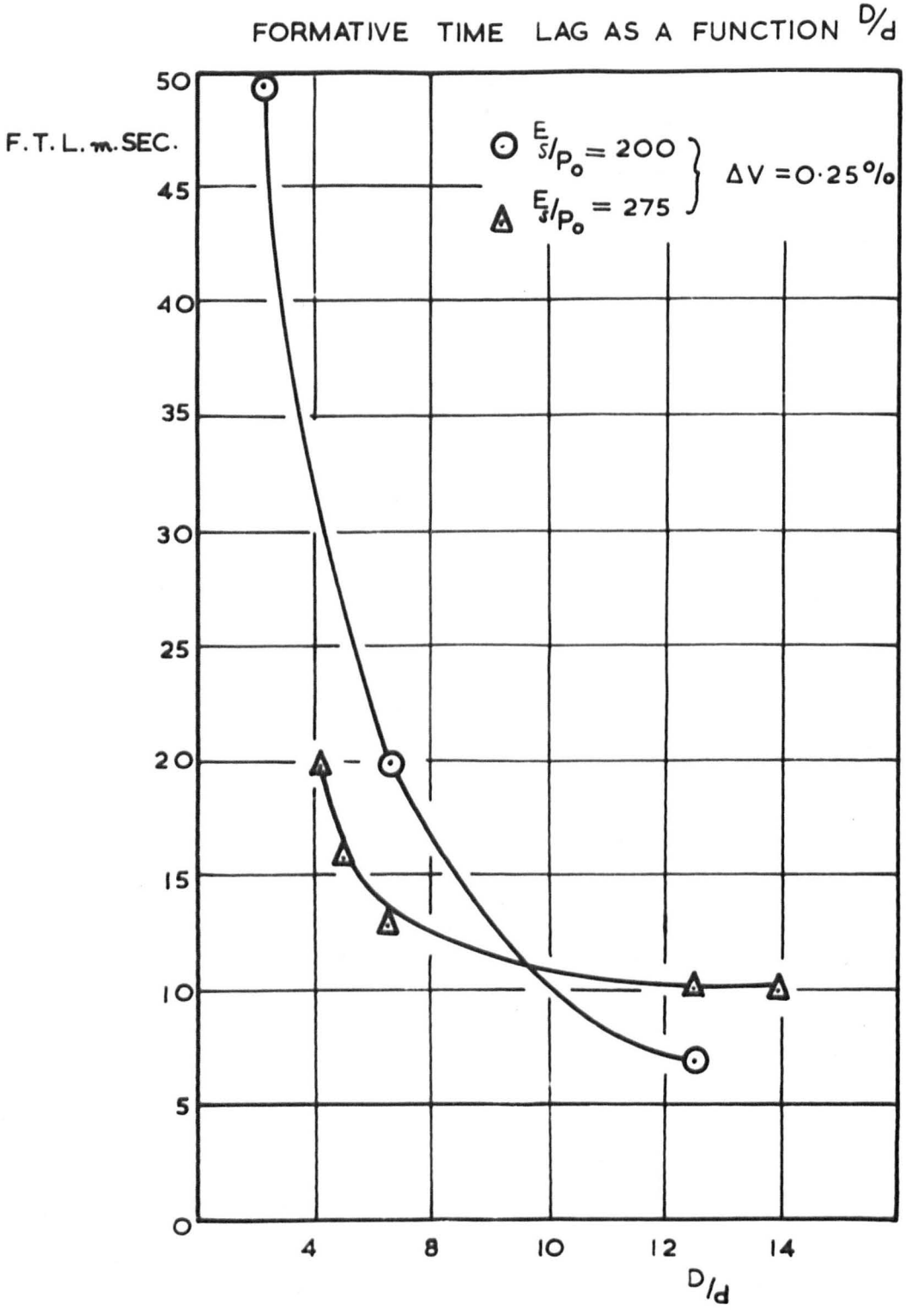
FORMATIVE TIME LAG AS A FUNCTION D/d
F.T.L. m.SEC.
50
45
40
35
30
25
20
15
10
5
0
4
8
10
12
14
D/d
E_S/P_o = 200
E_S/P_o = 275
ΔV = 0·25%

Fig. 54

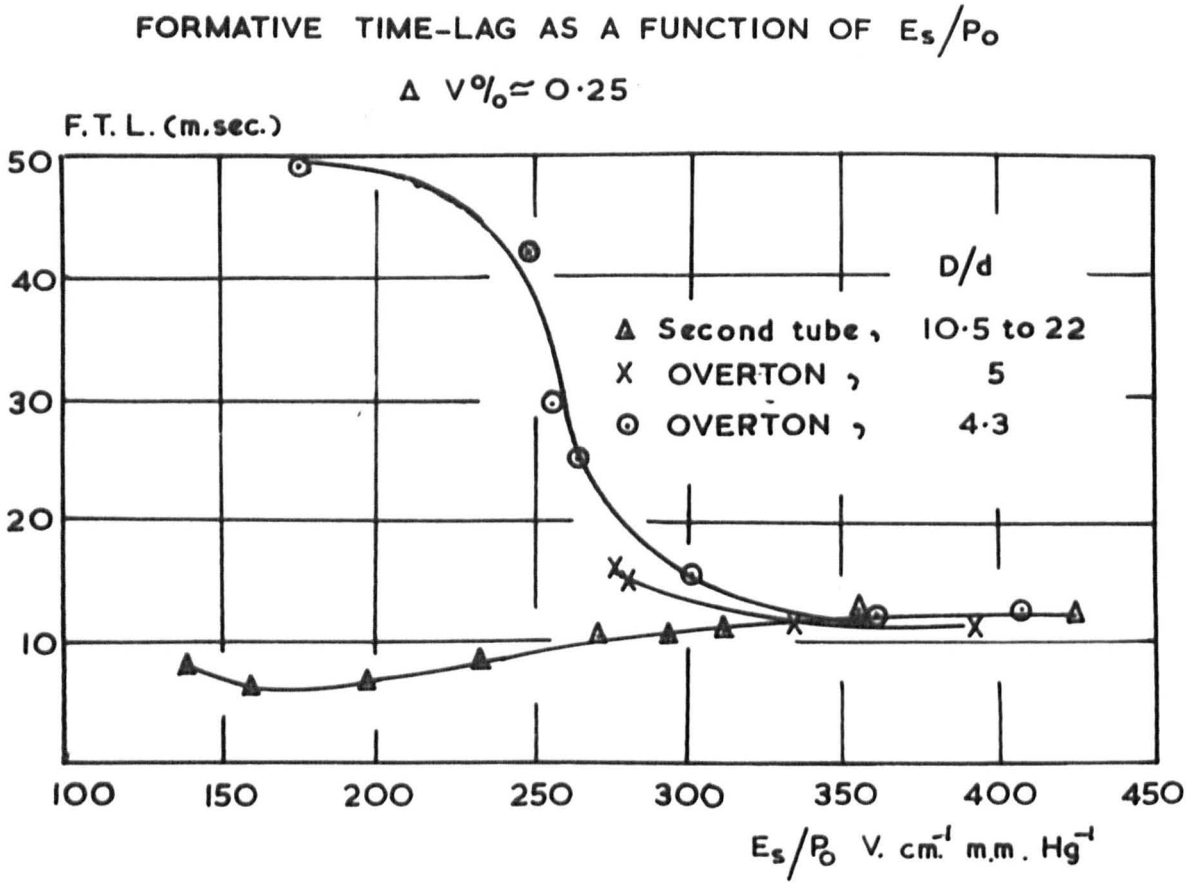
FORMATIVE TIME-LAG AS A FUNCTION OF E_s/P_o
Δ $V\%_o \simeq 0.25$
F. T. L. (m.sec.)
50
40
30
20
10
D/d
Δ Second tube, 10·5 to 22
X OVERTON, 5
⊙ OVERTON, 4·3
100
150
200
250
300
350
400
450
E_s/P_o V. cm^{-1} m.m. Hg^{-1}

fig.55

temperature of the oven to vary the pressure inside the tube (to obtain a new E_s/p_o) caused some evaporation of the mercury in the cup. Due to this evaporation, it was not possible to obtain a set of time-lag curves at the same electrode separation covering the wide range of E_s/p_o. No risk was taken to maintain the mercury surface level at the same point in the cup by evaporation of mercury from the side-arm, at the high temperatures used in the present measurements. The maximum variation of the mercury surface level was not greater than 0.05 cm., over the period(of 12 hours) required for stabilization of the temperature inside the oven. However, 1m.sec., was the maximum difference between any two readings of the time-lag at the same E_s/p_o and 0.25% overvoltage, observed for a difference o.15cm. in the electrode separations. This is not surprising, since a plot of the time-lag against D/d, at 0.25% overvoltage and at E_s/p_o 275 and 200v.cm^{-1}.mm.Hg^{-1}. fig(54) shows that the formative growth of ionization is less sensitive to variation in the electrode separation at this high ratio of D/d. The results used in the above two curves shown in fig(54) are taken from the present results (obtained from the first and second tube) and those of Overton.

The time-lag as a function of E_s/p_o for 0.25% overvoltage, obtained from the second experimental tube and those of Overton for the same per-cent overvoltage are shown in fig(55). In the range of E_s/p_o above 350v. cm^{-1}.mm.Hg^{-1}., they are almost the same. In the range of E/p_o below 350v.cm^{-1}. mm.Hg^{-1}., the present measured times, unlike the previous results, are showing that the breakdown mechanism is becoming progressively faster up to an E_s/p_o of about 160v.cm^{-1}.mm.Hg^{-1}. In the range of E_s/p_o below 160v.cm. mm.Hg^{-1}., despite the fact that the present measurements are showing a slow increase, these times and thus the breakdown mechanism is much faster than

in the previous results. The speeding up of the breakdown mechanism at these high ratios of D/d is most likely to be caused by the increase in the population of the active particles which are responsible for the breakdown mechanism. As will be seen later from the analysis of the results using Davidson's theory (section 6.2.3), it is found that at values of E/p_o below 350v.cm^{-1}.mm.Hg^{-1}., the secondary electron emission from the cathode by the incidence of delayed non-resonance photons are becoming very important. The photons are found to be produced by the volume destruction of the 2 $^3P_2$ metastable mercury atoms. Since the motion of the metastable atoms and the photons are entirely by their diffusion in the gas between the electrodes, then the rate of arrival of these photons at the cathode will depend on the solid angle between their point of formation and the cathode, since most of these photons are produced near the anode, then their rate of arrival at the cathode will generally depend on the ratio of D/d. For a tube for which the ratio D/d is large, the loss of the metastable atoms and photons from the gap will be small, and thus the rate of arrivals of photons at the cathode will be higher than in a tube for which D/d is small. This is most likely to be the explanation for the dependance of the growth times on D/d. At values of E_s/p_o above 350v.cm^{-1}.mm.Hg^{-1}., however, it is found from the analysis that the secondary emission is caused mainly by the mercury positive ions. Since that motion of the positive ions is confined to the field lines, therefore, it is not surprising to find the growth times are independant on the ratio of D/d in this region.

The speeding up of the temporal growth of current in the present results as E_s/p_o gets lower than 350v.cm^{-1}.mm.Hg^{-1}., is most likely to be caused by the increase in the population of 2 $^3P_2$ metastable mercury atoms as well

as of the increase in rates of their destruction in the gas. At these high ratios of D/d, as the pressure increases, (i.e. as E_s/p_o gets lower), it is to be expected that it will be accompanied by an increase in the population of the 2 $^3P_2$ metastable atoms and also by an increase in the rate of their destruction (i.e. decrease in the life-time). This will lead to an increase in the rate of formation of the non-resonance photons (the probability of excitation of the 2 $^3p_2$ metastable atoms, fig(4), starting to increase very steeply at an energy of about 14 eV. An energy of 14.3eV is expected to correspond to an E_s/p_o of 350v.cm^{-1}.mm.Hg^{-1}.) in the discharge gap, and thus will be accompanied by an increase of their arrival at the cathode. ~~It is of interest to notice.~~

6.2.3. ANALYSIS OF THE FORMATIVE TIME-LAG MEASUREMENTS USING DAVIDSON'S THEORY

6.2.3.1 INTRODUCTION

As it has been seen from section (6.2.1), the appearance of the peaks in the curves of ω/α against E_s/p_o at low values of E_s/p_o below 350v.cm^{-1}.mm.Hg^{-1}.) indicates the importance of the four P states of the mercury atoms together with the positive ions as secondary processes in a mercury discharge. The observed growth currents indicate that a slow process of a diffusive nature is operative. If undelayed photons produced from the de-excitation of the $^1p_1$ and $^3p_1$ states to the ground state ^1S_o are active, a time of the order of 10^{-8} to 10^{-7}sec. would be expected. In the case of delayed resonance photons, however, Overton(54) assuming an absorption coefficient of the order of 2000cm.$^{-1}$ and that the photons reach the cathode by a diffusion process, calculated times of the order of 10^{-6} to 10^{-5}sec. by using Davidson's growth equation (2.25). Thus

the calculated times for the last case differ little from those expected if an undelayed photon process is active. Mercury positive ions with a drift velocity of the order of 10^4cm.sec^{-1}, would give times of the order of 10^{-4}sec. For metastable mercury atoms ($^3p_2$) to act alone as a secondary process at the cathode, times of the order of 100m.sec. would be required for the breakdown to occur. Comparison of these times with the observed growth times, indicated that none of these processes could account alone for the breakdown mechanism. However it suggested that it could be accounted for by a combination between these last two processes and one or both of those discussed previously in section (2.3). Therefore a combination of either of the following two processes and the positive ion process were considered.

(a) The action of metastable atoms.

(b) The action of delayed non-resonance phctons.

Formative time-lags were calculated using the appropriate temporal growth of current equation from Davidson's theory (chapter 2) on the basis of the simultaneous action of the primary ionization process and one of the above combinations of secondary processes active at the cathode. The calculated times were compared with the observed time-lags to enable the unimportant secondary processes to be eliminated and the important secondary ionization coefficients to be estimated. The analysis was applied only to results obtained from the second tube. The time-lag was calculated at each particular E_s/p_o for a range of overvoltage between 0.2% and 2% and over a range of E/p_o from 138 to 422v.cm^{-1}.mm.Hg^{-1}. The calculations and their interpretation are presented in the following sections.

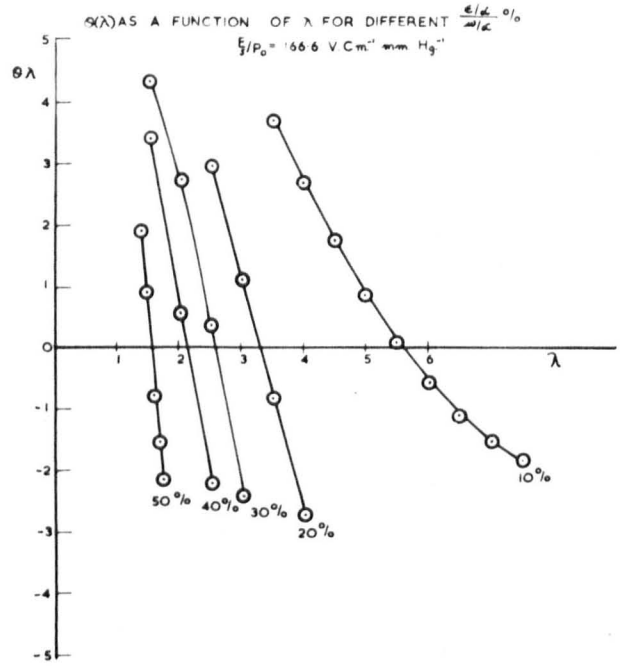
θ(λ) AS A FUNCTION OF λ FOR DIFFERENT
θλ
λ
50 %
40%
30%
20%
10%

Fig. 56

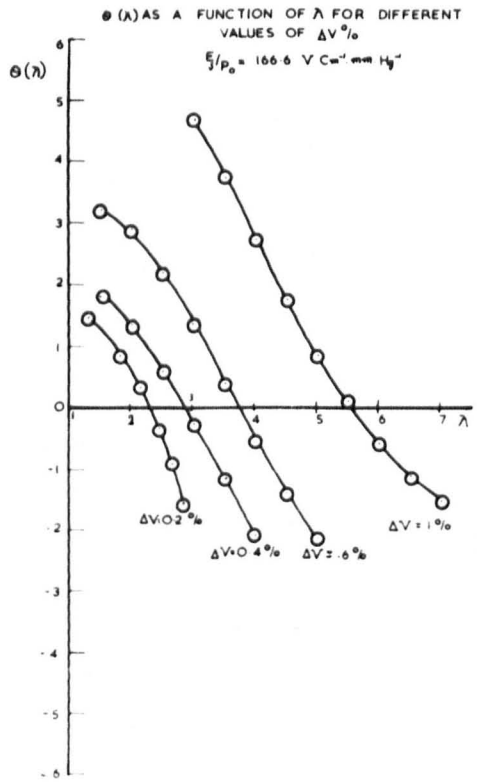
θ (λ) AS A FUNCTION OF λ FOR DIFFERENT VALUES OF ΔV %
θ(λ)
λ
ΔV=0.2 %
ΔV=0.4%
ΔV=.6%
ΔV=.1%

Fig. 57

6.2.3.2. CALCULATION OF THE IONIZATION GROWTH TIMES FOR SECONDARY ELECTRON EMISSION BY METASTABLE ATOMS.

In order to calculate the growth times from equation (2.2.5) under particular conditions, it is essential to find the real solution λ which satisfies the equation (2.27) $\theta(\lambda) = 0$. This function was solved firstly for λ graphically by plotting $\theta(\lambda)$ against λ. This was done in the preliminary calculations to find the behaviour of the function $\theta(\lambda)$ and the order of magnitude of the real solution (non-trivial solution) λ. Calculation of $\theta(\lambda)$ as a function of λ was performed for the experimental curves of time-lags at E_s/p_o of 422, 192 and 166.6v.cm^{-1}.mm.Hg^{-1}. For each of these curves the function $\theta(\lambda)$ was determined for six values of overvoltages and for nine choices of metastable atoms' contribution in (equation 2.29). Thus calculation of $\theta(\lambda)$ as a function of λ was performed for 54 different conditions for each of the experimental curves. Typical curves of the function $\theta(\lambda)$ as a function of λ are shown in figs.(56) and (57), which are for the experimental conditions of the formative time-lag curve at E_s/p_o of 166.6v.cm^{-1}.mm.Hg^{-1}. The curves in fig(56) were calculated for 1% overvoltage and different percent contribution ($\frac{\varepsilon/\alpha}{\omega/\alpha}$ x100) of the metastable atoms (ε/α in ω/α, those in fig(57) were calculated for 10% metastable atoms contribution and for different percent overvoltages. It can be seen from fig(56) that as the percent contribution of metastable atoms is decreased, the curves cut the $\theta(\lambda) = 0$ axis at shallow angles, and there is a real solution λ for each of the five curves. From fig(57) however, it can be seen that there is only a real solution λ for the first four percent overvoltages. In most cases, there was not a real solution λ for overvoltages above 2%, the only solution was found to be a trivial one (i.e. at $\lambda = \alpha$). Fulker (65),

studying the time-lag in neon, also could not find a real solution (non-trivial solution) at 2% percent overvoltage. It is difficult to see any physical reason which could account for this lack of a real solution at high overvoltages.

Knowing the characteristics of the function $\theta(\lambda)$, the formative time-lag was calculated using Davidson's theory as described in section (2.2) involving the emission of secondary electrons from the cathode by metastable atoms and positive ions and undelayed photons. An Elliott 4101 computer was used to facilitate the calculations. In the following program some of the symbols used in the equations in section (2.2) have been changed to make the program acceptable in the Fortran 4 computer language. The corresponding symbols are listed below.

A = α Primary ionization coefficient.

GS = ω/α Generalized Secondary ionization coefficient.

D = d electrode separation.

P = p_o reduced pressure.

T = T Temperature in degrees Kelvin.

E = ε/α Secondary ionization coefficient for metastable atoms.

E = $Y + \delta/\alpha$ positive ion and photon secondary ionization coefficients taken together.

Q = λ

FQ = $F(\lambda)$.

FQZ= $F^1(\lambda) = \frac{\delta F(\lambda)}{\delta \lambda}$

B = $e^{\alpha d} - 1$.

BA = $e^{\alpha d} - \alpha d - 1$.

F = $1 - (\gamma + \delta/\alpha)(e^{\alpha d} - 1)$.

S = $\frac{\varepsilon/\alpha \ (\alpha^2 d)(e^{\alpha d} - 1)}{e^{\alpha d} - \alpha d - 1}$.

$R = \frac{I(d,t)}{I_o}$

$RV = \frac{I(o,t)}{I_o}$

C = C^2 square of the average velocity of the metastable atoms.

STY = N number of atoms per cm^3.

DFM = D Diffusion coefficient of metastable atoms.

TF = t the formative time-lag.

The expressions Y, W, WV, U, FQA, and FQB were used to facilitate the program.

The program calculates TF (time-lag) for 8 curves of the time-lag in each run. For each curve, TF was calculated at 6 overvoltages corresponding to 0.2%, 0.4% 0.6%, 1%, 1.5% and 2%. At each percent overvoltage, TF was calculated for 9 choices of the secondary ionization coefficients satisfying the relation, GS = E + EP. Thus the time-lag was calculated for 54 different conditions for each experimental curve of time-lag. The real (non-trivial) solution λ was determined automatically by "DO" loop and "IF" statement to an accuracy of 0.01%. Equation (2.25) was simplified by neglecting the constant A(= $\frac{1}{1 \frac{\omega}{\alpha} (e^{\alpha d} - 1)}$) since it can be omitted at large observed times, without any serious error in the validity of the equation. The diffusion coefficient was determined from the relation,(70), $(2C^2)^{\frac{1}{2}}/3 \; S_{12}^2$, where C is the mean velocity of the atom, N is the number of atoms per C.C.(= $p_o \times 10^{17}/2.827$), and S_{12} is the average diameter of the normal and metastable atoms of being 3.75×10^{-8}cm.

The program.

```
      DO 500 N=1,8
      READ(7,100)D,GS,P,T
      DO 400 M=1,6
      READ(7,100)A
RV=2  RV=200000.0
      REX=0.1
      DO 200 K=1,9
      E=GS*REX
      REX=REX+0.1
      EP=GS-E
      B=(EXP(A*D))-1.0
      BA=B-(A*D)
      F=1.0-EP*B
      S=(E*(A**2.0)*D*B)/BA
35    Q=0.0
      ZINC=0.1
      DO 30 J=1,4
40    Q=Q+ZINC
      Y=(Q+A)*(((Q-A)*F)-S)
      W=EXP((A-Q)*D)
      WV=EXP(-2.0*Q*D)
      FQ=(Y*(1.0-WV))+(2.0*S*Q*W)-(2.0*S*WV*Q)
      IF(FQ+0.0)50,60,40
50    Q=Q-ZINC
      ZINC=ZINC/10.0
```

```
30  CONTINUE
60  Y=(Q+A)*(((Q-A)*F)-S)
    W=EXP((A-Q)*D)
    WV=EXP(-2.0*Q*D)
    U=(2.0*((Q**2.0)-A**2.0))*(1.0-WV))/Q
    FQA=(2.0*Q*F)-S-(2.0*S*((Q*D)-1.0)*W
    FQB=(WV*((2.0*F*D*((A**2.0)-(Q**2.0)))+(2.*D*S*(A-Q))+(2.*Q*F)+S))
    FQZ=FQZ-FQB
    R=RV/B
    C=1.25*(10.0**6.0)*T
    STY=P*(10.0**17.0)/2.826642
    DFM=((2.0*C)**0.5)/(STY*1.90755*(10.0**(-14.0)))
    TF=(ALOG((R*FQZ)/U))/(DFM*(Q**2.0))
    WRITE(2,300)TF,A,REX,Q,DFM
200 CONTINUE
400 CONTINUE
500 CONTINUE
100 FORMAT(4F0.0)
300 FORMAT(1H0,6E12.5)
    STOP
    END
```

The calculated time-lags were plotted against percent overvoltage and compared with the experimental ones. At all percent contribution of ε/α and $\gamma + \delta/\alpha$ in ω/α, the calculated growth times proved to be slow. For 90% of the metastable atoms in ω/α the calculated times were about one order of magnitude higher than the measure ones. At an

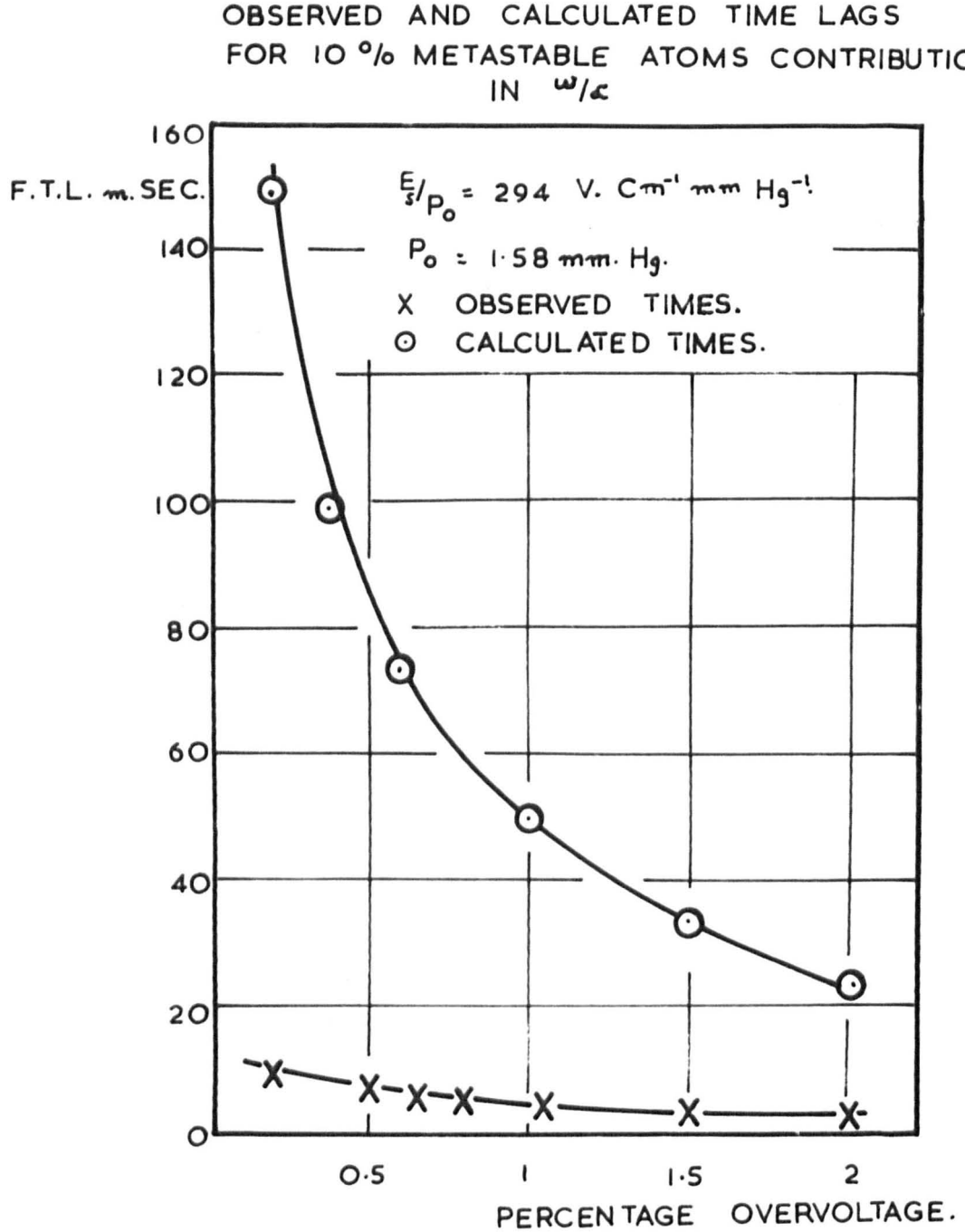
OBSERVED AND CALCULATED TIME LAGS
FOR 10 % METASTABLE ATOMS CONTRIBUTION
IN ω/α
F.T.L. m. SEC.
160
140
120
100
80
60
40
20
0
E/P0 = 294 V. Cm-1 mm Hg-1.
P0 = 1·58 mm. Hg.
X OBSERVED TIMES.
⊙ CALCULATED TIMES.
0·5
1
1·5
2
PERCENTAGE OVERVOLTAGE.

Fig. 58

E_s/p_o of 294v.cm^{-1}.mm.Hg^{-1}., the calculated time-lag was 15 times too great for 0.2% overvoltage, and 6 times too great for 2% overvoltage. The theoretical and the observed time-lag curves, at this value of E_s/p_o can be seen in fig(58). The theoretical curve is for 10% metastable atom contribution in ω/α . Therefore, it was concluded that the combination of secondary processes considered above, can not account for the breakdown in mercury vapour in the range of E_s/p_o considered.

6.2.3.3 CALCULATION OF THE FORMATIVE TIME-LAG FOR SECONDARY ELECTRON EMISSION BY DELAYED NON-RESONANCE RADIATION.

In the modified theory by Davidson discussed in section (2.3) it is shown that by applying equation (2.51) to a particular gas, the formative time-lag can be calculated for delayed radiation and positive ion action at the cathode. It has been shown also that there are several collisional processes known to occur in the gas which can ultimately give rise to secondary emission after a relatively long delay between the initial electron-atom exciting collisions and the release of a cathode electron. The most likely delayed processes to occur in a mercury discharge are,

(1) Imprisoned resonance radiation which proceeds to the cathode according to Hoelstein-Biberman transport theory.

(2) Collision induced non-resonance radiation.

If the motion of the imprisoned resonance photons is governed by the Hoelstein-Biberman transport law, then the total delay time τ_1, has been shown (equation 2.32) to depend on the life-time of the resonance state τ_o, and on the number of absorptions and re-emissions made in traversing the discharge gap. It has been seen in section (6.2.1.3) that the phonons of most importance are those produced in the transition $^1P_1$ to ^1S_o

with a wavelength of 1849Å. An average of 2.56×10^3 absorptions and re-emissions will take place when these photons travel through 1cm.gap distance. The average life-time of this state is about 1.3×10^{-9}sec.(66), therefore a delay time τ_1 of the order of 3.33×10^{-6}sec. would be expected, which is very low to account for the measured growth times. In the case of the photons which correspond to the transition $^3P_1$ to ^1S_o, of average life-time 1.18×10^{-7}sec.(67), a total delay time of 1.2×10^{-4}sec. would be expected for the same gap distance. During this time a large number of the atoms in the state $^3P_1$ will degenerate to the state ^3P_o (7) in two body collisions with the ^1S_o ground state atoms. The cross-section for this transition, being 3.1×10^{-17}cm.^{2}, is about 14 times higher than the cross-section for the transition $^3p_1$ to ^1S_o, being 2.2×10^{-18} cm^2 (68). Yavorskii(69) determined the maximum excitation cross-section to the state $^3P_1$ from the ground state to be 1.05×10^{-16}cm^2. Comparison of the above values and the one given in section (6.2.1.3) suggests that the delayed photons emitted in the transition $^3p_1$ to ^1S_o would not lead to a substantial photoelectric emission in a mercury discharge.

In collision-induced non-resonance radiation, metastable atoms emit non-resonance photons through a straight transition to the ground states by breaking the selection rules. As it has been seen from section (6.2.1.3) the most likely non-resonance photons which are capable of emitting secondary electrons from the cathode, are those emitted in the transition $^3p_2$ to ^1S_o. Couillette (70) has concluded that there is a dissipative process in which one collision in 1300 with normal mercury atoms results in the metastable mercury atom losing its excitation energy Zemansky (71) has also shown that there is a probability of 9×10^{-4} of the

mercury metastable atoms losing their excitation energies in two-body collisions with ground state mercury atoms. For an electrode separation of 1cm., mercury metastable atom, moving through the gap without lateral deflection, will on the average make 200 collisions at pressure of 1mm. Hg. At a pressure of 4mm.Hg., however it will make about 900 collisions. Therefore it seems likely that the $^3P_2$ metastable mercury atom will have ample opportunity of losing its excitation energy in this manner, resulting in volume destruction with a subsequent emission of non-resonance photons. If the secondary electron emission is caused by these non-resonance photons, the delay time τ_1 (i.e. the average life-time of $^3P_2$ state) would be expected to depend on the pressure, since the number of dissipative collisions per cm. is dependant on the pressure. According to Couillette and Zemansky's values, a life-time of the order 67 to 51×10^{-6} sec. and 280 to 215×10^{-6} sec. would be expected at pressures of 4 and 1mm.Hg. respectively.

Aubrecht (56) working on the afterglow spectrum of a rf mercury discharge, has determined the life-time of the $^3P_2$ state to be 46.8×10^{-6} sec. in the region of pressure between 0.5 and 3 mm.Hg. This determination was based on the assumption that the $^3P_2$ metastable atom is destroyed in a two body collision with another $^3P_2$ metastable atom.

On these semi-quantative grounds, it would appear unlikely that the imprisoned resonance radiation produced from the transitions $^1P_1$ to ^1S_o and $^3P_1$ to ^1S_o will lead to a substantial secondary emission, and any photoelectric emission is more likely to be caused by the action of the non-resonance radiation which is produced in the volume destruction of the

state $^3P_2$. However a detailed quantative analysis of the observed growth times using Davidson's theory (section 2.3) is necessary before a reliable conclusion concerning the relative importance of these two possible delayed radiation processes can be obtained.

The formative time lag was calculated from equation (2.51) on the assumption that a combination of positve ions and delayed radiation is active at the cathode as the secondary process. It can be seen from equation (2.45), that at a particular value of overvoltage and a given choice of secondary ionization coefficients (δ_1/α and γ in equation 2.53), the value of γ of P which satisfies F(P), and therefore the calculated growth times, will depend on the value of the delay time τ_1. Now it has just been seen that there are two possible delayed radiation processes and each of them has a variable delay time ranging from $5x10^{-5}$ to $5x10^{-4}$ sec. Therefore in the calculation of the time-lag at a particular value of overvoltage and choice of the secondary ionization coefficients ($\delta_1/\alpha + \gamma = \omega/\alpha$), τ_1 was treated as a variable and given 12 choices of delay times. Preliminary analysis showed that the values of τ_1 required to account for the observed growth times are equal or higher than $50x10^{-6}$ sec. Therefore in the analysis of the present results τ_1 was varied between $50x10^{-6}$ sec. to $600x10^{-6}$ sec., in steps of $50x10^{-6}$ sec. The following program was written by the present author to facilitate the calculation of the time-lag using the equations (2.45) to (2.53). Some of the variables used in these equations had to be changed to suit computer Fortran 4 language. The corresponding variables are given below:-

A = α primary ionization coefficient.

D = d electrode separation.

EP = γ' positive ions secondary ionization coefficient.

ED = δ_1/α Delayed photons secondary ionization coefficient.

GS = ω/α generalized (or total) secondary ionization coefficient.

EB = E/p_o ratio of the field strength to reduced pressure of mercury vapour.

WB = W_+ drift velocity of positive ions.

RE = ε average electron energy in election volt unit (Overton).

WE = W_- drift velocity of electrons.

TE = τ_1 average total delay time in the case of resonance photons or the average life-time of the metastagle states in case of non-resonance radiation.

Q = λ of P which satisfies the equation F(P) = 0

FQ = F(P)

FQD = $F^1(P)$ the first differential with respect to P of F(P) evaluated at the λ of P which satisfies the equation F(P) = 0.

RV = $\frac{i(d,t)}{I_o}$

R = $\frac{i(o,t)}{I_o}$

FTL = t the formative time-lag, $\frac{1}{W} = \frac{1}{W+} + \frac{1}{W-}$

X = $\psi = \alpha - \lambda/W_-$

XZ = $\phi = \alpha - \lambda/W$

B = $e^{\psi d}$

BA = $e^{\phi d}$

V = $(1 + \lambda . \tau_1)$

FLD, FCD and FDD are intermediate expressions used to simplify the program.

The Program:

```
      DO 6ØØ N=1,12
      READ(3,1ØØ)D,GS,EB
      DO 55Ø M=1,6
      READ(3,1ØØ)A
      DO 5ØØ K=1,2
      READ(3,1ØØ)WB
      REX=Ø.Ø8
      DO 52Ø I = 1,1Ø
      REZ=REX*1ØØ.Ø
      EP=GS*REX
       ED=GS-EP
      REX=REX+Ø.Ø8
      TE=Ø.Ø
      ACD=Ø.ØØØØ5
      DO 45Ø J=1,12
      TE=TE+ACD
      RE=((EB/42.Ø)+6.Ø)*1.6*(1Ø.Ø**(-12.Ø))
      WE=(2.Ø*RE /(9.1Ø7*(1Ø.Ø**(-28.Ø))))**Ø.5
      W=(WE*WB)/(WE+WB)
      Q=Ø.Ø
      ZINC=5Ø.Ø
      DO 4ØØ IJ=1,5
35Ø   Q=Q+ZINC
      X=A-(Q/WE)
      XZ=A-(Q/W)
```

```
      B=EXP(X*D)
      BA=EXP(XZ*S)
      V=1.Ø+(Q*TE)
      FQ=1.-((A*ED*(B-1.Ø))/(V*X))-((A*EP*(BA-1.))/XZ)
      IF(FQ-Ø.Ø)35Ø,6Ø,3ØØ
3ØØ   Q=Q-ZINC
      ZINC=ZINC/1Ø.Ø
4ØØ   CONTINUE
 6Ø   X=A-(Q/WE)
      XZ=A-(Q/W)
      B=EXP(X*D)
      BA=EXP(XZ*D)
      V=1.Ø+(Q*TE)
      FLD=(A*ED)/(WE*(X**2.Ø)*(V**2.Ø))
      FCD=FLD*((WE*X*TE*(B-1.))+(V*((((X*D)-1.)*B)+1.)))
      FDD=((A*EP)*((((XZ*D)-1.Ø)*BA)+1.Ø))/(W*(XZ**2.Ø))
      FQD=FCD+FDD
      RV=2ØØØØØ.Ø
      R=RV/((EXP(A*D))-1.Ø)
      FTL=(ALOG(Q*FQD*R))/Q
      WRITE(2,2ØØ)FTL,REZ,A,TE,W,Q,EB
52Ø   CONTINUE
5ØØ   CONTINUE
55Ø   CONTINUE
6ØØ   CONTINUE
25Ø   FORMAT(F15.7)
2ØØ   FORMAT(1HØ,1ØE17.5)
```

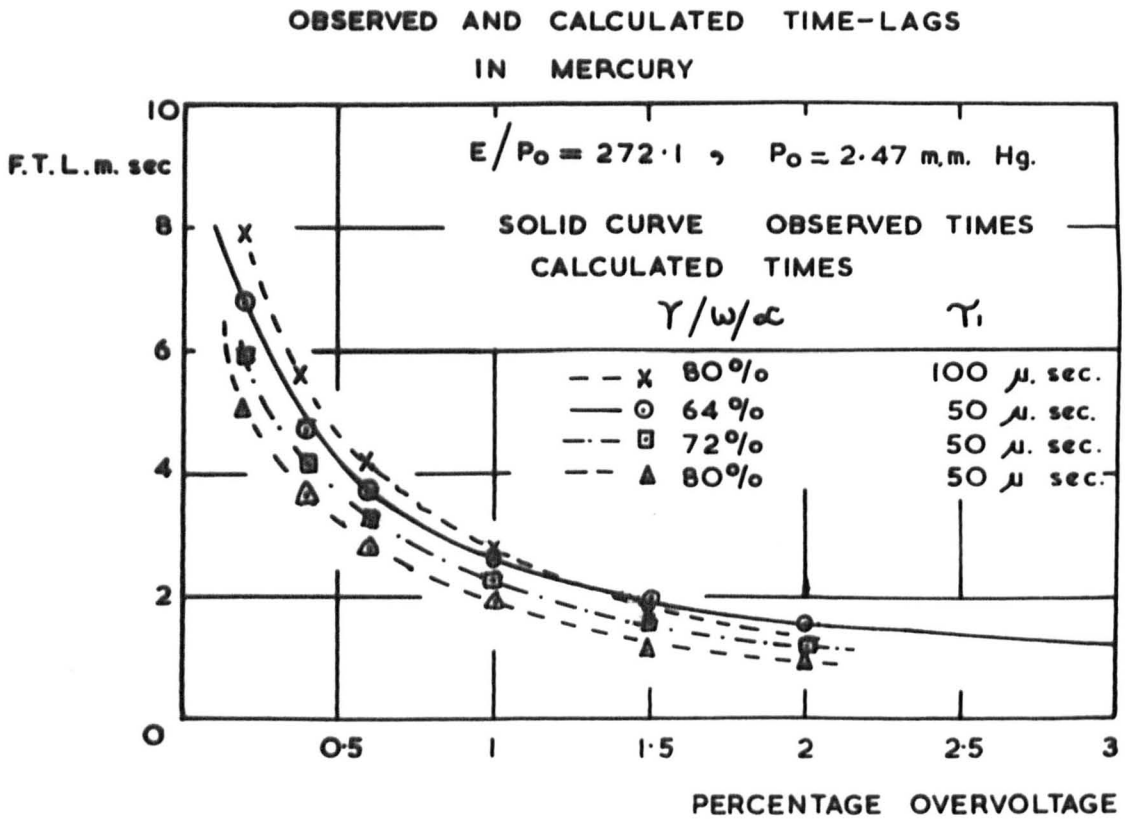
OBSERVED AND CALCULATED TIME-LAGS
IN MERCURY
F.T.L.m. sec
10
8
6
4
2
0
E/P₀ = 272·1 , P₀ = 2·47 m.m. Hg.
SOLID CURVE OBSERVED TIMES
CALCULATED TIMES
ϒ/ω/α ϒ₁
80% 100 μ. sec.
64% 50 μ. sec.
72% 50 μ. sec.
80% 50 μ sec.
0·5
1
1·5
2
2·5
3
PERCENTAGE OVERVOLTAGE

fig.59

```
1ØØ   FORMAT(3FØ.Ø)
      STOP
      END
```

This program has five loops. The first loop enabled the measured time-lag at twelve values of E_s/p_o to be analysed in one sum. The second loop enabled the time-lag to be calculated at each E/p_o, for six values of over-voltages which covered a range between 0.2% and 2%. The third loop helped to find out the effect of the drift velocities of the atomic and molecular mercury positive ions on the time-lag. The values of the drift velocities were those determined by Kovar (55). The fourth loop enabled the calculation to be performed for ten choices of δ_1/α and γ, such that $\delta_1/\alpha + \gamma = \omega/\alpha$. Finally the fifth one enabled the time-lag to be determined for each of the above variables (i.e. 10 choices of secondary coefficients, 2 choices of drift velocities and six choices of overvoltages) at 12 values of τ_1. The accuracy of determining the value of Q of FQ=0 was better than 0.001%.

The analysis applied to all the present experimental curves of time-lag against overvoltage. It was found in all cases, that the difference between the drift velocities of the atomic and molecular ions had negligible effect on the calculated time-lag, a difference of 11500 cm.per sec. resulted in a difference of only 0.07 m.sec., in the calculated times. The theoretical time-lag at constant E_s/p_o was then plotted as a function of percent overvoltage and compared to the experimental curves. At any particular value of E_s/p_o, the agreement between the theoretical and experimental curves, over the whole range of overvoltage, was found at only one particular value of τ_1. Fig(59) shows a typical plot of the observed and calculated time-lags at E_s/p_o of 272.lv.cm^{-1}.mm.Hg^{-1}., and

reduced pressure of 2.47 mm.Hg. Only the 4 closest theoretical curves are included. The four theoretical curves show that the best fit is at a value of τ_1 of 50×10^{-6} sec. and 36% of $\frac{\delta_1/\alpha}{\omega/\alpha}$.

The values of τ_1 required in order to obtain agreement to within 10% between calculated and measured growth times, obtained in this way, are given below in table (6.2.1)

Table (6.2.1)

p_o (mm.Hg.)	d(cm)	E_s/p_o	$\tau_1 \times 10^{-6}$ sec.
5.8	0.72	13.8	150
5.6	0.4776	166.6	50
4.5	0.45	192.35	50
4.2	0.7	160.2	50
3	0.42	240.5	50
2.47	0.465	272.1	50
2.45	0.8	196.4	50
2	0.71	236.3	100
1.58	0.6563	294.4	150
1.4	0.83	271.9	100
0.95	0.72	422	250
0.9	0.9	357	300

In order to decide, from these values of τ_1 which of the two delayed photon processes is the more important, the role of each process will be discussed separately in the following two sections.

6.2.3.4. THE ROLE OF IMPRISONED RESONANCE RADIATION.

It has been seen earlier in this section the delay time for the ($^1P_1 \rightarrow {}^1S_o$) photons was only ~3 x 10^{-6} sec., which is far too short compared with the lowest required value of τ_1. However for the ($^3P_1 \rightarrow {}^1S_o$) photons the delay times are between 75 to 120x10^{-6} sec. for electrode separations between 0.4 and 1cm. These delay times are of the order of magnitude of some of the required values of τ_1 in table (6.21). The relation $\tau_1 = \tau_o \frac{(3\pi^2 d)^{\frac{1}{2}}}{\lambda} \times 0.87$, shows that if this process is solely responsible for the delayed photoelectric emission, then the required times should be a function of the gap separation d over the whole range of E_s/p_o analyzed. Comparison of the values of τ_1 and the electrode separation in table (6.2.1) shows that τ_1 is not a function of d. Therefore it is concluded that this process is not of great importtance, which agrees with the conclusion reached earlier in the section.

6.2.3.5 THE ROLE OF COLLISION-INDUCED NON-RESONANCE RADIATION.

It has been seen earlier in this section that if non-resonance photons produced in the volume destruction of the $^3P_2$ metastable atoms are responsible for the observed ionization growth times, then the required delay time τ_1 should depend on the pressure (i.e. density) (38). Comparison of the values of pressure and the required values τ_1 (table 6.2.1.) shows that for pressures up to 2.5mm.Hg. τ_1 is dependant on the pressure which indicates the dominance of the volume destruction process of $^3P_2$ metastable atoms. In the range of pressures from 2.5 to 5.6mm.Hg., however, the required values of τ_1 show independance of the pressure. Since the lowest value of τ_1 involved in the calculation of the growth

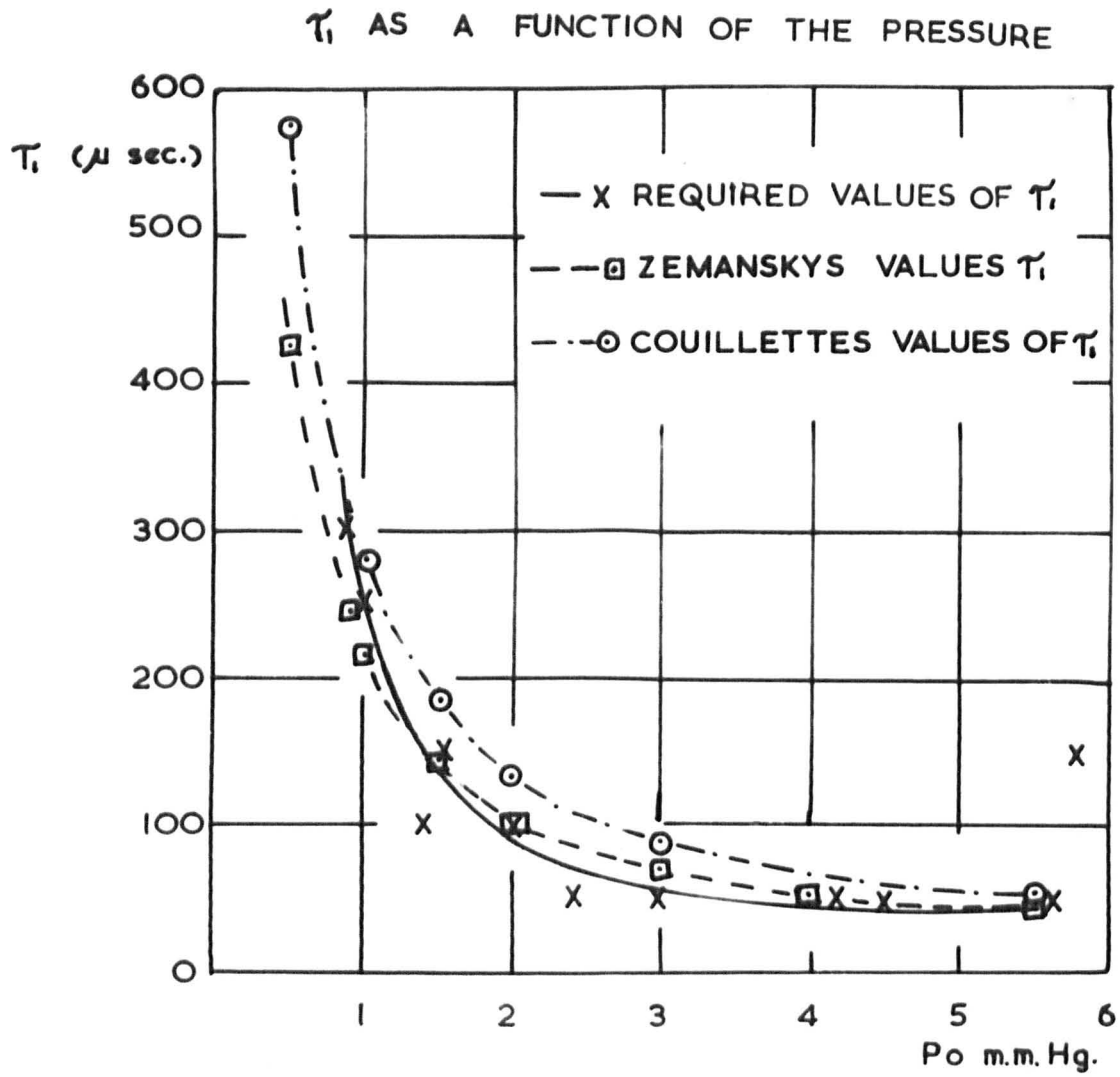
τ_i AS A FUNCTION OF THE PRESSURE
τ_i (μ sec.)
600
500
400
300
200
100
0
— X REQUIRED VALUES OF τ_i
— — ZEMANSKYS VALUES τ_i
— · — COUILLETTES VALUES OF τ_i
1
2
3
4
5
6
Po m.m. Hg.

fig.60

times is 50×10^{-6} sec., it is difficult to be sure that τ_1 would be independant of the pressure.

Assuming that $^3P_2$ metastable mercury atoms are de-excited in two body collisions with the ground state atoms within the discharge volume, and that the value of the dissipative collision probability is 9×10^{-4} (71), the life-time was calculated as the reciprocal of the number of the dissipative collisions per sec. The life-times obtained in this way show a reasonable agreement with the required values of τ_1, fig (60) (except the point at $p_o = 5.8$). When the calculation was repeated, using Coulíette's value for the probability of dissipative collisions (7.77×10^{-4}), the calculated life-times were slightly higher than the required values of τ_1, especially in the range of p_o from 1 to 4 mm.Hg.(fig(60)). The above two agreement suggests that in the range of pressure 0.9 to 5.6 mm.Hg., the active non-resonance photons are produced by the volume destruction of $^3P_2$ metastable mercury atoms in two body collisions with the ^1S_o ground state mercury atoms. Aubrecht's (56) value of 47×10^{-6} sec. is in good agreement with the required values of τ_1 at pressures between 2.5 and 5.6 mm.Hg., however the agreement is poor in the range of pressures below 2.5 mm.Hg., where he had made his observations. The rate of the de-excitation process, of the $^3P_2$ state, considered by Aubrecht would be proportional to the pressure, and therefore the life time would be inversely proportional to it. Consequently the life-time would be expected to vary by a factor of 6 over the range of pressure (0.5 to 3 mm.Hg.) that he studied. Therefore a life-time of 47×10^{-6} sec. would not be expected to account for the observed growth times over the whole range of pressure, unless there was some other destfuction process in Aubrecht's discharge

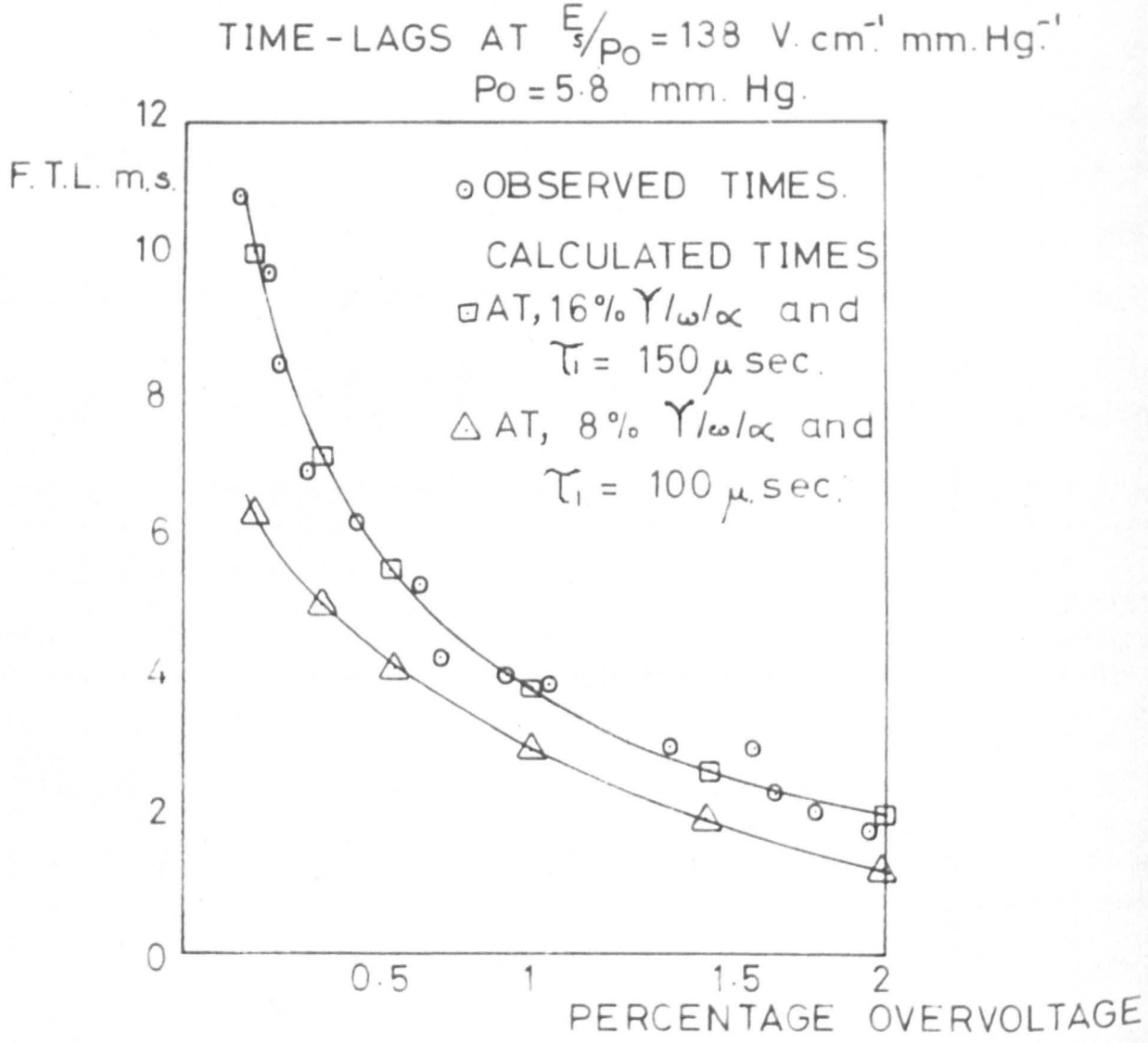
TIME-LAGS AT E_s/P_o = 138 V.cm^{-1} mm.Hg^{-1}
Po = 5·8 mm. Hg.
F.T.L. m.s.
12
10
8
6
4
2
0
OBSERVED TIMES.
CALCULATED TIMES
AT, 16% $\gamma/\omega/\alpha$ and
τ_i = 150 μ sec.
AT, 8% $\gamma/\omega/\alpha$ and
τ_i = 100 μ sec.
0·5
1
1·5
2
PERCENTAGE OVERVOLTAGE

Fig. 61

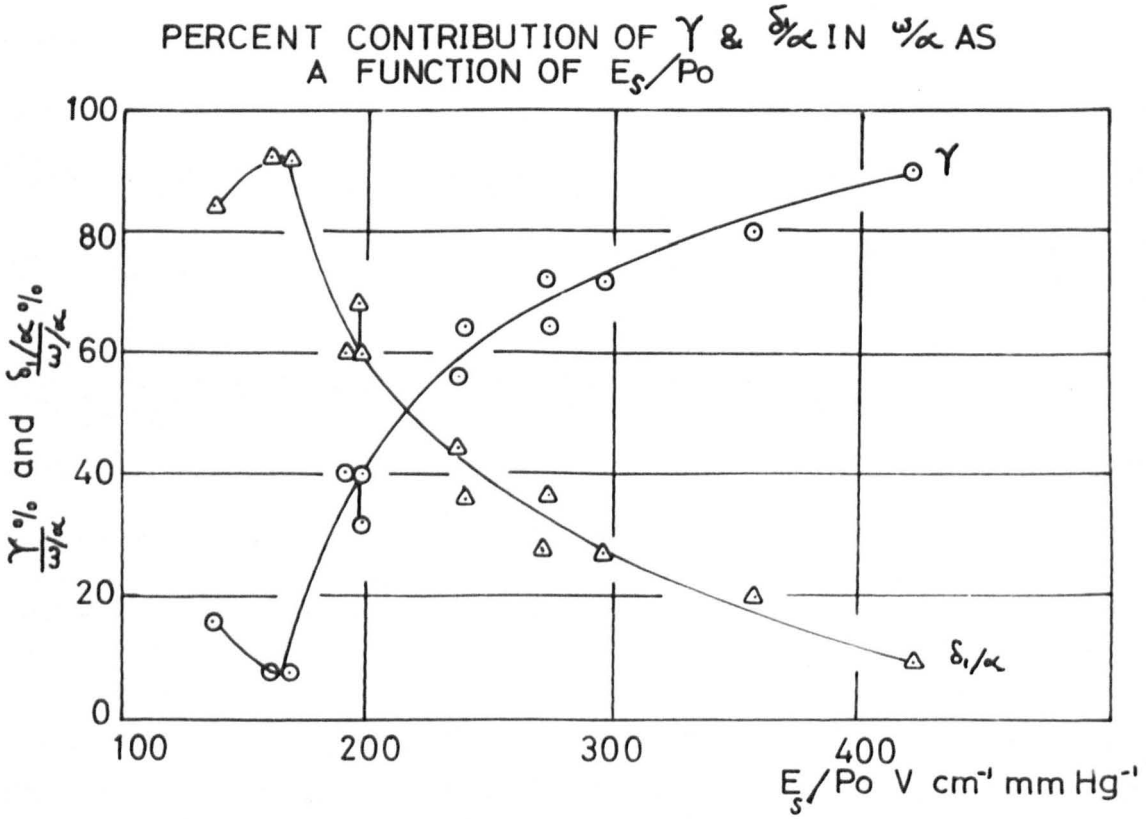
PERCENT CONTRIBUTION OF γ & δ/α IN ω/α AS A FUNCTION OF Es/Po
100
80
60
40
20
0
γ% and δ1/α% / ω/α
γ
δ1/α
100
200
300
400
Es/Po V cm⁻¹ mm Hg⁻¹

Fig. 62

which he did not consider. It is of interest to notice that an extrapolation of the required values of τ_1 fig(60), gives a value of 0.5m.sec. at a pressure of 0.6mm.Hg. This is the required value of the life-time of the $^3p_2$ metastable mercury atoms which is given by Overton, section (3.2.2.), for his interpretation of the time-lags observed at pressures from 0.6 to 0.63mm.Hg.

The observed time-lag at E_s/p_o of 138v.cm^{-1}.mm.Hg^{-1}. and pressure of 5.8mm.Hg. is rather unexpected, since the lowest life-times found to give an agreement was 150×10^{-6} sec. The closest calculated and experimental time-lags at this value of E_s/p_o, are shown in fig(61). It must be mentioned here, that the breakdown potential, at the value of p_od at this value of E_s/p_o, confirmed that the cathode conditions had not changed. Also the secondary ionization coefficient (δ_1/α and γ) obtained by the analysis was not anomalous.

6.2.3.6. THE VARIATION OF THE SECONDARY IONIZATION COEFFICIENTS WITH E_s/p_o.

Fig(62) shows the percent contribution of the positive ion, and the nonresonance radiation, δ_1/α_1 in ω/α obtained by the present analysis as a function of E_s/p_o. The increase in the percent contribution of the non-resonance radiation $\left(\frac{\delta_1/\alpha}{\omega/\alpha}\,100\right)$ at low E_s/p_o is a reflection of the increase in the probability of excitation to the $^3p_2$ mercury metastable state (fig(4)) at low energies. The decrease of the percent contribution of δ_1/α in the region of E_s/p_o below 160v.cm^{-1}.mm. Hg^{-1}. is more interesting since the probability of excitation to this state ($^3p_2$) starts decreasing sharply beyond this region. However this can be better seen from the curves in fig(63) showing the variation of secondary ionization coefficients δ_1/α and γ as a function of E_s/p_o. These

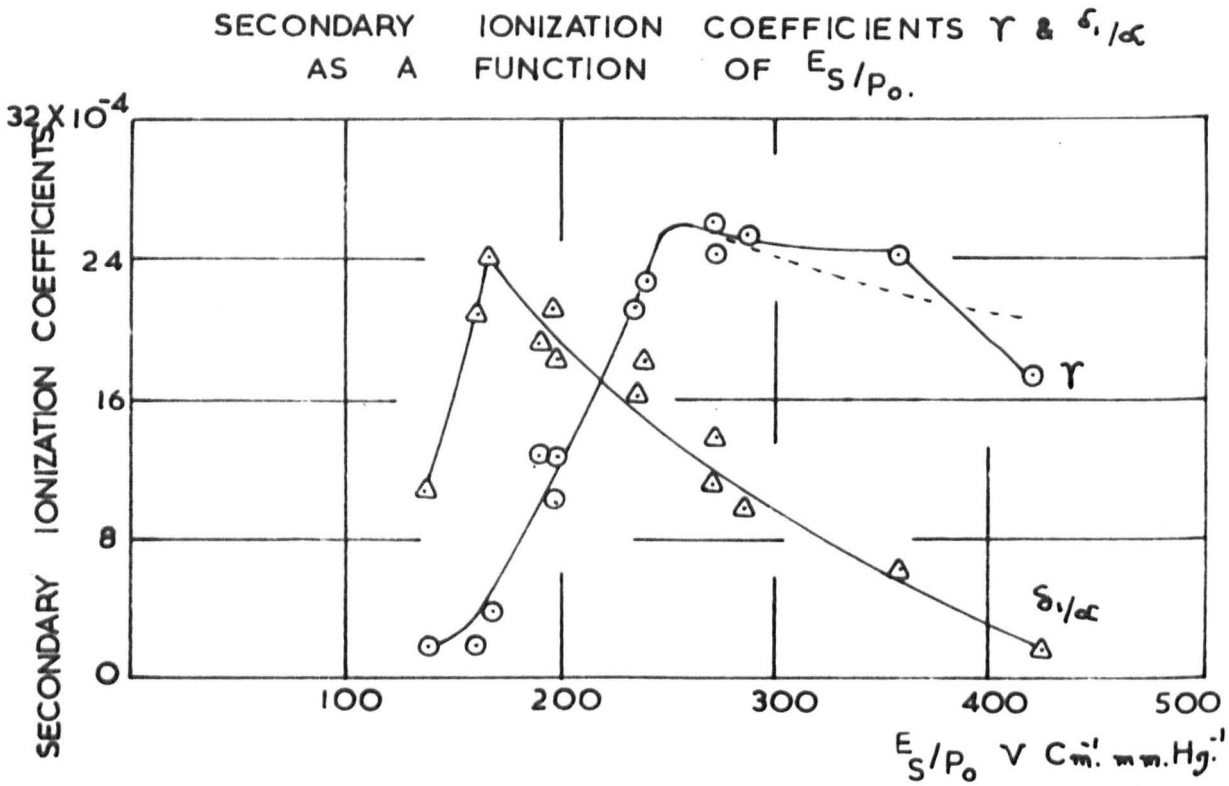
SECONDARY IONIZATION COEFFICIENTS γ & δ1/α
AS A FUNCTION OF ES/Po.
SECONDARY IONIZATION COEFFICIENTS
32 X 10⁻⁴
24
16
8
0
100
200
300
400
500
γ
δ1/α
ES/Po V Cm⁻¹. mm.Hg⁻¹

fig.63

values of δ_1/α and γ are obtained by multiplying the appropriate percent contribution by ω/α which are shown in fig(43). The most striking feature of these curves is the dominance of δ_1/α in the region of E_s/p_o below 250v.cm^{-1}.mm.Hg^{-1}. The feature of the curve of the secondary ionization coefficient δ_1/α is that it bears a very close resemblance to the excitation probability curve of the $^3P_2$ state. As E_s/p_o is increased from low values (i.e. as the energy is increased) the probability of excitation increases very sharply to a maximum and then starts decreasing more slowly. Therefore the similar variation of the δ_1/α with E_s/p_o is not surprising since it would be expected if the photoelectric emission (δ_1/α) by the non-resonance radiation produced by the volume destruction of the $^3p_2$ metastable atoms was operative. If it is assumed that the relation given by Overton (54) for the mean electron energy, $\bar{\varepsilon} = \frac{E/p_o}{42} + 6$, is within 10% accuracy, then a maximum of δ_1/α at E_s/p_o of 166v.cm^{-1}.mm.Hg^{-1} would correspond to an energy of 10ev. The maximum probability of excitation of the $^3P_2$ state (4) is at 8.3eV. The points joined by a vertical solid line in figs(62) and (63) are due to difficulties in finding the right percent contribution. The broken line drawn between the two points on the γ curve in fig (63) is believed to be the most likely variation of γ with E_s/p_o. A sudden change in γ is not expected since the action of positive ions at the cathode is entirely by virtue of their potential energy. Probably the sudden change is caused by error in ω/α it must be remembered that ω/α is very sensitive to any errors in determining α (due to the exponential factor.). As it has been seen, the computations are insufficiently sensitive to the values assigned to ionic velocities to enable a

distinction to be made between the roles of atomic and molecular mercury ions in this present investigation. The work of Kovar (55) on the ion mobilities of mercury ions in a Townsend discharge could not detect any Hg_2^+ at an E_s/p_o above 200v.cm^{-1}.mm.Hg^{-1}. The work of von-Engel and Aubrecht (18,56) has confirmed that there is a high cross-section($5x10^{-14}$cm^2) for the formation of Hg_2^+ at pressures above 1.5mm.Hg. Therefore, if there is a Hg_2^+ ion contribution to ω/α it would be expected only at low E_s/p_o, generally lower than 250v.cm^{-1}.mm.Hg^{-1}., where the pressure is high and thus the excitation probability to the states ^3p_o and $^3p_1$ are high (which are mainly responsible for the formation of Hg_2^+ in a mercury discharge). It would be expected therefore that at E_s/p_o above 250 volts cm^{-1} mmHg^{-1}, γ is mostly the contribution of atomic mercury positive ions. From Overton's analysis, 55% and 60% γ contribution would be expected at an E_s/p_o of 358 and 391v.cm^{-1}.mm.Hg^{-1}. respectively. From the present analysis, 80% and 85% would be expected at the same values of E_s/p_o. The difference between these values can be easily caused by inaccuracy of 1m.sec. difference in the measurements of the time-lag. However his analysis, shown in section (3.2.2) tables (3.2.) and (3.2.) shows that the agreement between his calculated and experimental time-lag is restricted to high overvoltages ($\geq$ 1.15%).

His results indicate that a big deviation (much more than 20%) would be expected at low values of overvoltage($\leq$ 0.5%).

6.2.4. CONCLUSIONS AND SUGGESTIONS FOR FUTURE WORK IN MERCURY.

The present measurements of the time-lags, together with those of Overton, indicate the importance of the gap geometry in the mercury discharge. The loss of the active particles, at small ratios of D/d, not only will effect the ionization growth rates, but also as we have seen, the breakdown potential and thus the total secondary ionization coefficient. At high ratio (10-20), the use of Davidson's analysis shows that a combination of delayed non-resonance photon and positive ion secondary processes together with the primary ionization processes can account for the observed growth times in the region of E_s/p_o between 138 and 422v.cm^{-1}.mm.Hg^{-1}., and in the range of pressure used between 0.9 to 5.6mm.Hg. Comparison of the required values of τ_{1-} with that calculated by using Zemansky's value of the probability of destruction shows that the non-resonance photons are produced by the volume destruction of the triplet $^3p_2$ metastable atoms in two body collisions with the ground mercury atoms.

The contribution of the non-resonance photons produced in the de-excitation of ^3p_o metastable atoms to the ground state has been eliminated on the basis of its low energy (4.66eV) compared to the work function of the liquid mercury cathode (~4.5eV) and also on the basis of the low ^3p_o excitation probability. Comparison of the delay times, associated with the imprisoned photons ($^3p_1 - {}^1S_o$), with the required times τ_1 has shown that these photons are unimportant as a secondary process. The last conclusion is supported by the low energies (4.86 eV) and the cross-section of deactivation of the $^3P_1$ state to the ^3p_o state which is higher than to the ^1S_o ground state. Due to the high energy (6.6eV) and the high numbers of the undelayed photons produced in the transition ($^1P_1$ to ^1S_o),

it may contribute to the secondary ionization coefficient. Since the calculations are not sensitive to distinguish between the fast secondary processes (i.e. atomic positive ion, molecular positive ion, and undelayed photons (δ/α)), therefore the calculated values of γ includes any ionization resulting from the action of undelayed photons at the cathode. Also, there may be some molecular ion contribution at values of E_s/p_o below 250v.cm^{-1}.mm.Hg^{-1}. The required value of τ_1 is taken as the average life-time of the $^3p_2$ metastable mercury atoms. To confirm the values of τ_1 and the other conclusions reached from the application of Davidson's analysis, measurements of the life-time of the $^3p_2$ metastable state, and its variation with pressure are needed by direct methods (i.e. optical absorption methods, or observation of the mercury after glow). Also Data on the electron drift velocities and electron energy distribution needed to be obtained to enable the use of the theory of Emeleus, Lunt and Meek, since values of α/p_o as a function of E/p_o has already been established in mercury discharge.

APPENDIX I

DAVIES-MILNE ANALYSIS

Three simultaneous current growth equations of the form

$$i = \frac{i_o \, e^{\eta(V-V_o)}}{1 - \omega/\alpha\,(e^{\eta(V-V_o)}-1)}$$

are taken for three values of current and voltage (i_1,V_1), (i_2,V_2) and (i_3,V_3) at a given value of E/p_o, ω/α, i_o and V_o can then be eliminated, producing

$$f(\eta) = i_1(i_3-i_2)\, e^{\eta(V_3-V_1)} - i_2(i_3-i_1)\, e^{\eta(V_3-V_2)} + i_3(i_2-i_1) = 0$$

By using Newton's method of successive approximation a value of η may be obtained to any required accuracy, by estimating a value of η and substituting this in the expression

$$\eta^1 = \eta - \frac{f(\eta)}{f^1(\eta)}$$

where η^1 is a closer approximation to the true value of η, and $f^1(\eta)$ is the first derivative of $f(\eta)$.

APPENDIX.3

SATURATED CAESIUM VAPOUR PRESSURE AS A FUNCTION OF THE ABSOLUTE TEMPERATURE.

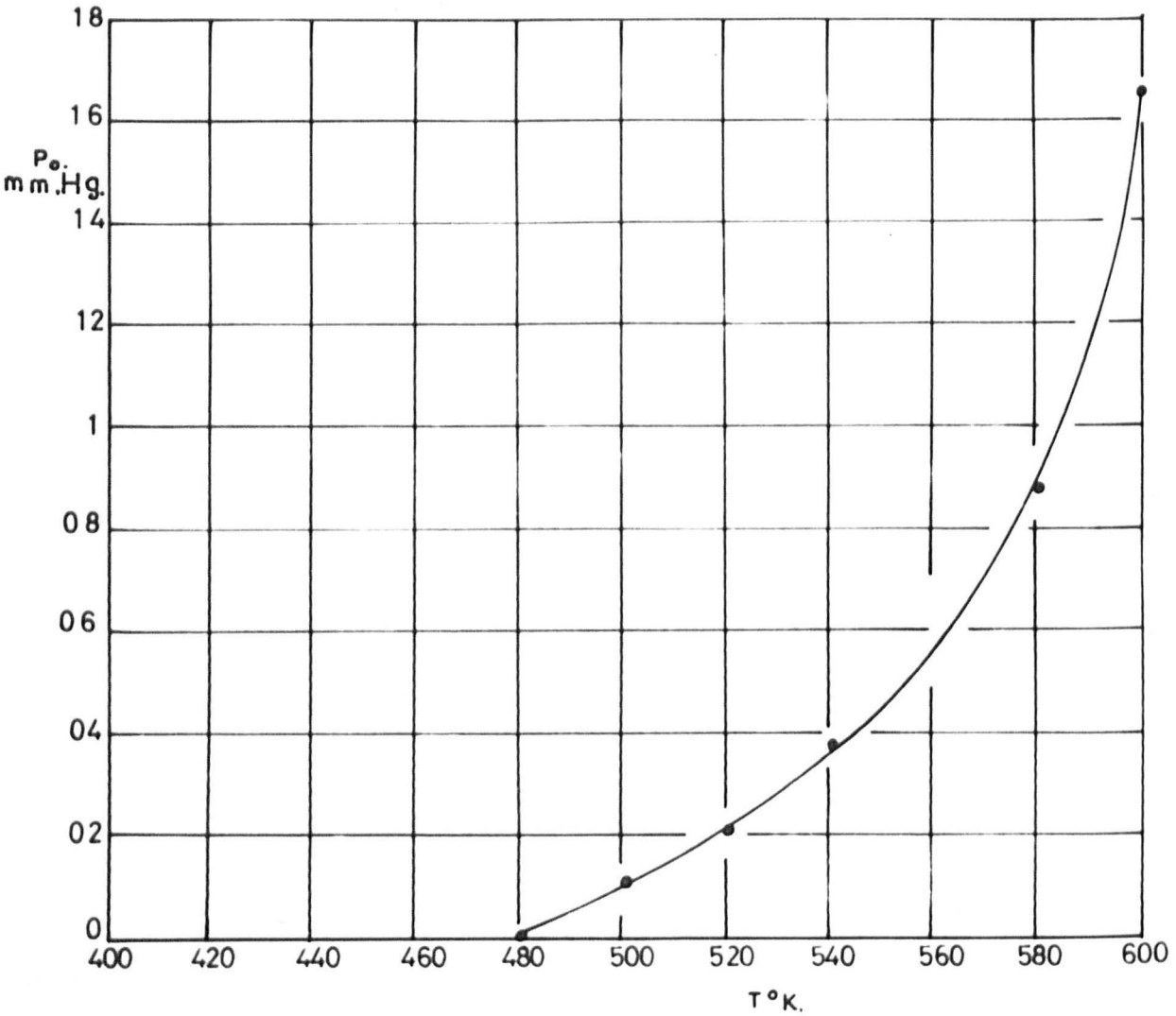

APPENDIX.2

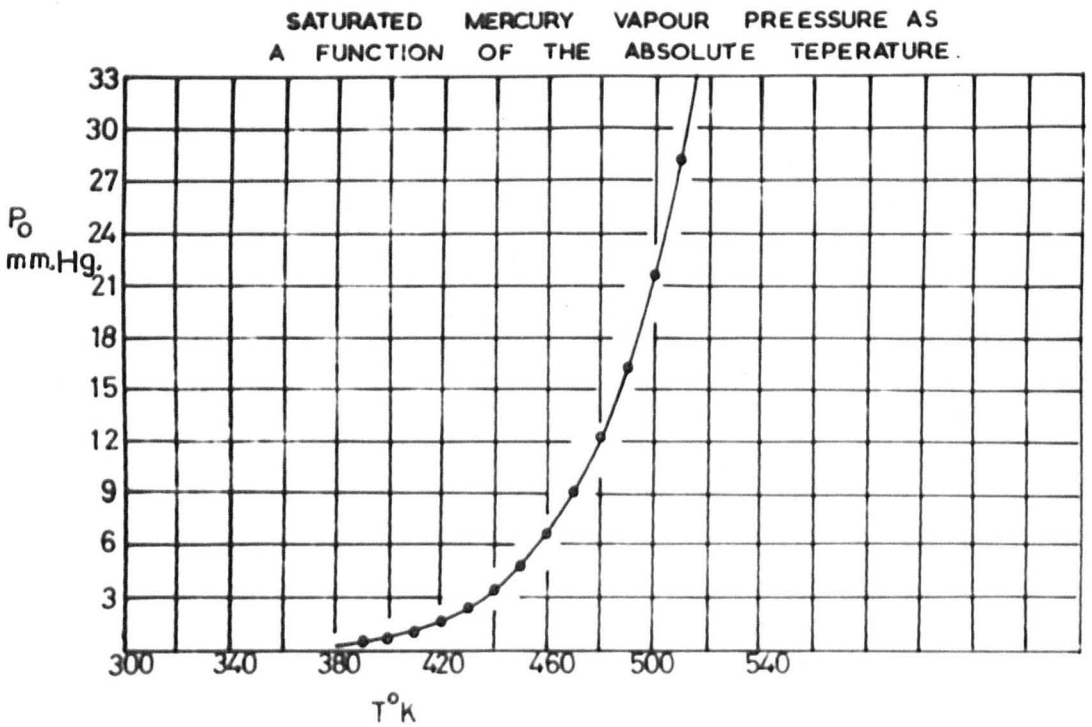
SATURATED MERCURY VAPOUR PREESSURE AS
A FUNCTION OF THE ABSOLUTE TEPERATURE.
Po
mm.Hg.
33
30
27
24
21
18
15
12
9
6
3
300
340
380
420
460
500
540
T°K

TEXT BOUND CLOSE TO THE SPINE IN THE ORIGINAL THESIS

LIST OF FIGURES

31. Photographs of the second mercury experimental tube.
32. The second mercury experimental tube.
33. The voltage source.
34. Circuit for the measurement of breakdown potentials.
35. Circuit for the measurement of first ionization coefficients.
36. Circuit for the measurement of the formative time lag.
37. Oscilloscope traces of the formative time lags at $E/p_o = 160$.
38. Breakdown potentials in caesium vapour.
39. Lag I as a function of E/p_o in caesium vapour.
40. First ionization coefficient in caesium vapour.
41. Breakdown potentials in Caesium vapour.
42. First ionization coefficient in mercury vapour.
43. ω/α as a function of E/p_o in mercury vapour.
44. to 45. Formative time lags in mercury vapour, first tube.
46. Formative time lag as a function of E_s/p_o for 0.25% overvoltage, first tube.
47. to 52. Formative time lags in mercury vapour, second tube.
54. Formative time lags as a function of D/d.
55. Formative time lag as a function of E_s/p_o for 0.25% overvoltage, second tube.
56. to 57. $\theta(\lambda)$ as a function of λ.
58. Observed and calculated time lags as a function of $\Delta V\%$ for 10% metastable atoms contributions in ω/α at E_s/p_o of 294V $cm^{-1}.mm.Hg^{-1}$.
59. Observed and calculated time lags as a function of $\Delta V\%$ at E_s/p_o of 272.1 Vcm^{-1} $mm.Hg^{-1}$.
60. Calculated and required values of τ_1 as a function of p_o.
61. Observed and calculated time lags as a function of $\Delta V\%$ at E_s/p_o of 138V.cm^{-1} $mm.Hg^{-1}$.
62. Percent contribution of γ and δ_1/α in ω/α as a function of E_s/p_o.
63. The secondary ionization coefficients γ and δ_1/α as a function of E_s/p_o.

References

1. Townsend, J.S. Electricity in Gases (Oxford Clarendon Press 1915).
2. Cravath, A.M. Phys. Rev. 36, 248, (1930), Phys. Rev. 47, 254A, (1935).
3. Penning, F.M. Druyvesteyn, M.J. Rev. Mod. Phys. 12, 27, (1940).
4. Ramsauer, C. Ann. d. Physik. 64, 513, (1921).
5. Penney, W.G. Phys. Rev. 35, 504, (1930).
6. Francis, G.E. Ionization Phenomena in Gases (London, 1960).
7. Houtermans, F.G. Z. Phys. 41, 619, (1927).
8. Von Engel, A., Steenbeck, M., Elektrische Gasentladungen (Berlin,, 1932).
9. Llewellyn-Jones, F., Ionization and Breakdown in Gases (Metheun, 1957).
10. Crowe, R.W., Bragg, J.K. and Thomas, V.G., Phys. Rev. 96, 10, (1954).
11. Emeleus, K.G., Lunt, R.W. and Meek, C.A., Proc. Roy. Soc. A156, 394, (1936).
12. Von Engel, A, Ionized Gases (Clarendon Press, 1955).
13. Varney, R.N. Phys. Rev. 47, 483, (1935).
14. Horton, F. and Millest, D.M. Proc. Roy. Soc. 61, 134, (1946).
15. Penning, F.M. and Addenk, C.C.T. Physica 1, 1007, (1934).
16. Mohler, F.L. and Boeckner, C, J. Res. Nat. Bur. Stand. 3, 303, (1929).
    Mohler, F.L. et al. Phys. Rev. 27, 37, (1927).
17. Rouse, G.F. and Giddingings, G.W., Proc. Nat. Acad. Sci. (U.S.A.)
    11, 514, (1925), 12, 447, (1926).
18. Tan, K.L. and Von Engel, A., Brit. J. Appl. Phys. (J. Phys. D.) 2, 258, (1968).
19. Loeb, L.B. and Meek, J.M., The Mechanism of Electric Sparks (California:
    Standford University Press, 1941).
20. Reather, H.Z. Angew. Phys. 7, 50, (1955).
21. Massey, H.S.W. Electr nic and Ionic Impact Phenomena (Oxford: Clarendon Press, 1952)
22. Kapitza, L., Phil. Mag. 45, 989, (1923).
23. Oliphant, M.L.E. and Moon, P.B. Proc. Roy. Soc. A127, 388, (1930).
24. Newton, R.R. Phys. Rev. 73, 570, (1948).
25. Molnar, J.P. Phys. Rev. 83, 933, (1951).
26. Weissler, G.L. Handbuck de Phys. 21, 347, (1956).
27. Loeb, L.B. Basic Processes of Gaseous Electronics (University of California
    Press, 1955).

28. Meek, J.M. and Graggs, J.D. Electrical Breakdown of Gases (Oxford Clarendon Press, 1953).
29. Overton, G.D.N. et al. Brit. J. Appl. Phys. 16, (1965).
30. Hornbeck, J.A. Phys. Rev. 2, 83, (1951).
31. Varney, R.N. Phys. Rev. 93, 1156, (1954).
32. Molnar, J.P. Phys. Rev. 83, 933, (1951).
33. Dutton, T. et al. Brit. J. Appl. Phys. 4, 170, (1953).
34. Davidson, P.M. Proc. Roy. Soc. A249, 237, (1958).
35. Davidson, P.M. Proc. Roy. Soc. 80, 143, (1962).
36. Biondi, M., Phys. Rev. 88, 660, (1952).
37. Menes, M., Phys. Rev. 116, 481, (1959).
38. Phelps, A.V. Phys. Rev. 99, 1307, (1958).
Phys. Rev. 117, 619, (1960).
39. Holstein, T. Phys. Rev. 72, 1212, (1947).
Phys. Rev. 83, 1159, (1951).
40. Bibermann, L.M., Zh Eksper. Teor. Fiz, 17, 416, (1947).
41. Bartholomeyczyk, W. Z. Phys. 116, 235, (1940).
42. Stephenson, G., Mathematical Methods for Science Students (Glasgow University Press, 1966).
43. Betts, B.P., M.Sc. Thesis, Birmingham, (1963).
44. Bulker, M.J. M.Sc. Thesis, Birmingham, (1963).
45. Davies, D.K. et al., Proc. Phys. Soc. 81, 677, (1963).
Proc. Phys. Soc. 83, 137, (1964).
46. Bratescu, G.G. Revue de Phys. (Rumania) 7, 131, (1962).
47. Ditchburn, R.W. and Gilmor, J. C., Rev. Mod. Phys. 13, 310, (1941).
48. Bratescu, G.G. Revue de Phys (Rumania) 2, 1 (1957).
49. Lepeshinskaya, V.N. et al. Fizika Tverdogo Tela 1, 1656, (1959).
50. Llewellyn-Jones, F. and Galloway, W.R. Proc. Phys. Soc. 50, 207, (1938).
51. Grigorovici, R.Z. Phys. 111, 596, (1939).
52. Badareu, E. and Bratescu, G.G. Bull.Soc. Roum. 42, 82, (1944).
53. Smith, D. Ph.D. Thesis, University of Birmingham (1962).
54. Overton, G.D.N. Ph.D. Thesis, University of Keele (1965).
55. Kovar, F.R. Phys. Rev. 3A, 133, (1964).

56. Aubrecht, J.A. et al., J. Otic. Soc. Amer. 58, 196, (1968).
58. Colin, J.S., Metals Reference Book (London Butterworths, 1955).
59. Colin, J.S., Metals Reference Book (London Butterworths, 1955).
60. Colin, J.S., Metals Reference Book (London Butterworths, 1955).
61. McCallum, S.P., and Klatzow, L., Phil. Mag. S. 7, 111, (1934).
62. Davies, D.E. and Milne, J.G.C. Brit. J. Appl. Phys. 10, 301, (1959).
63. Sonkin, S. Phys. Rev. 43, 788, (1933).
64. Gurevich, I.M. and Yavarsky, B.M. C.R. Acad. Sci. U.S.S.R. 53, 789, (1946).
65. Fulker, M.J. Ph.D. Thesis, University of Keele, (1967).
66. Wolfsohn, G, Z. Fur. Phys. 83, 634, (1930).
67. Barrat, J.P. J. Phys. Radium 20, 541, (1959).
68. Samson, E.W., Phys. Rev. 40, 940, (1932).
69. Yavorskii, B., C.R. Acad. Sci. U.R.S.S. 55, 307, (1947).
70. Couillette, J.H. Phys. Rev. 32, 636, (1928).
71. Zemansky, M.A. Phys. Rev. 29, 313, (1927).